Models and Performances of Wireless MIMO and Cooperative Communication Systems

Guchun Zhang

Doctor of Philosophy

ASTON UNIVERSITY

July 2009

Summary

Aston University

Models and Performances of Wireless MIMO and Cooperative Communication Systems

Guchun Zhang
Doctor of Philosophy, 2009

Multiple-antenna systems offer significant performance enhancement and will be applied to the next generation broadband wireless communications. This thesis presents the investigations of multiple-antenna systems – multiple-input multiple-output (MIMO) and cooperative communication (CC) – and their performances in more realistic propagation environments than those reported previously.

For MIMO systems, the investigations are conducted via theoretical modelling and simulations in a double-scattering environment. The results show that the variations of system performances depend on how scatterer density varies in flat fading channels, and that in frequency-selective fading channels system performances are affected by the length of the coding block as well as scatterer density.

In realistic propagation environments, the fading correlation also has an impact on CC systems where the antennas can be further apart than those in MIMO systems. A general stochastic model is applied to studying the effects of fading correlation on the performances of CC systems. This model reflects the asymmetry fact of the wireless channels in a CC system. The results demonstrate the varied effects of fading correlation under different protocols and channel conditions.

Performances of CC systems are further studied at the packet level, using both simulations and an experimental testbed. The results obtained have verified various performance trade-offs of the cooperative relaying network (CRN) investigated in different propagation environments. The results suggest that a proper selection of the relaying algorithms and other techniques can meet the requirements of quality of service for different applications.

Key words: MIMO; cooperative communication; scatterer density; fading correlation; performance trade-offs.

To my parents,

Acknowledgement

I would like to first express the most sincere appreciation to my supervisors, Dr. Xiaohong Peng (Academic Supervisor, Aston University) and Dr. Xuanye Gu (Industrial Supervisor, BT Group plc). Without their generosity of knowledge sharing, endless support and encouragement, it would not be possible to carry out this research programme and complete the thesis. Moreover, I am grateful for other members, Richard Haywood, Dr. Saty Mukherjee, Timothy Porter and Dr. Scott Fowler, in the Adaptive Communications Network Research Group, Aston University for the discussions, their selfless help and expertise whenever I needed throughout the project. Also, many thanks should be delivered to Dr. Terence Broderick for his mathematical assistance for some of the issues in this thesis. Last but not least, I would like to thank Aston University and BT Group plc for the financial sponsorships offered to this doctoral programme.

Contents

Abbreviations

AF	amplify-forward
AOA	angle of arrival
AOD	angle of departure
AWGN	additive white Gaussian noise
B3G	beyond third generation
BS	base station
CC	cooperative communication
CDF	cumulative distribution function
CF	compress-forward
cor	correlation
CRC	cyclic redundancy check
CRN	cooperative-relaying network
CSI	channel state information
DDF	dynamic DF
DF	decode-forward
FAF	fixed AF
FDF	fixed DF
FSK	frequency shift keying
GAF	generalised AF
GSM	global system for mobile communications
IAF	incremental AF
i.i.d.	identical and independently distributed
i.n.d.	independent and non-identically distributed
KLT	Karhunen–Loève transform
LOS	line-of-sight
MAC	medium access control
MIMO	multiple-input multiple-output
MISO	multiple-input single-output
MU	mobile user

NAF	non-orthogonal AF
NLOS	non-LOS
OFDM	orthogonal frequency division multiplexing
PDF	probability density function
PHY	physical
QOS	quality of service
QPSK	quadrature phase-shift keying
RMS	root mean square
RSSI	received signal strength indication
Rx	receive
SAF	selection AF
SDF	selection DF
sel	selection
SIMO	single-input multiple-output
SISO	single-input single-output
SNR	signal-to-noise ratio
S-R-DF	selection repetition-based DF
S-STC-DF	selection (distributed) space-time-coding-based DF
TDMA	time division multiple access
Tx	transmit
UIU	unitary-independent-unitary
WLAN	wireless local area network
YCR	you-can-relay

Symbols

$\mathbf{\Psi}$	covariance matrix
Φ	correlation coefficient
$\Phi(\bullet)$	phase shift
$\mathbf{H}$	MIMO channel matrix
$H(\bullet)$, $h(\bullet)$	entropy
$\mathbf{X}$, $\mathbf{X}_i$, X	transmitted codeword
$\mathbf{Y}$, $\mathbf{Y}_i$, Y	received codeword
$\mathbf{Z}$, Z	noise
$\mathbf{I}$	identity matrix
$x(\bullet)$	baseband transmit signal
$r(\bullet)$	baseband received signal
B	bandwidth
P	power
G	complex array antenna gain pattern
$g(\bullet)$	real-valued antenna gain
L	path loss; number of symbols; packet length
f_d	Doppler shift
f_c	carrier frequency
R	attenuation coefficient; receiver; spectral efficiency
λ	carrier wavelength; parameter of the exponential distribution; eigenvalue
d	path length; diversity gain; destination
D	path length; distance
c	velocity of carrier; codebook; capacity
τ	delay
θ	phase of signals; angular spread; phase of complex correlation coefficient
h	antenna height
l	horizontal distance between the transmitter and the receiver

ε	dielectric constant; beamforming; energy efficiency
v	dimensionless Fresnel-Kirchoff diffraction parameter; tap number; speed
σ	radar cross-section; standard deviation
σ^2	variance
γ	path loss exponent
T_c	coherence time
E(•), E[•], E{•}	expectation
B_c	coherence bandwidth
D_c	coherence distance
α	channel gain; angle
s	parameter of the Rice distribution
K	Rice factor; number of scatterers
m	fading figure; mth receive antenna
ω	parameter of the Nakagami-m distribution
$\Gamma(\bullet)$	Gamma function
$I_0(\bullet)$	modified Bessel function of the first kind with zeroth order
n	number of path; nth transmit antenna
$\otimes$	operator of Kronecker product
T	transmitter; time; coding block length; transpose
C	capacity
Pr[•]	probability
$p, f(\bullet)$	PDF
$I(\bullet)$	mutual information
$\|\bullet\|_F$	Frobenius norm
*	matrix transpose conjugation/Hermitian transpose
N	AWGN; number of transmit antennas; number of relay nodes; number of delay taps; number of packets; number of nodes
r_x	receiver
N_0	double power spectral density of AWGN
det(•)	determinant

log	logarithm
$\mathbf{\Lambda}$	diagonal matrix
$\mathbf{R}$	upper triangular matrix; correlation matrix
Π	multiple product
Σ	summation
$\mathbf{U}$	unitary matrix
M	number of receive antennas
r	multiplexing gain
P_e	error probability
∞	infinity
$\cong$	statistically equal
$\propto$	proportional to
$\approx$	approximately equal to
$\sim$	asymptotically equal to
SNR	SNR
d_t	transmit antenna spacing
d_r	receive antenna spacing
S	number of scatterers
ϕ	dielectric property and radial displacement
$\lvert\bullet\rvert$	absolute value
Δ	angular spread of the transmitter; absolute variation
$S(\bullet)$	a scatterer
TA	transmit antenna
RA	receive antenna
Θ	AOA of transmitter
$\Im$	steering matrix
$\Gamma\exp(j\phi)$	complex reflection coefficient
η	scatterer density; data throughput; constant
ψ	pointing angle of terminals related to x-axis
$\psi(\bullet)$	Doppler power spectrum

$s_{(\cdot)}$	source node
$r_{(\cdot)}$	relay node
$(x)^+$	$\max(0, x)$
g	threshold
$\rightarrow$	approaching
lim	limitation
$D(\cdot)$	decoding set
V	number of delay taps
β	magnitude of complex correlation
υ	amplification factor
k	length of data packets in coded packets
ρ	packet loss rate
$P(\cdot)$	permutation
$\exp(\cdot)$	exponential
CN	complex circularly symmetric Gaussian
$\Re$	set of real numbers
w	white; message
f	flow
$\mathcal{A}$	arc
$\mathcal{C}$	cut

Tables

Figures

1 Introduction

In the past decade, multiple-antenna systems have attracted so much attention from the research community as well as system vendors, as they can provide significant performance improvement in terms of data throughput, coverage and error probabilities. Due to ever growing demands for faster and more reliable wireless access to various applications, including web browsing, email and video streaming, the multiple-antenna technology has been adopted by many broadband wireless access systems, such as Long Term Evolution (LTE) [1], future wireless local area network (WLAN) [2] and worldwide interoperability for microwave access (WiMAX) [3]. Many technical challenges and research issues, however, have been raised, such as the understanding of the performance differences between multiple-antenna channels and single-antenna channels, the design of proper coding schemes, the construction of realistic system models and the evaluation of system performances.

With respect to the formation of antenna arrays, multiple-antenna systems can be divided into two categories: multiple-input multiple-output (MIMO) systems and cooperative communication (CC) systems. In MIMO systems, each transmission terminal is equipped with multiple antennas, which forms a real antenna array. In CC systems, however, a number of single antennas on different terminals or devices tend to work together, forming virtual antenna arrays. So far, many research efforts have been focused on:

- Construction of multiple-antenna channel models for different wireless propagation environments;
- Design of space-time coding schemes for MIMO systems;
- Design and optimization of cooperative protocols for CC systems;
- Design of coding schemes for CC systems;
- Channel capacity formulation and analysis for multiple-antenna systems;
- Analysis of performance trade-offs in multiple-antenna systems.

This thesis is focused on investigating the performance of MIMO and CC systems, through the construction of channel models, the formulation and analysis of channel

capacity and the analysis of performance trade-offs. The next section is an overview of these multiple-antenna systems.

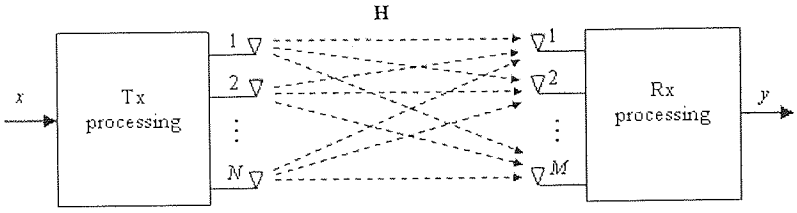

H: MIMO channel matrix; N: number of transmit antennas; M: number of receive antennas;

Figure 1-1 MIMO systems.

1.1 Systems description

MIMO systems, as shown in Figure 1-1, offer a significant performance improvement over single-input single-output (SISO) systems that are deployed in the current wireless systems, by exploiting spatial diversity and multiplexing gains with space-time coding employed at both the transmitter and the receiver. MIMO systems are suitable for both indoor wireless systems, i.e., short range propagation, and outdoor wireless systems, i.e., long distance propagation. According to the Shannon channel capacity $C = B\log_2(1+SNR)$, higher channel capacity can only be achieved when the frequency bandwidth, B, becomes wider for a fixed signal-to-noise ratio (SNR), SNR. MIMO systems, however, can increase the capacity dramatically without a bandwidth penalty. It has been shown that if the wireless channels experience independent and identically distributed (i.i.d.) Rayleigh fading [4-6], the channel capacity of a MIMO system increases linearly with the minimum number of antennas, i.e., $C = \Sigma_{i=\min(M,N)} B\log_2(1+SNR_i)$, for given SNRs, where N and M are respectively the numbers of the transmit and the receive antennas, as indicated in Figure 1-1. Nevertheless, the fading correlation between wireless channels is inevitable in real propagation environments. Therefore, many research efforts have been spent on the channel characterization, i.e., channel modelling, of MIMO systems and analysis of the channel capacity performance with the correlation factor taken into account in different scattering

environments, such as ring scattering [7, 8], linear scattering [9] and general scattering environments [10, 11]. However, some of these reported models are over-simplified, which leads to the over-estimated performance of MIMO systems. Therefore, in the MIMO system part of this thesis, the performance of channel capacity is evaluated in a more realistic propagation environment.

Although it has been shown that MIMO systems can increase the channel capacity dramatically, the size of portable devices limits the full exploitation of the advantages provided by MIMO. CC systems are therefore proposed to deal with this limitation problem, in order to achieve the diversity gain in this situation. A sample topology of CC systems is shown in Figure 1-2.

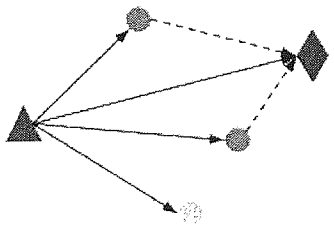

Triangle: the source node; Circle: the relay nodes; Diamond: the destination node.

Figure 1-2 A sample topology of CC systems.

CC systems are the descendants of relaying communication systems that were first introduced by van der Meulen in [12-14]. In relaying communication systems, the transmitter (the source node) communicates with the receiver (the destination node) via the relay nodes. Later in [15], T. Cover and A. Gamal allowed the destination node to listen to the source node directly, which is now known as CC systems. As the source node and the relay nodes are individual devices, some mechanisms, termed as *protocols*, are designed to control the way how relay nodes process and forward the source information. According to the action required in relay nodes, various protocols proposed fall into three categories: amplify-forward (AF), decode-forward (DF) and compress-forward (CF). AF, first proposed in [16], is the simplest protocol, where relay nodes only need to enhance the signal strength of the received source information and then forward it. Although the noise received at relay nodes is also amplified and forwarded, AF is an ideal candidate for the so-called two-way relaying systems [17].

DF and CF are both proposed in [15]. In DF, relay nodes decode the received source information and forward the error-free re-encoded source information. In CF, the source information received by relay nodes is compressed or quantised and then forwarded to the destination node. The main purpose of employing relay nodes is to exploit the spatial diversity gain in the network, in order to reduce the error probability or information loss of wireless channels. If feasible space-time or network coding schemes can be found for CC systems, spatial multiplexing gain can also be achieved, resulting higher data rate.

So far, all the investigations in the areas of CC systems are confined in the ideal channel assumption and the results reported are most based on theoretical analysis and simulations. Therefore, it is essential to evaluate system performances in more realistic environments, i.e., considering fading correlation and, as the best option, through experiments. The work in the CC system part of this thesis is focused on accomplishing these two tasks.

1.2 Objectives

To better understand the behaviour of MIMO propagation channels, it is essential to model the scattering environment as realistically as possible. In this thesis, therefore, the performance of MIMO systems is studied in a double-scattering model modified to reflect the real propagation environment as closely as possible. The performance variations are subject to the change of the scatterer density, one of the key parameters in a scattering environment.

In real-world environments, two wireless fading channels in a multiple-antenna system can be correlated, i.e., the variation in one channel causes the other to vary correspondingly. As is well known, the fading correlation can have significant impacts on system performances, such as channel capacity, and thus should not be ignored in performance evaluation. Nevertheless, not much work has been done for finding the effect of fading correlation on CC systems. Therefore, it is necessary to evaluate the performance of CC systems in realistic propagation environments by theoretical modelling of correlated channels in CC systems and by experiments and simulations.

1.3 Methodology and contributions

To meet the objectives of this thesis, investigations are carried out through theoretical analysis and modelling, experimental tests and simulations. Theoretical models and their simulations are based on the scattering models that can closely reflect real propagation environments. They show the insight into the system being modelled and can be used to predict system performances with respect to different system parameters and conditions. Experimental tests give true system performances that are sometimes overestimated by theoretical and simulation models. The results obtained from experimental tests can help refine the theoretical and simulation models accordingly. Those refined models can then be used to evaluate system performances in other propagation environments that are difficult to establish in a laboratory.

For investigating the performance of MIMO systems, a theoretical channel model is developed in this work for a modified double-scattering fading environment where both of remote and local scatterers are considered to be essential to represent a realistic wireless environment. The key technical challenge in the MIMO channel modelling is how to present the scattering model to closely reflect the real-world environment.

Performances of CC systems in realistic propagation environments are studied in two aspects. Firstly, they are evaluated in a theoretical manner, where a general correlated fading channel model is incorporated into the existing ideally modelled protocols. Secondly, an experimental testbed is built to verify the simulation models created, allowing the investigations to be extended to other propagation environments. There are several challenges in investigating CC systems, such as how to deal with the asymmetrical feature of wireless channels in a CC system when modelling the system in realistic environments; how to adjust simulation models with respect to the results obtained from testbed experiments; and how to construct a proper testbed for carrying out experiments and data analysis.

Based on the above methodology, a MIMO channel model is developed for a double-scattering environment in which both remote and local scatterers are considered. This model provides insight into signal propagation in this double-scattering environment and can be conveniently manoeuvred by the governing

parameters, such as the scatterer density. For CC systems, a general channel model has been applied to the existing ideal channel models, in order to evaluate the effect of fading correlation on these systems. Moreover, a simulation model is created to investigate the performance trade-offs in CC systems for different wireless propagation environments; and the performance results are verified by the real-world testbed used.

1.4 Outline

The thesis begins with the wireless propagation theory that is essential for studying the multiple-antenna systems. Based on the theory, the multiple-antenna systems are investigated in more realistic environments than those described in previous work, through theoretical analysis and modelling, experimental tests and simulations.

The thesis is organised as follows. In Chapter 2, large-scale path loss models and small-scale fading models for signal propagating in wireless channels are discussed, respectively. The large-scale path loss models are used to estimate the mean received power at the receiver when the transmission range is expected to be large. The small-scale fading models characterise the rapid fluctuation of the received power over a short transmitter-receiver distance, over a short period of time or at different close locations. These models are essential for studying multiple-antenna systems.

Chapter 3 gives the capacity formulation of general wireless channels and addresses the modelling techniques for multiple-antenna systems. This chapter also highlights the fundamental trade-off, i.e., diversity-multiplexing trade-off, in performance evaluation. Some classic MIMO channel models are re-constructed, providing better understanding of MIMO channels and the use of modelling techniques. These models are extended in Chapter 5 for the investigation in a more realistic propagation environment.

Chapter 4 is focused on examining the protocols for CC systems. Different protocols are designed for the relay nodes to cope with different system conditions. The performance of these CC systems is evaluated through the channel capacity and diversity-multiplexing trade-off. Later in Chapter 6, some of the protocols are re-evaluated with the fading correlation being taken into account.

The effects of the scatterer density on MIMO channel performances in a double-scattering model are the main topic of Chapter 5. It is begun with constructing a new channel model for the more realistic propagation model that includes both remote and local scatterers. The critical results are produced through theoretical modelling and simulations by using different parameter sets for the propagation environment. The outcome of this work extends the results reported in previous work, and explains why and how the scatterer density has varied impacts on channel performances.

In Chapter 6, the effects of fading correlation on the performance of CC systems are investigated. A general correlated fading channel model is adopted under the consideration of special channel conditions in CC systems. The results indicate that the fading correlation does have a noticeable effect on the performance of CC systems. Hence, it is necessary to take this factor into account in performance evaluation.

The performance trade-offs of CC systems are studied at the packet level in Chapter 7. The approach of the work is to build a CC system in both simulations and a tested. The results obtained from the testbed are used to verify the simulation models, which are then extended to address other propagation environments that are unlikely to set up in a laboratory.

The conclusions and the contributions of the work and the recommendations for future research are given in Chapter 8.

2 Signal Propagation in Wireless Channels

Transmitting signals in wireless environments is challenging, since signals are subject to the severe impairment in wireless channels. In contrast, wired communication systems can offer better performances. Here is an example. 1Gbps Ethernet card has become the standard configuration for new personal computers, while WLAN can only achieve 54Mbps at maximum. In wireless channels, there are many signal-impairing factors that do not exist in wired channels, such as reflection, diffraction, scattering, shadowing and fading. These factors can distort the waveform of a signal, decrease the signal strength, and make the received signals added destructively. To investigate these factors, it is pivotal to first model the transmitted signal as [18]

$$\begin{aligned} s(t) &= \mathrm{Re}\left\{x(t)e^{j2\pi f_c t}\right\} \\ &= \mathrm{Re}\{x(t)\}\cos(2\pi f_c t) - \mathrm{Im}\{x(t)\}\sin(2\pi f_c t) \\ &= x_I(t)\cos(2\pi f_c t) - x_Q(t)\sin(2\pi f_c t), \end{aligned} \tag{2.1}$$

where $x(t) = x_I(t)+jx_Q(t)$ is a complex baseband signal with in-phase component $x_I(t) = \mathrm{Re}\{x(t)\}$, quadrature component $x_Q(t) = \mathrm{Im}\{x(t)\}$, bandwidth B_x (found through the *Fourier Transform* of $x(t)$) and power P_x (the square of the magnitude of $x(t)$). $x(t)$ can represent either analogue or digital information of the transmitter. For digital information, $x_I(t)$ and $x_Q(t)$ are evident on the constellation diagram. For example, if Quadrature Phase-Shift Keying (QPSK) is the modulation method, information "11" can be expressed by $x_I(t) = x_Q(t) = (P_x/2)^{1/2}$, where P_x is the power of the symbol representing "1". The quality of the received signal depends on that of the channel through which the signal propagates. Wireless channel models can be categorised into two types: *large-scale path loss* models and *small-scale fading* models. The large-scale path loss models estimate the average received signal strength over large transmitter-receiver distance (several hundreds or thousands of meters). These models are useful in approximating the coverage of transmitters. The small-scale fading models characterise the rapid fluctuation of the signal strength over short transmitter-receiver distance or very short duration (on the order of seconds). The models discussed in this

chapter are essential for understanding and modelling multiple-antennas systems in the later chapters.

2.1 Ray tracing

Ray tracing is a modelling method that is used to mathematically present the phenomena of signal propagation in wireless channels. Using this method, one can explicitly model signal attenuation in power, delay in time and shift in phase and/or frequency relative to the signal on the line-of-sight (LOS) path. In ray tracing, it is usually assumed that the number of reflectors in the wireless channel is finite and the reflectors' location and dielectric properties are known. Corresponding to the transmitted signal expressed in (2.1), the received signal can be modelled as, using ray tracing,

$$r(t) = \mathrm{Re}\left\{ \sum_{i\in(1,\cdots,n)} \sqrt{G_i}\sqrt{L_i}\, x(t-\tau_i) e^{j2\pi\left(f_c - f_{d|i}\right)t} e^{-j2\pi d_i/\lambda} \right\}, \tag{2.2}$$

where n is the number of paths between the transmitter and the receiver; $G_i = G_{tx,i}G_{rx,i}$ is the total antenna gain of the transmit antenna and the receive antenna for the ith path; L_i is the path loss due to reflection, diffraction or scattering; τ_i is the delay; f_c is the carrier frequency; $f_{d|i}$ is the *Doppler shift*[1]; λ is the carrier wavelength; $-2\pi d_i/\lambda$ is the phase shift with respect to the length of the ith path.

2.2 Path loss

Path loss may be due to many effects such as free space loss, refraction, diffraction, reflection, aperture-medium coupling loss and absorption. Path loss is also affected by terrain contours, type of environments (urban, rural, vegetation or foliage), propagation

[1] Doppler shift will be discussed in more details in Subsection 2.3.1.

medium (dry or moist air), the distance between the transmitter and the receiver, the height and the location of the antennas involved, etc.

2.2.1 Free space loss

Free space loss is associated with the phenomenon of beam divergence and the inverse square law of electromagnetic radiation. As the name implies, free space loss counts the power attenuation of the wireless signals when they travel on an unobstructed path. It omits the antenna gains and other sources of loss such as reflection, absorption and diffraction. If a signal propagates on a LOS path, as shown in Figure 2-1, then the received signal can be presented as [18]

$$r(t) = \mathrm{Re}\left\{ \frac{\lambda \sqrt{G} e^{-j2\pi d/\lambda}}{4\pi d} x(t) e^{j2\pi f_c t} \right\}. \tag{2.3}$$

where d is the path length and G is the product of transmitter and receiver antenna gains. Thus, by comparing (2.1) and (2.3), free space loss can be expressed as [19]

$$L_f(d) = \frac{P_t}{P_r} = \left(\frac{4\pi d}{\lambda} \right)^2 = \left(\frac{4\pi f d}{c} \right)^2, \tag{2.4}$$

where f and c are the frequency and velocity of the carrier, respectively.

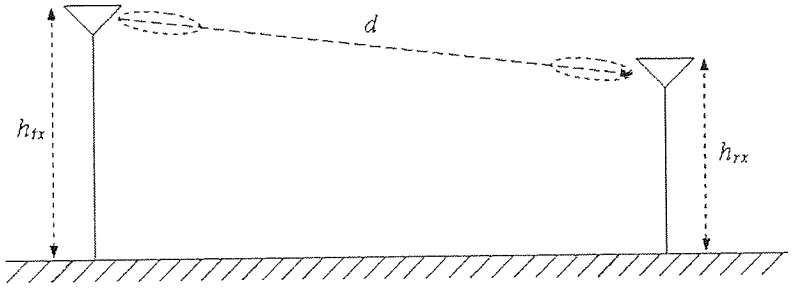

Figure 2-1 Signal propagation on a LOS path.

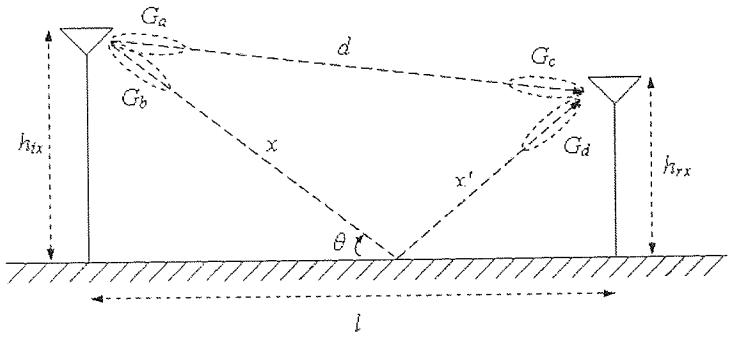

Figure 2-2 The two-ray model (ground reflection).

2.2.2 Reflection

When the radio wave of a signal impinges on another medium with different electric properties, the signal is partially reflected and partially transmitted [19]. If another medium is a perfect dielectric, then part of the energy of the signal is transmitted into the second medium and rest of the energy is reflected back to the first medium. There is no energy loss. If the second medium is a perfect conductor, then all the energy is reflected back to the first medium.

The two-ray model shown in Figure 2-2 is a useful propagation model and found to be reasonably accurate for estimating the signal strength over the distance of several kilometres for the mobile systems with the base station (BS) height exceeding 50m, as well as for LOS microcellular channels in urban environments [18]. In this model, once the locations of the transmitter and the receiver antennas are fixed, θ can be determined according to the law of reflection[1]. Using the ray tracing modelling technique, the received signal in the two-ray model can be found as

$$r(t) = \mathrm{Re}\left\{\frac{\lambda}{4\pi}\left[\frac{\sqrt{G_l}\,x(t)e^{-j2\pi d/\lambda}}{d} + \frac{R\sqrt{G_r}\,x(t-\tau)e^{-j2\pi(x+x')/\lambda}}{x+x'}\right]e^{j2\pi f_c t}\right\}, \tag{2.5}$$

where $G_l = G_a G_c$ and $G_r = G_b G_d$ are the products of transmitter and receiver antenna gains on the LOS and reflection paths, respectively; $\tau = (x+x'-d)/c$ is the time delay of the reflected signal relative to the LOS path; R is the ground reflection coefficient. If

[1] The law of reflection states that the direction of incoming light (the incident ray), and the direction of outgoing light reflected (the reflected ray) make the same angle with respect to surface normal.

the transmitted signal $x(t)$ is narrowband[1], i.e., $u(t) \approx u(t-\tau)$, then the received signal power of the two-ray model is

$$P_r = P_t\left(\frac{\lambda}{4\pi}\right)^2\left|\frac{\sqrt{G_l}}{d}+\frac{R\sqrt{G_r}e^{-j\theta_\Delta}}{x+x'}\right|^2, \tag{2.6}$$

where $\theta_\Delta = 2\pi(x+x'-d)/\lambda$ is the phase difference between the two received signals from two paths. When $l >> h_{tx}+h_{rx}$, θ_Δ can be approximated as

$$\theta_\Delta = \frac{2\pi\left(\sqrt{(h_{tx}+h_{rx})^2+l^2}-\sqrt{(h_{tx}-h_{rx})^2+l^2}\right)}{\lambda} \approx \frac{4\pi h_{tx}h_{rx}}{\lambda l}, \tag{2.7}$$

where h_{tx} and h_{rx} are the heights of the transmit antenna and the receive antenna, respectively; l is the horizontal distance between the transmitter and receiver; the following Taylor series approximation is used to obtain (2.7),

$$\sqrt{1+a} = \sum_{n=0}^{\infty}\frac{(-1)^n(2n)!}{(1-2n)n!^2 4^n}a^n \quad \text{for } |a|<1.$$

The ground reflection coefficient R is given by [18, 20, 21]

$$R = \frac{\sin\theta - Z}{\sin\theta + Z}, \tag{2.8}$$

where

$$Z = \begin{cases}\sqrt{\varepsilon_r - \cos^2\theta}\,/\varepsilon_r & \text{for vertical polarization,}\\ \sqrt{\varepsilon_r - \cos^2\theta} & \text{for horizontal polarization,}\end{cases}$$

and ε_r is the dielectric constant of the ground. Assume that $x+x' \approx d \approx l$, $\theta \approx 0$, $G_l \approx G_r$ and $R \approx -1$, for asymptotically large l. Then, the received signal power can be approximated as

[1] Narrowband will be discussed with more details in Subsection 2.3.2.

$$P_r \approx P_t G_l \frac{h_{tx}^2 h_{rx}^2}{l^4}. \tag{2.9}$$

Thus the path loss (without antenna gain) is found as

$$L_r(l) = \frac{P_t}{P_r} = \frac{l^4}{h_{tx}^2 h_{rx}^2}. \tag{2.10}$$

Comparing (2.10) with (2.4), it can be noticed that the path loss in (2.10) increases more rapidly than that in (2.4). Also, the received signal power in (2.9) and path loss in (2.10) are independent of carrier frequency at large value of l. As this two-ray model is more suitable for the long distance transmission, the parameter assumptions for (2.9) and (2.10) are rational and widely agreed.

This two-ray ground reflection model is useful to predict the path loss for mobile communications in rural and suburban areas where the distance between the transmitter and receiver is large and terrain can be rather flat. In the urban area, however, the two-ray model no longer works well, due to the size of mobile cells and high object density. Amitay [22] developed a model for urban microcells, where in total ten rays are considered and a similar approach as discussed above is used to model the received signal.

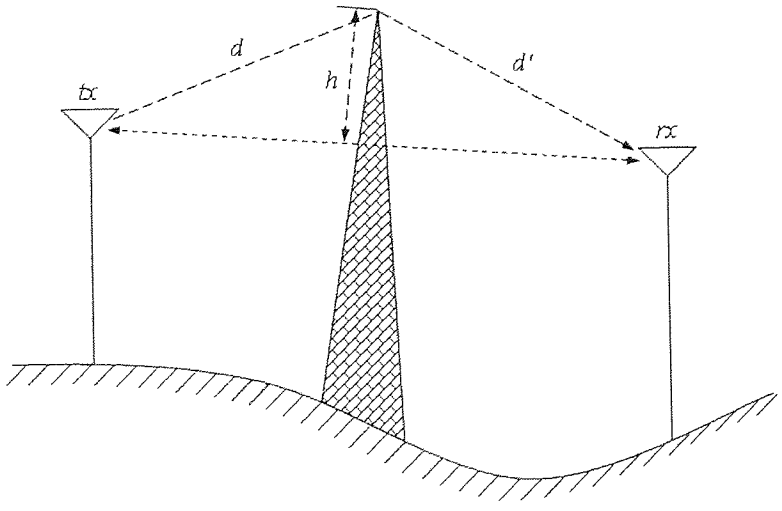

Figure 2-3 The geometry of the knife-edge model. The receiver, r_x, is in the shadow region.

2.2.3 Diffraction

Diffraction is the bending or spreading of waves that encounter an object (a barrier or an opening) in their path. The phenomenon occurs for all the types of waves, such as radio waves, sound waves, water waves and so on. Here is a common example of diffraction. One can hear a sound even when he/she is not in a direct line to the sound source. For diffraction to occur, the size of the object must be of the order of the wavelength of the incident waves. When the wavelength is much smaller than the size of the object diffraction is usually not observed and the object casts a sharp shadow [23].

For radio wave propagation, diffraction is commonly modelled by the *Fresnel knife-edge diffraction model* because of its simplicity. In this model, the diffracting object is assumed to be asymptotically thin and the object's parameters, such as polarization, conductivity and surface roughness, are ignored. Figure 2-3 shows a typical geometry of the model. For $h << d, d'$, the length difference of a travelling signal wave between the diffracted and LOS paths is [18]

$$d_{\Delta} = \frac{h^2(d+d')}{2dd'}. \tag{2.11}$$

Thus the corresponding phase difference of the received signals is found as

$$\theta_{\Delta} = \frac{2\pi d_{\Delta}}{\lambda} \approx \frac{\pi}{2} v^2, \tag{2.12}$$

where v is the dimensionless *Fresnel-Kirchoff diffraction* parameter, given as

$$v = h\sqrt{\frac{2(d+d')}{\lambda dd'}}. \tag{2.13}$$

where h can be negative. It is rather complex to compute the knife-edge diffraction path loss. Lee [21] has given approximations for the diffraction path loss as follows in dB,

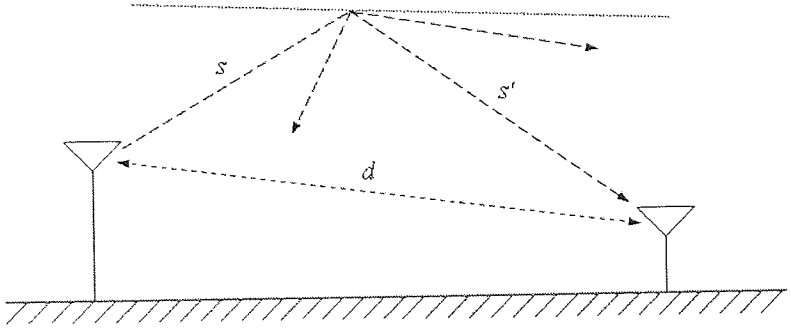

Figure 2-4 Scattering.

$$L_{k-e}(v)(\mathrm{dB}) = \begin{cases} 0 & v \le -1, \\ 20\log_{10}(0.5 - 0.62v) & -1 \le v \le 0, \\ 20\log_{10}(0.5e^{-0.95v}) & 0 \le v \le 1, \\ 20\log_{10}\left(0.4 - \sqrt{0.1184 - (0.38 - 0.1v)^2}\right) & 1 \le v \le 2.4, \\ 20\log_{10}\left(\dfrac{0.225}{v}\right) & v > 2.4. \end{cases} \tag{2.14}$$

2.2.4 Scattering

In fact, reflection includes *diffuse* reflection and *specular* reflection. The reflection theory discussed in Subsection 2.2.2 is for specular reflection. Diffuse reflection is caused by scattering, where the energy of a radio wave will spread out when it impinges on a rough surface. Objects such as lamps posts and trees can scatter energy in all direction and thus the receiver can receive radio energy from different directions. In wireless environments, scattering is usually caused by large objects. Figure 2-4 illustrates the geometry of signal scattering, where the spot of scattering taking place depends on the direction of the incoming signal. The scattered received signal can be given by the bi-static radar equation [18, 24],

$$r(t) = \mathrm{Re}\left\{ x(t-\tau) \frac{\lambda\sqrt{G_s \sigma}\, e^{-j2\pi(s+s')/\lambda}}{(4\pi)^{3/2} ss'} e^{j2\pi f_c t} \right\}, \tag{2.15}$$

where $\tau = (s+s'-d)/c$ is the delay of the scattered signal relative to the LOS path; σ in m^2 is the area of the radar cross-section of the scattering object, depending on the

roughness, size and shape of the object; and G_s represents the product of antenna gains. Apart from scattering, (2.15) assumes that signal waves only experience free space loss. Then, the scattering path loss in dB is found as

$$\begin{aligned} L_s(\text{dB}) &= P_t(\text{dBm}) - P_r(\text{dBm}) \\ &= 30\log_{10}(4\pi) + 20\log_{10}(s) + 20\log_{10}(s') - 10\log_{10}(G_s) - 20\log_{10}(\lambda) - 10\log_{10}(\sigma) \end{aligned} \tag{2.16}$$

Seidel, *ed al.* [25] have given the empirical values of $10\log_{10}(\sigma)$ for different buildings in four European cities.

2.2.5 Simplified path loss model

In the practical system design, the following simplified path loss model is commonly used [18],

$$P_r = P_t K \left[\frac{d_0}{d}\right]^{\gamma}, \tag{2.17}$$

where K is a unitless constant that depends on the antenna characteristics; d_0 is a reference distance; d is the distance between the transmitter and the receiver; and γ is the path loss exponent. The values for K and γ can be approximated through measurements and analytical models [18, 19, 26].

2.2.6 Shadowing

In wireless propagation channels, signals can be not only reflected, diffracted and scattered, but also blocked by the objects in the signal path. The attenuation of signal strength due to signal blocking is most commonly modelled by the log-normal shadowing [18], a stochastic model given as follows [27],

$$p(\gamma) = \frac{\kappa}{\sqrt{2\pi}\sigma_{\gamma\text{dB}}\gamma} \exp\left[-\frac{\left(10\log_{10}\gamma - \mu_{\gamma\text{dB}}\right)^2}{2\sigma^2_{\gamma\text{dB}}}\right], \quad \gamma > 0, \tag{2.18}$$

where $\gamma = P_t/P_r$, $\kappa = 10/\ln 10$, $\mu_{\gamma dB}$ (dB) $= E[\gamma_{dB} = 10\log_{10}\gamma]$, and $\sigma_{\gamma dB}$ is the standard deviation of γ_{dB}, where $E[x]$ calculates the expectation value of random variable x. The mean, $\mu_{\gamma dB}$, can be obtained through analytical models and empirical measurements.

2.3 Multipath fading

When the received signal strength is concerned for a short transmitter-receiver distance (on the order of tens to hundreds of meters) or time duration (on the order of seconds), the models discussed above are no longer available for characterising the wireless channels. This is because in this scenario the received signal strength can fluctuate rapidly for merely over one meter or one second. This phenomenon arises due to the multiple paths that radio signals propagate on and any object movement on these paths. Herein, fading is concerned in three domains: time, frequency and space. Figure 2-5 illustrates the received signal power over the distance between the transmitter and the receiver, in a multipath fading channel.

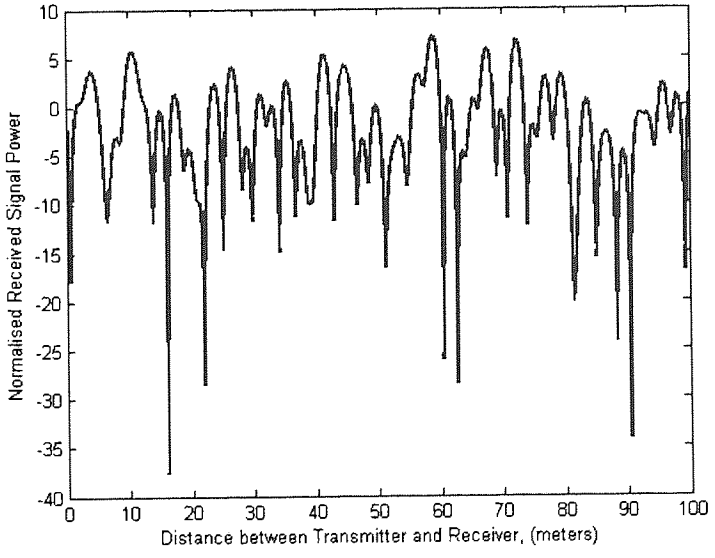

Figure 2-5 Received signal power in a multipath fading channel.

2.3.1 Fast and slow fading

When any object, including the transmitter and the receiver themselves, is moving on a signal path, the radio signals on that path tend to spread their bandwidth with a small amount, $f_{d\max}$, to a finite bandwidth ($f_c \pm f_{d\max}$). This small amount is the maximum value of Doppler shift on that signal path. "Maximum" is used because there can be more than one object moving on the path. Doppler shift is defined as [28]

$$f_d = f_c \frac{v}{c} \cos\theta, \tag{2.19}$$

where c is the velocity of carrier, v is the velocity of the moving object, and θ is the angle between the moving object and the point of reception of the frequency-shifted signal. If the receiver is moving and others remain static, then θ represents the angle between the moving direction of the receiver and the transmitter or the scatterer. When the receiver is moving towards the transmitter, the received signal frequency is greater than the transmitted signal frequency, f_c, and vice versa.

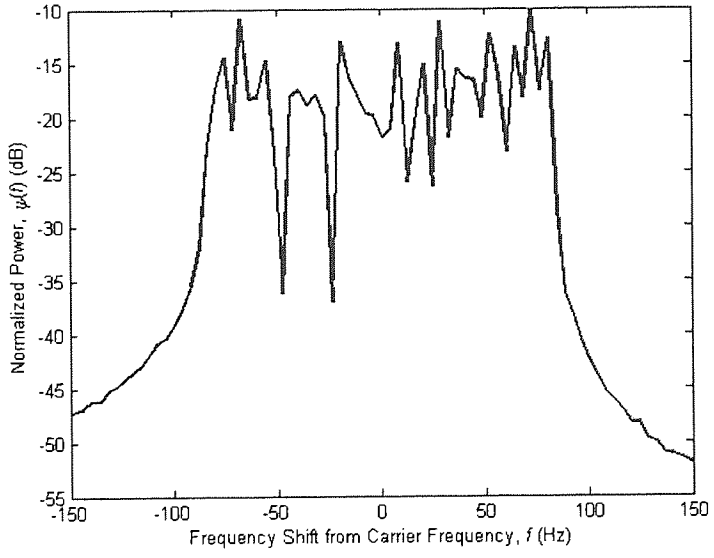

Figure 2-6 Doppler power spectrum with 100 Hz Doppler shift.

By performing Fourier transform of the autocorrelation[1] of the channel response in the time domain to that in the frequency domain, the Doppler power spectrum $\psi(f)$ with $f_c - f_{dmax} \leq f_c \leq f_c + f_{dmax}$ can be found. Figure 2-6 shows a Doppler power spectrum with 100 Hz Doppler shift. The Doppler spread can be derived from the Doppler power spectrum, where the former is the root mean square (RMS) bandwidth of the latter. The Doppler spread is given by [28]

$$f_{RMS} = \sqrt{\frac{\int (f - \overline{f})^2 \psi(f) df}{\int \psi(f) df}}, \tag{2.20}$$

where $\overline{f}$ is the average frequency of the Doppler power spectrum and is defined as [28]

$$\overline{f} = \frac{\int f \psi(f) df}{\int \psi(f) df}. \tag{2.21}$$

The RMS bandwidth, f_{RMS}, is critical to defining the coherence time of the channel, which is the time lag at which the signal autocorrelation coefficient reduces from 1 (full autocorrelation) to 0.7. The coherence time, T_c, is evaluated by [28]

$$T_c \approx \frac{1}{f_{RMS}}. \tag{2.22}$$

If the duration of the baseband signal symbol is longer than the coherence time, then the autocorrelation of two consecutive symbols will be lower than 0.7. In this case, the symbols are regarded as propagating in a fast fading channel and equalization is required at the receiver. Otherwise, it is slow fading channel.

---

[1] Autocorrelation can be defined as the correlation of the values of a function observed at different points. For instance, the autocorrelation of a radio signal in the frequency domain is defined as

$$\Theta(\varphi) = \frac{E[(r(f) - \mu_r)(r(f + \varphi) - \mu_r)]}{\sigma_r^2},$$

where φ is the frequency difference, E is the expectation operator, μ is the mean, and σ is the standard deviation.

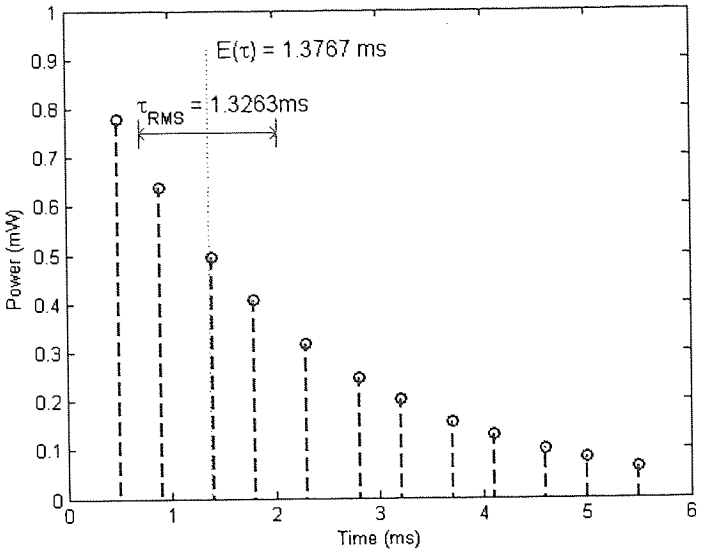

Figure 2-7 A plot of power delay profile.

2.3.2 Frequency selective and flat fading

When an impulse is transmitted in an object-scattered channel, the receiver can receive multiple taps of the impulse over a short period of time, where the first tap often presents the LOS path and usually has the strongest signal strength. These multiple arrivals form the *power delay profile* of this wireless channel due to an impulse sent. An example is shown in Figure 2-7. An important parameter that can be extracted from the power delay profile is the RMS delay spread, which can be used to measure how dispersive the channel is in the time domain. It is defined as [28]

$$\tau_{RMS} = \sqrt{\mathrm{E}\left(\tau^2\right) - \left(\mathrm{E}(\tau)\right)^2}, \tag{2.23}$$

where

$$\mathrm{E}(\tau) = \frac{\sum_l P_l \tau_l}{\sum_l P_l} \tag{2.24}$$

and

$$\mathrm{E}\left(\tau^2\right) = \frac{\sum_l P_l \tau_l^2}{\sum_l P_l} \tag{2.25}$$

are the first and the second moment of the instantaneous power delay profile. Eq. (2.24) is also known as the *mean excess delay*. P_l is the detected power of the lth tap. τ_l is the delay of the lth tap related to the first tap.

The selectivity of frequency dependent fading can be characterised in terms of coherence bandwidth, B_c, which is the frequency lag at which the channel's autocorrelation function reduces to 0.7. The coherence bandwidth is defined as [28]

$$B_c \approx \frac{1}{\tau_{RMS}}. \tag{2.26}$$

When the coherence bandwidth is comparable to or narrower than the signal bandwidth, the channel is said to be frequency selective fading and the signals are regarded as wideband signals. Otherwise, the channel is frequency flat or non-selective fading and the signals are narrowband signals.

In frequency selective fading channels, a wideband signal experiences different fading conditions at different frequencies, which is quite difficult for the receiver to cope with. On the contrary, in flat fading channels, a narrowband signal fades almost the same across its frequency spectrum. Because flat fading is better for signal reception and recovery, a powerful technology – orthogonal frequency division multiplexing (OFDM) – was invented to deal with the wideband signals. OFDM divides a wideband signal into a series of parallel and frequency-orthogonal narrowband signals.

2.3.3 Space selective and non-selective fading

Space selective fading is more concerned in the multiple antenna systems which will be discussed with more details later. It is caused by the angular spread referred as to the angle of arrival (AOA) at the receiver and the angle of departure (AOD) at the transmitter. The definition of angular spread resembles that of delay spread, which is given by [28]

$$\theta_{RMS} = \sqrt{\mathrm{E}\left(\theta^2\right) - \left(\mathrm{E}(\theta)\right)^2}, \tag{2.27}$$

where

$$\mathrm{E}(\theta)=\frac{\sum_l P_l\theta_l}{\sum_l P_l} \tag{2.28}$$

and

$$\mathrm{E}(\theta^2)=\frac{\sum_l P_l\theta_l^2}{\sum_l P_l}, \tag{2.29}$$

θ_l is the angle of the lth tap relative to the angle of the first detected signal received by the receiver.

The RMS angle spread is used to determine the coherence distance between antennas. The autocorrelation coefficient of the spatial fading decreases to be below 0.7, when the spacing between any two antennas is longer than the coherence distance. The coherence distance, D_c, is given by [28]

$$D_c \propto \frac{1}{\theta_{RMS}}. \tag{2.30}$$

Note that in (2.30), the operator is $\propto$ (proportional to) rather than $\approx$ (approximately equal to). The value of D_c varies from typically 10 to 16 wavelengths at a BS and from 3 to 5 wavelengths at the mobile user (MU).

2.4 Fading distributions

Channel fading can be statistically presented using probability distributions. The following three *probability density functions* (PDF) are commonly used to describe fading phenomenon in wireless channels.

2.4.1 Rayleigh distribution

When the channel between the transmitter and the receiver is non-LOS (NLOS), the magnitude of channel gain in a flat fading channel usually exhibits the *Rayleigh distribution*. If the channel is considered to be frequency selective, the Rayleigh

distribution describes the magnitude of channel gain of each individual multipath tap of the received signal. The magnitude of channel gain is mathematically denoted as $|\alpha|$ ~ Rayleigh(σ), where $|\alpha|$ is the magnitude of channel gain. The phase, θ, of channel gain is usually modelled to be *uniformly* distributed, i.e., $\theta \sim$ uniform[0, 2π). With the magnitude and the phase at hand, the complex channel gain can be presented as $\alpha = |\alpha|e^{j\theta}$ or $\alpha = \alpha_r + j\alpha_i = |\alpha|cos\theta + j|\alpha|sin\theta$, where α_r and α_i are *independent and identically distributed* (i.i.d.) Gaussian random variables with the mean zero and the variance σ^2. In fact, such α is a *circularly symmetric* Gaussian variable, denoted as $\alpha \sim CN(0, 2\sigma^2)$. The squared Rayleigh-distributed random variables follow the *chi-square distribution* with two degrees of freedom [29], i.e.,

$$p(y) = \frac{1}{2\sigma^2}\exp\left(-y/2\sigma^2\right), \quad y \geq 0, \tag{2.31}$$

where $y = |a|^2 = \alpha_r^2 + \alpha_i^2$. The PDF of the Rayleigh distribution can be found through finding the integral of (2.31) (a.k.a. the *cumulative distribution function* [CDF]) and making necessary variable substitutions as,

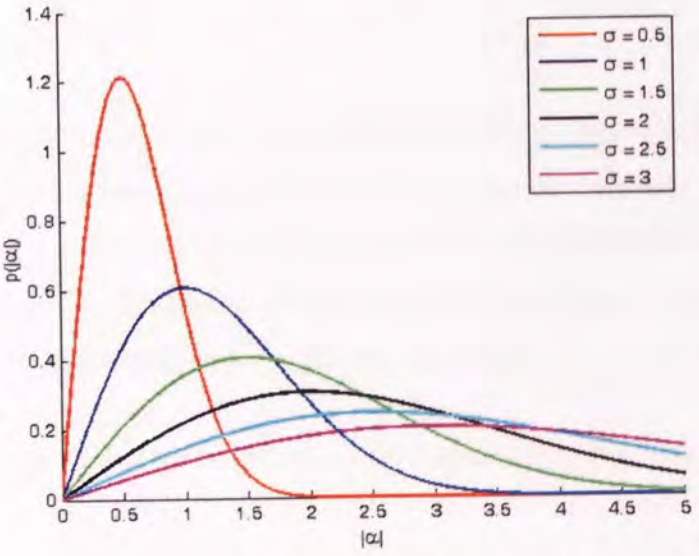

Figure 2-8 The PDF of the Rayleigh distribution.

since $$\int p(|\alpha|)d|\alpha| = \int p(y)dy \overset{y=|\alpha|^2}{=} \int p\left(|\alpha|^2\right)2|\alpha|d|\alpha|,$$

$$p(|\alpha|) = \frac{|\alpha|}{\sigma^2}\exp\left(-|\alpha|^2/2\sigma^2\right), \quad |\alpha| \geq 0. \tag{2.32}$$

The PDF of the Rayleigh distribution is drawn in Figure 2-8, with respect to different values of σ. If $2\sigma^2$ in (2.31) is substituted by $1/\lambda$, the signal power variation can be found to obey the *exponential distribution* as

$$p(y) = \lambda e^{-\lambda y}, \quad \lambda > 0, y \geq 0. \tag{2.33}$$

2.4.2 Rice distribution

When there is a strong LOS channel between the transmitter and the receiver, the channel gain can be described using the *Rice distribution* that is a generalization of the Rayleigh distribution. Note that a LOS channel is deterministic. The NLOS channel is still Rayleigh distributed. The PDF of the Rice distribution is [29]

$$p(|\alpha|) = \frac{|\alpha|}{\sigma^2}\exp\left[-\left(|\alpha|^2 + s^2\right)/2\sigma^2\right]I_0\left(\frac{|\alpha|s}{\sigma^2}\right), \quad |\alpha| \geq 0, \tag{2.34}$$

where $s^2 = (\mathrm{E}[\alpha_r])^2+(\mathrm{E}[\alpha_i])^2$ in which $\mathrm{E}[a]$ calculates the expected value of a, α_r and α_i are still i.i.d. Gaussian random variables with a common variance σ^2 and non-zero means, and $I_0(\bullet)$ is the modified *Bessel function*[1] of the first kind with the zeroth order. Similar to the Rayleigh distributed magnitudes of channel gain, the Rice distributed magnitudes can be expressed as $|\alpha| \sim \mathrm{Rice}(s, \sigma)$. When $s = 0$, the Rice distribution

[1] The first kind of Bessel function can be defined in several presentations. Here is one of them, which was used by Bessel,

$$J_n(x) = \frac{1}{\pi}\int_0^{\pi}\cos(n\tau - x\sin\tau)d\tau,$$

where n is the order. The modified Bessel function is used for complex variable x, which is defined as

$$I_n(x) = i^{-n}J_n(ix).$$

reduces to the Rayleigh distribution. The PDF of the Rice distribution is drawn in Figure 2-9 for varying σ and Figure 2-10 for varying s, respectively.

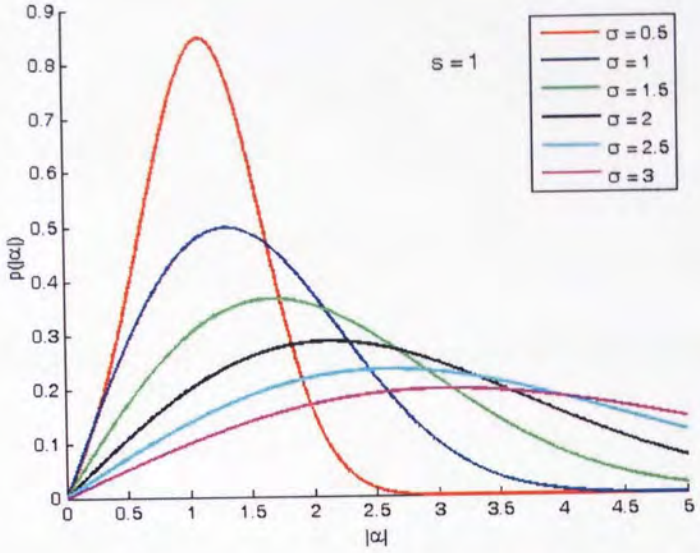

Figure 2-9 The PDF of the Rice distribution with varying σ.

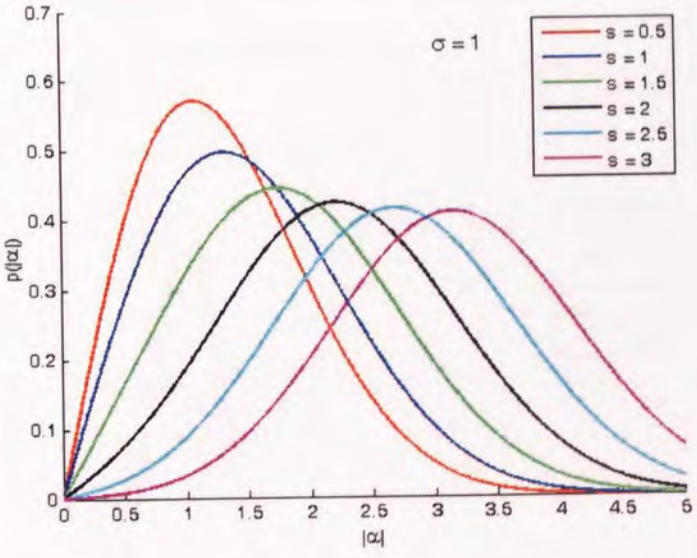

Figure 2-10 The PDF of the Rice distribution with varying s.

Define K as the Rice factor, the ratio of the power of the LOS channel component to the mean power of the NLOS channel component. When K increases, the LOS channel component dominates the channel gain and the entire channel tends to be deterministic.

Note that s^2 equals the power of the received signals on the LOS channel and $2\sigma^2$ is the mean power of the received signals on the NLOS channel. Then, the Rice factor can be found as $K = s^2/2\sigma^2$. For the Rayleigh distribution, $K = 0$. It is observed that the mean received power $E[|\alpha|^2] = \Omega_p = s^2+2\sigma^2$. Therefore, with the following expressions,

$$s^2 = \frac{K\Omega_p}{K+1} \tag{2.35}$$

and

$$2\sigma^2 = \frac{\Omega_p}{K+1}, \tag{2.36}$$

the PDF of the Rice distribution in terms of the mean received power can be found as [30]

$$p(|\alpha|) = \frac{2(K+1)|\alpha|}{\Omega_p}\exp\left[-K-\frac{(K+1)|\alpha|^2}{\Omega_p}\right]I_0\left(2|\alpha|\sqrt{\frac{K(K+1)}{\Omega_p}}\right), \quad |\alpha| \geq 0, \tag{2.37}$$

and is shown in Figure 2-11 with varying K. The estimation of K is discussed in [31], which is rather useful for real data analysis.

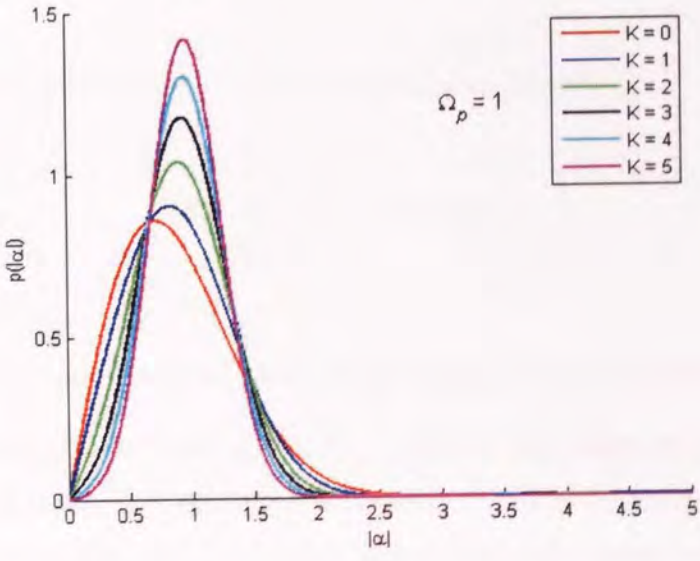

Figure 2-11 The PDF of the Rice distribution with varying *K*.

Considering the power components on the LOS and the NLOS channels in (2.35) and (2.36), the normalised channel gain of a Rice-faded channel can be modelled as the combination of the channel gains of the LOS and the NLOS channel components, i.e.,

$$\alpha = \sqrt{\frac{K}{K+1}}\alpha_{LOS} + \sqrt{\frac{1}{K+1}}\alpha_{NLOS}. \tag{2.38}$$

2.4.3 Nakagami-*m* distribution

Another probability distribution that is frequently used to describe fading is the Nakagami-*m* distribution, which was developed with adjustable parameters to match empirical data better than other models. Thus, it is considered as a more general distribution and can describe severe fading better than either Rayleigh or Rice distribution. Nakagami gave the PDF of the distribution in 1960 as [29]

$$p(|\alpha|) = \frac{2}{\Gamma(m)}\left(\frac{m}{\omega}\right)^m |\alpha|^{2m-1} \exp\left(-m|\alpha|^2/\omega\right), \tag{2.39}$$

where ω is defined as

$$\omega = \mathrm{E}\left[|\alpha|^2\right],$$

m is defined as the ratio of moments, termed the *fading figure*,

$$m = \frac{\omega^2}{\mathrm{E}\left[\left(|\alpha|^2 - \omega\right)^2\right]}, \quad m \geq \frac{1}{2},$$

and $\Gamma(\bullet)$ is the Gamma function, defined as $\Gamma(m) = \int_0^\infty t^{m-1}e^{-t}dt$. When $m = 1$, (2.39) reduces to a Rayleigh PDF. For $m = (K+1)^2/(2K+1)$, the Nakagami-*m* distribution is approximately the Rice distribution with parameter K. The PDF of the Nakagami-*m* distribution is illustrated in Figure 2-12 and Figure 2-13 with varying m and ω, respectively.

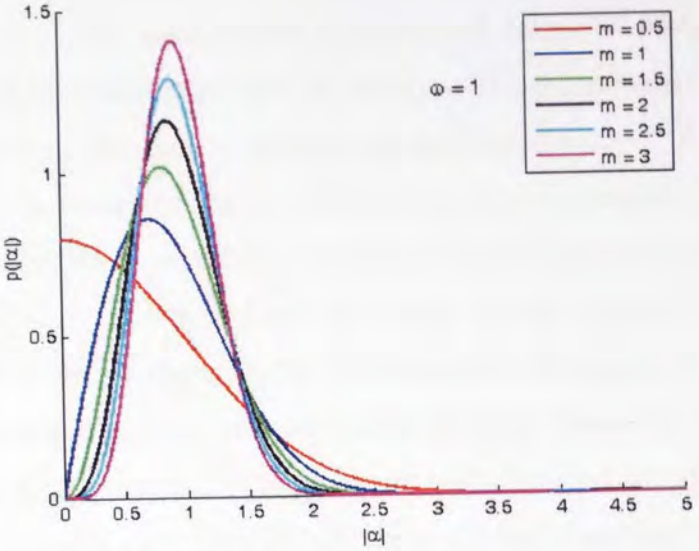

Figure 2-12 The PDF of the Nakagami-*m* distribution with varying *m*.

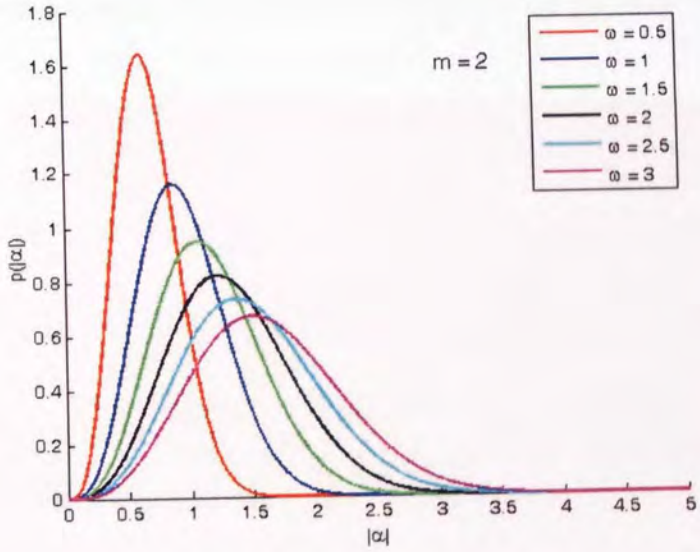

Figure 2-13 The PDF of the Nakagami-*m* distribution with varying *ω*.

2.5 Summary

Understanding how signals propagate in wireless channels is essential for modelling complex wireless systems, such as MIMO and CC systems. In this chapter, large-scale path loss models and small-scale fading models for signal propagation in wireless

channels are discussed, respectively. When the distance between the transmitter and the receiver is in the range from several hundreds to a couple of thousands meters, the large-scale path loss models are used to estimate the mean received power at the receiver. The small-scale fading models characterise the rapid fluctuation of the received power over short transmitter-receiver distance (on the order of tens of meters up to a couple of hundreds of meters), over short period of time or at different close locations. The fading selectivity in time, frequency or space domain is not only related to the wireless propagation channels, but also dependent on signal (time and frequency domain) properties and antenna spacing (space domain). Since the received power is observed as "rapidly fluctuating", the probability distributions are used to present this kind of models. Usually, one wireless environment is best described by one particular model. In modern mobile networks, such as the Global System for Mobile Communications (GSM), more than one channel model are applied, letting BS and MU choose the most suitable channel model and achieving the best quality of service (QOS).

3 MIMO Systems

A key feature of MIMO systems is the ability to exploit multipath propagation that has long been considered as a pitfall in wireless SISO communications. MIMO effectively takes advantage of random fading and, when available, multipath delay spread for multiplying transmission rates. The prospect of capacity improvement by deploying MIMO technology has stimulated many new research areas ranging from fundamental information theory, modelling and simulations, to prototyping and system trials.

In this thesis, modelling the physical channels of the outdoor MIMO systems is one of the major concerns. Channel modelling is essential to understand the behaviour and performances of MIMO systems in different propagation environments and under various configurations of the systems. A number of MIMO models and measurements have been reported for both indoor channels [32-35] and outdoor channels [7, 9, 36-42]. When a MIMO outdoor channel is modelled, some critical parameters, such as antenna pattern, path loss, alignment of antenna array, scatterer properties and fading distributions, have significant impact on the system performance.

This chapter is focused on re-constructing some of classic wireless MIMO channel models, which demonstrate the modelling techniques for MIMO systems and will be extended in Chapter 5 for a more realistic propagation environment. Also in this chapter, some critical performance parameters, such as channel capacity and diversity-multiplexing trade-off, are discussed in details. A MIMO channel model can be represented by a channel matrix $\mathbf{H}$ that is constructed by the channel gains between the antenna-pairs[1].

3.1 Channel modelling

The methods for modelling multiple-antenna channels are no difference to those for single-antenna channels, i.e., ray-tracing modelling and stochastic modelling. The gains of multiple-antenna channels are in the form of a matrix or a vector in multiple-antenna channels instead of a singular value as in single-antenna channels.

[1] One transmit antenna and one receive antenna form an antenna pair.

One advantage of the ray-tracing method is that it is able to present a wireless channel explicitly. Furthermore, the ray-tracing models can include the transmission factors, such as antenna pattern and free space loss, for inspecting a wireless channel. The ray-tracing method is particularly popular for modelling outdoor channels where the signal paths are more distinctive than indoor channels. There are, however, some disadvantages in the ray-tracing method, one of which is that it cannot reflect the changing channel conditions in real systems. Fortunately, this drawback can be overcome by applying Monte Carlo simulation methods, where the values of certain parameters can be randomly chosen without changing original conditions. For example, in [7], the positions of scatterers are randomly chosen but they still comply with the uniform distribution.

The stochastic models view the channels in a more abstract way. The elements in each model obey certain probability distributions. For multiple-antenna channels, each model can be the result of the multiplication of several sub-matrices or sub-vectors, such as correlation matrices, fading channel matrices and/or steering vectors. Stochastic models are easier for mathematical manipulation.

3.2 Multipath fading correlation

When two multipath channels are close to each other, these two channels may interfere with each other. The correlation is the measure of how much one channel is affected by the other. The multipath fading correlation can be described in two related ways: channel correlation and antenna correlation. If $\mathbf{H}_{m,n}$ is used to represent the channel gain of the channel of one antenna-pair (from the nth transmit antenna to the mth receive antenna) and so is $\mathbf{H}_{m',n'}$ (from the n'th transmit antenna to the m'th receive antenna), then the fading correlation coefficient Φ between different channels can be found as [18]

$$\Phi\left(\mathbf{H}_{m,n},\mathbf{H}_{m',n'}\right)=\frac{\mathrm{E}\left[\mathbf{H}_{m,n}\mathbf{H}^{*}_{m',n'}\right]-\mathrm{E}\left[\mathbf{H}_{m,n}\right]\mathrm{E}\left[\mathbf{H}_{m',n'}\right]}{\sqrt{\left(\mathrm{E}\left(\left|\mathbf{H}_{m,n}\right|^{2}\right)-\mathrm{E}\left(\left|\mathbf{H}_{m,n}\right|\right)^{2}\right)\left(\mathrm{E}\left(\left|\mathbf{H}_{m',n'}\right|^{2}\right)-\mathrm{E}\left(\left|\mathbf{H}_{m',n'}\right|\right)^{2}\right)}}. \tag{3.1}$$

For a 2×2 MIMO channel matrix $\mathbf{H}$,

$$\mathbf{H} = \begin{bmatrix} \mathbf{H}_{1,1} & \mathbf{H}_{1,2} \\ \mathbf{H}_{2,1} & \mathbf{H}_{2,2} \end{bmatrix},$$

which includes four channels (channel 1 to 4: (1, 1), (1, 2), (2, 1) and (2, 2)), the channel correlation matrix $\mathbf{\Phi}$ can be found as

$$\mathbf{\Phi} = \begin{bmatrix} \Phi(\mathbf{H}_{1,1}, \mathbf{H}_{1,1}) & \Phi(\mathbf{H}_{1,1}, \mathbf{H}_{1,2}) & \Phi(\mathbf{H}_{1,1}, \mathbf{H}_{2,1}) & \Phi(\mathbf{H}_{1,1}, \mathbf{H}_{2,2}) \\ \Phi(\mathbf{H}_{1,2}, \mathbf{H}_{1,1}) & \Phi(\mathbf{H}_{1,2}, \mathbf{H}_{1,2}) & \Phi(\mathbf{H}_{1,2}, \mathbf{H}_{2,1}) & \Phi(\mathbf{H}_{1,2}, \mathbf{H}_{2,2}) \\ \Phi(\mathbf{H}_{2,1}, \mathbf{H}_{1,1}) & \Phi(\mathbf{H}_{2,1}, \mathbf{H}_{1,2}) & \Phi(\mathbf{H}_{2,1}, \mathbf{H}_{2,1}) & \Phi(\mathbf{H}_{2,1}, \mathbf{H}_{2,2}) \\ \Phi(\mathbf{H}_{2,2}, \mathbf{H}_{1,1}) & \Phi(\mathbf{H}_{2,2}, \mathbf{H}_{1,2}) & \Phi(\mathbf{H}_{2,2}, \mathbf{H}_{2,1}) & \Phi(\mathbf{H}_{2,2}, \mathbf{H}_{2,2}) \end{bmatrix}. \tag{3.2}$$

Using $\Phi = \beta e^{j\theta}$, (3.2) can be presented as

$$\mathbf{\Phi} = \begin{bmatrix} 1 & \beta_{1,2}e^{j\theta_{1,2}} & \beta_{1,3}e^{j\theta_{1,3}} & \beta_{1,4}e^{j\theta_{1,4}} \\ \beta_{2,1}e^{j\theta_{2,1}} & 1 & \beta_{2,3}e^{j\theta_{2,3}} & \beta_{2,4}e^{j\theta_{2,4}} \\ \beta_{3,1}e^{j\theta_{3,1}} & \beta_{3,2}e^{j\theta_{3,2}} & 1 & \beta_{3,4}e^{j\theta_{3,4}} \\ \beta_{4,1}e^{j\theta_{4,1}} & \beta_{4,2}e^{j\theta_{4,2}} & \beta_{4,3}e^{j\theta_{4,3}} & 1 \end{bmatrix}, \tag{3.3}$$

where $\beta_{a,b}$ is the magnitude of correlation coefficient between channels a and b (a = 1, …, 4; b = 1, …, 4), θ is the corresponding phase of correlation coefficient, and self-correlation is equal to 1. According to (3.1), $\mathbf{\Phi}$ is a Hermitian matrix (self-adjoint matrix) so that (3.3) can be simplified to

$$\mathbf{\Phi} = \begin{bmatrix} 1 & \beta_{1,2}e^{j\theta_{1,2}} & \beta_{1,3}e^{j\theta_{1,3}} & \beta_{1,4}e^{j\theta_{1,4}} \\ \beta_{1,2}e^{-j\theta_{1,2}} & 1 & \beta_{2,3}e^{j\theta_{2,3}} & \beta_{2,4}e^{j\theta_{2,4}} \\ \beta_{1,3}e^{-j\theta_{1,3}} & \beta_{2,3}e^{-j\theta_{2,3}} & 1 & \beta_{3,4}e^{j\theta_{3,4}} \\ \beta_{1,4}e^{-j\theta_{1,4}} & \beta_{2,4}e^{-j\theta_{2,4}} & \beta_{3,4}e^{-j\theta_{3,4}} & 1 \end{bmatrix}. \tag{3.4}$$

To calculate the correlation coefficient between the transmit antennas or the receive antennas, simply replace n' with n or m' with m in (3.1). The correlation coefficient Φ has the following relationship with covariance Ψ that

$$\Phi(\mathbf{H}_{m,n}, \mathbf{H}_{m',n'}) = \frac{\Psi(\mathbf{H}_{m,n}, \mathbf{H}_{m',n'})}{\sigma(\mathbf{H}_{m,n})\sigma(\mathbf{H}_{m',n'})}, \tag{3.5}$$

where σ is the standard deviation. If $\mathbf{H}$ is the matrix of a NLOS channel, then [7, 43]

$$\mathrm{vec}(\mathbf{H}) \cong \mathbf{\Phi}^{1/2}\mathrm{vec}(\mathbf{H}_{\text{i.i.d.}}), \tag{3.6}$$

where $\mathbf{\Phi} = \mathbf{\Phi}^{1/2}(\mathbf{\Phi}^{1/2})^*$, vec is the matrix vectorization operator[1], $\cong$ denotes *statistically equal*, and $\mathbf{H}_{\text{i.i.d.}}$ is i.i.d. $CN(0, \sigma^2)$. Sometimes, the channel correlation coefficient is estimated as the *Kronecker product*[2] of the correlation coefficients between the transmit antennas and between the receive antennas, i.e., $\mathbf{\Phi} \approx \mathbf{\Phi}^R \otimes \mathbf{\Phi}^T$, where $\mathbf{\Phi}^R$ and $\mathbf{\Phi}^T$ are the correlation matrices for the transmit antenna array and the receive antenna array, respectively. For manipulation convenience, it is therefore preferred to use the statistical equivalent of correlated $\mathbf{H}$,

$$\mathbf{H} \cong \left(\mathbf{\Phi}^R\right)^{1/2} \mathbf{H}_{\text{i.i.d.}} \left(\mathbf{\Phi}^T\right)^{1/2}. \tag{3.7}$$

3.3 Channel capacity formulation

In this section, the capacity of various wireless channels is presented. Channel capacity measures the maximal amount of error-free information that a channel, no matter wireless or wired, can deliver per unit time. When the channel capacity is below the targeted transmission rate set by the transmitter, an outage will occur and the receiver no longer receives error-free information. The outage probability is used to measure the outage percentage in a wireless channel, given a targeted transmission rate. Usually,

---

[1] Let $\mathbf{A} = [\mathbf{A}_1\ \mathbf{A}_2\ \ldots\ \mathbf{A}_N]$. Thus it can be vectorized to

$$\mathrm{vec}(\mathbf{A}) = \left[\mathbf{A}_1^T\ \ \mathbf{A}_2^T\ \ \cdots\ \ \mathbf{A}_N^T\right]^T,$$

where ^{T} stands for transpose.

[2] The Kronecker product of two matrices, $\mathbf{A}$ and $\mathbf{B}$, is calculated as

$$\mathbf{A} \otimes \mathbf{B} = \begin{bmatrix} \mathbf{A}_{1,1}\mathbf{B} & \mathbf{A}_{1,2}\mathbf{B} & \cdots \\ \mathbf{A}_{2,1}\mathbf{B} & \mathbf{A}_{2,2}\mathbf{B} & \cdots \\ \cdots & \cdots & \cdots \end{bmatrix}.$$

wireless channels are considered as discrete memoryless, i.e., "the probability distribution of the output depends only on the input at that time and is conditionally independent of previous channel inputs or outputs" [44]. Then, the capacity of such channel is defined as the maximum of *mutual information* [44]

$$C = \max_{p(x)} I(X;Y), \tag{3.8}$$

where I is the mutual information that the receiver can extract from the received codeword Y given codeword X is transmitted, and the maximum is taken over all possible input distribution $p(x)$. The mutual information $I(X;Y)$ in discrete time is defined as the relative *entropy* [44]

$$\begin{aligned} I(X;Y) &= \sum_{x\in X}\sum_{y\in Y} p(x,y)\log_2 \frac{p(x,y)}{p(x)p(y)} \\ &= \mathrm{E}_{p(x,y)} \log_2 \frac{p(X,Y)}{p(X)p(Y)}, \end{aligned} \tag{3.9}$$

where E stands for expectation; $p(x, y)$ is the joint probability of $X = x$ and $Y = y$. The mutual information can also be expressed by the subtraction of the entropy of the received codeword with the conditional entropy of the received codeword on the transmitted codeword as

$$I(X;Y) = H(Y) - H(Y|X), \tag{3.10}$$

where $H(Y) = -\Sigma_y p(y)\log_2 p(y)$ and $H(Y|X) = -\Sigma_{x,y} p(x, y)\log_2 p(y|x)$ are the entropy and conditional entropy, respectively, and $p(y|x)$ is the conditional probability of $Y = y$ on $X = x$.

Power constraint is commonly used as a limitation on the input codeword X. The total transmit power for all input codeword $(x_1, x_2, \ldots, x_n)$ cannot exceed the total transmitter power P, i.e.,

$$\frac{1}{n}\sum_{i=1}^{n} x_i^2 \le P \tag{3.11}$$

for single-antenna channels; for multiple-antenna channels, the power constraint is

$$\frac{1}{c}\sum_{i=1}^{c}\|\mathrm{X}(i)\|_F^2 \le P, \tag{3.12}$$

where c represents the codebooks used and $\|\bullet\|_F$ is the Frobenius norm of a matrix,

$$\|\mathrm{X}\|_F^2 = \mathrm{trace}\left(\mathrm{X}\mathrm{X}^*\right),$$

where * indicates matrix transpose conjugation manipulation or Hermitian transpose.

The mutual information $I(X;Y)$ in continuous time is defined as [44]

$$\begin{aligned} I(X;Y) &= \int f(x,y)\log_2\frac{f(x,y)}{f(x)f(y)}dxdy \\ &= h(Y) - h(Y|X) \ge 0, \end{aligned} \tag{3.13}$$

where $h(Y) = -\int_S f(y)\log_2 f(y)dy$ is the differential entropy of a continuous random variable Y with density $f(y)$ and S is the support set of the random variable; $h(Y|X) = -\int f(x,y)\log_2 f(y|x)dxdy$ is the conditional differential entropy.

3.3.1 AWGN channel

The received codeword, Y, in an additive white Gaussian noise (AWGN) channel can be modelled as

$$Y = X + Z, \tag{3.14}$$

where Z is the Gaussian noise $\sim N(0, \sigma^2)$. Thus, the mutual information $I(X;Y)$ of a discrete-time channel is bounded by [44]

$$\begin{aligned} I(X;Y) &= H(Y) - H(Y|X) \\ &= H(Y) - H(X+Z|X) \\ &= H(Y) - H(Z|X) \\ &= H(Y) - H(Z) \\ &\le \frac{1}{2}\log_2\left(1+\frac{P}{\sigma^2}\right) \text{ bits per transmission,} \end{aligned} \tag{3.15}$$

where P is the power constraint of the transmitted codeword, σ^2 is the noise power, and Z is independent of X. The upper bound is the channel capacity of this AWGN channel and achieved when X is $\sim N(0, P)$. For discrete-time channels, "per transmission" means every time the transmitter accesses the channel for transmission.

The channel capacity of a continuous-time Gaussian channel can be derived from (3.15) with essential redefinition of the signal power and the noise power. Considering that most of the signal energy is contained in bandwidth B and in a finite time interval, say $(0, T)$, it is sufficient to state that any signal can be described within a set of almost time-limited and almost band-limited signals in about $2TB$ basis [44]. According to the *Nyquist-Shannon sampling theorem*, a band-limited signal has $2B$ degrees of freedom per second. If the noise is regarded as white and Gaussian and has power spectral density $N_0/2$ watts/hertz and bandwidth B hertz as well, then the noise has the total power $N_0/2\times 2B = N_0B$ and each of the $2TB$ samples in time T has the variance $N_0B\times T/2TB = N_0/2$. If the signal power in the continuous channel is P_c, then the signal power per sample in the discrete-time channel is $P = P_c\times T/2TB = P_c/2B$. Thus, the channel capacity per sample is [44]

$$C = \frac{1}{2}\log_2\left(1+\frac{P}{\sigma^2}\right) = \frac{1}{2}\log_2\left(1+\frac{P_c}{N_0B}\right) \quad \text{bits per sample.} \tag{3.16}$$

Because there are $2B$ samples per second for bandwidth B, the channel capacity in bits/s is found as

$$C = B\log_2\left(1+\frac{P_c}{N_0B}\right) \quad \text{bits/s,} \tag{3.17}$$

which is known as the *Shannon capacity*. It is also common to present the channel capacity normalised with bandwidth, i.e.,

$$C = \log_2\left(1+\frac{P_c}{N_0B}\right) \quad \text{bits/s/Hz.} \tag{3.18}$$

3.3.2 Block fading channels

In addition to AWGN, multipath fading is another factor that affects the quality of received signals at the receiver. If the realization of a fading channel remains constant within a block of L symbols, i.e., the block length is much shorter than the channel coherence time, then this channel is said to experience *block fading*.

In multiple-antenna channels, the received codeword $\mathbf{Y}$ can be presented as that the transmitted codeword $\mathbf{X}$ experiences non-linear fading $\mathbf{H}$ and linear channel noise $\mathbf{Z}$[1],

$$\mathbf{Y} = \sqrt{\frac{P}{N}}\mathbf{H}\mathbf{X} + \mathbf{Z}, \tag{3.19}$$

where $\mathbf{H}_{M\times N}$ contains the channel gain between N transmit antenna and M receive antennas; $\mathbf{X}_{N\times L}$ has the entries $\mathbf{x}_{i,j}$ ($i = 1, \ldots, N, j = 1, \ldots, L$), containing L codeword $\mathbf{X}_j$ of length N; each column of $\mathbf{Z}_{M\times L}$ is considered to be AWGN $\sim CN(0, \sigma^2\mathbf{I}_M)$; P is the total transmit power. As the same as (3.13), the mutual information of this multiple antenna channel is $I(\mathbf{X}_j;\mathbf{Y}_j) = h(\mathbf{Y}_j)-h(\mathbf{Z}_j)$. If $\mathbf{X}_j$ is zero-mean with covariance matrix $\mathrm{E}[\mathbf{X}_j\mathbf{X}_j^*] = \mathbf{\Psi}_\mathbf{X}$, then

$$\begin{aligned}\mathrm{E}\left[\mathbf{Y}_j\mathbf{Y}_j^*\right] &= \mathbf{\Psi}_\mathbf{Y} \\ &= \frac{P}{N}\mathrm{E}\left[\mathbf{H}\mathbf{X}_j\mathbf{X}_j^*\mathbf{H}^*\right] + \mathrm{E}\left[\mathbf{Z}_j\mathbf{Z}_j^*\right] \\ &= \frac{P}{N}\mathbf{H}\mathbf{\Psi}_\mathbf{X}\mathbf{H}^* + \sigma^2\mathbf{I}_M.\end{aligned} \tag{3.20}$$

By Lemma 2 in [5], $h(\mathbf{Y}_j)$ is maximised when $\mathbf{Y}_j$ are circularly symmetric Gaussian variables; and by Lemma 3 and 4 in [5], for $\mathbf{Y}_j$ to be such variables, $\mathbf{X}_j$ should be circularly symmetric Gaussian variables. For circularly symmetric Gaussian random variables, the differential entropy of $\mathbf{Y}_j$ is

$$h(\mathbf{Y}_j) = \log_2\left[\det(\mathbf{\Psi}_\mathbf{Y})\right] + N\log_2(\pi e), \tag{3.21}$$

[1] For single-antenna channels, $\mathbf{X}$, $\mathbf{Y}$, $\mathbf{H}$ and $\mathbf{Z}$ reduce to singular values.

where det stands for the determinant. Similarly, $h(\mathbf{Z}_j) = \log_2[\det(\sigma^2\mathbf{I}_M)]+N\log_2(\pi e)$. Therefore, the mutual information of the channel can be calculated as

$$\begin{aligned} I(\mathbf{X}_j;\mathbf{Y}_j) &= h(\mathbf{Y}_j) - h(\mathbf{Z}_j) \\ &= \log_2\left[\det(\boldsymbol{\Psi}_\mathbf{Y})\det\left(\sigma^2\mathbf{I}_M\right)^{-1}\right] \\ &= \log_2\left[\det\left(\frac{\boldsymbol{\Psi}_\mathbf{Y}}{\sigma^2\mathbf{I}_M}\right)\right] \\ &= \log_2\left[\det\left(\mathbf{I}_M + \frac{SNR}{N}\mathbf{H}\boldsymbol{\Psi}_\mathbf{X}\mathbf{H}^*\right)\right], \end{aligned} \tag{3.22}$$

where the third equation stands because $\det(\mathbf{AB}) = \det(\mathbf{A})\det(\mathbf{B})$ and $\det(\mathbf{C})^{-1} = \det(\mathbf{C}^{-1})$ for $\det(\mathbf{C}) \neq 0$, and $SNR = P/\sigma^2$ is the average received SNR without fading; which is valid under equal power assumption and total transmit power constraint. If the transmit codeword is carefully designed so that $\boldsymbol{\Psi}_\mathbf{X} = \mathbf{I}$, the mutual information is maximised to

$$I(\mathbf{X}_j;\mathbf{Y}_j) = \log_2\left[\det\left(\mathbf{I}_M + \frac{SNR}{N}\mathbf{H}\mathbf{H}^*\right)\right]. \tag{3.23}$$

If $\mathbf{H}$ is i.i.d. $CN(0, 1)$, then $\mathbf{H}_w$ is used to replace the notation of such channel matrix, where the subscript w means "white". Applying QR decomposition to $\mathbf{H}_w$[1] and using the facts that for any diagonal matrix $\boldsymbol{\Lambda}$ and any upper triangular matrix $\mathbf{R}$ [7],

$$\det\left(\boldsymbol{\Lambda}\boldsymbol{\Lambda}^* + \mathbf{R}\mathbf{R}^*\right) \geq \prod_l \left(\left|\boldsymbol{\Lambda}_{l,l}\right|^2 + \left|\mathbf{R}_{l,l}\right|^2\right), \tag{3.24}$$

where $\mathbf{R}_{l,l}$ is the lth diagonal element of $\mathbf{R}$, and for any nonnegative definite matrix $\mathbf{A}$ [7],

$$\det(\mathbf{A}) \leq \prod_l \mathbf{A}_{l,l}, \tag{3.25}$$

---

[1] $\mathbf{H}_w$ is QR-decomposed to

$$\mathbf{H}_w = \mathbf{QR},$$

where $\mathbf{Q}$ is a complex unitary matrix, defined as $\mathbf{I} = \mathbf{QQ}^*$ and $\mathbf{R}$ is an upper triangular matrix.

(3.23) can be bounded by [7]

$$\sum_{l=1}^{N}\log_2\left(1+\frac{SNR}{N}\left|\mathbf{R}_{l,l}\right|^2\right)\le I\left(\mathbf{X}_j;\mathbf{Y}_j\right)\le\sum_{l=1}^{N}\log_2\left(1+\frac{SNR}{N}\left(\left|\mathbf{R}_{l,l}\right|^2+\sum_{k=l+1}^{N}\left|\mathbf{R}_{l,k}\right|^2\right)\right). \tag{3.26}$$

Since $\mathbf{W} = \mathbf{HH}^*$ in (3.23) is a Hermitian matrix, it can be diagonalised (*eigenvalue decomposition*) to

$$\mathbf{W} = \mathbf{U}\Lambda\mathbf{U}^*, \tag{3.27}$$

where $\Lambda = \mathrm{diag}(\lambda_1, \ldots, \lambda_M)$ in which λ_i, $i = 1, \ldots, M$, are the eigenvalues of $\mathbf{W}$ in the descending order and $\mathbf{U}$ is the unitary matrix. Given $\det(\mathbf{A}) = \lambda_{A1}, \ldots, \lambda_{AM}$, the mutual information in (3.23) can also be presented as

$$I\left(\mathbf{X}_j;\mathbf{Y}_j\right)=\log_2\left[\prod_{i=1}^{M}\left(1+\frac{SNR}{N}\lambda_i\right)\right]=\sum_{i=1}^{M}\log_2\left(1+\frac{SNR}{N}\lambda_i\right). \tag{3.28}$$

The mutual information derived in (3.22), (3.23) and (3.28) is for the so-called *non-coherent* channels where only the receiver is aware of the channel condition, or more precisely, the *channel state information* (CSI). If the transmitter also has the knowledge of the CSI through a feedback channel from the receiver, the channel is regarded to be coherent and the *Waterfilling algorithm* [1] can be applied at the transmitter to enhance the channel capacity. Thus, the mutual information under the Waterfilling algorithm is [43]

$$I_{\mathrm{WF}}\left(\mathbf{X}_j;\mathbf{Y}_j\right)=\sum_{i=1}^{M}\log_2\left(\mu\lambda_i\right)^+, \tag{3.29}$$

where $(x)^+ = \max(0, x)$ and μ is chosen to satisfy

[1] In some literatures, the "waterfilling" algorithm is also known as the "waterpouring" algorithm. When the transmitter has the (partial or full) knowledge of the wireless channel, it can set the different power levels of the transmit signals sent out from different transmit antennas, letting stronger signals propagate on better channels. The major difficulty of implementing this algorithm is how the transmitter can obtain the CSI with as few errors as possible.

$$\sum_{i=1}^{M}\left(\mu-\lambda_i^{-1}\right)^{+} \geq \text{trace}(\boldsymbol{\Psi}_{\mathbf{X}}). \tag{3.30}$$

For the correlated channels in (3.7), the mutual information under equal power assumption is found as

$$\begin{aligned} I\left(\mathbf{X}_j;\mathbf{Y}_j\right) &= \log_2\left[\det\left(\mathbf{I}_M+\frac{SNR}{N}\mathbf{H}\mathbf{H}^*\right)\right] \\ &= \log_2\left[\det\left(\mathbf{I}_M+\frac{SNR}{N}\left(\boldsymbol{\Phi}^R\right)^{1/2}\mathbf{H}_w\left(\boldsymbol{\Phi}^T\right)^{1/2}\left(\left(\boldsymbol{\Phi}^R\right)^{1/2}\mathbf{H}_w\left(\boldsymbol{\Phi}^T\right)^{1/2}\right)^*\right)\right] \\ &= \log_2\left[\det\left(\mathbf{I}_M+\frac{SNR}{N}\mathbf{H}_w\boldsymbol{\Phi}^T\mathbf{H}_w^*\boldsymbol{\Phi}^R\right)\right], \end{aligned} \tag{3.31}$$

where the last equation stands because det(**I**+**AB**) = det(**I**+**BA**).

3.3.3 Ergodic fading channels

On the contrast to block fading channels, the length of each of L symbols in a coding block in ergodic channels is much longer than the channel coherence time. Fast fading channel is one example of ergodic channels. Importantly, the Shannon capacity is well defined for this type of channels. In ergodic channels, the *ensemble averages*[1] of the channel gain matrix $\mathbf{H}(t)$ equal its appropriate *time averages*[2], i.e., any statistics of $\mathbf{H}(t)$ can be determined from a single sample $\mathbf{H}(t, \tau)$ [45]. Therefore, the channel capacity of the ergodic fading channels is found as [4, 5]

---

[1] Ensemble average of a process $x(t)$ is used to estimate the mean $\eta(t)$ of $x(t)$,

$$\eta(t) \approx \frac{1}{n}\sum_{i=1}^{n} x(t,\tau_i),$$

where n is the number of samples.

[2] Time average of $x(t)$ is defined as

$$\bar{x} = \lim_{T\to\infty}\frac{1}{2T}\int_{-T}^{T} x(t,\tau)dt,$$

where only one single sample $x(t, \tau)$ of $x(t)$ is accessible.

$$C = \mathrm{E}\left\{\log_2\left[\det\left(\mathbf{I}_M + \frac{SNR}{N}\mathbf{H}\mathbf{H}^*\right)\right]\right\}. \tag{3.32}$$

The wireless channel is able to support such data rate constantly with arbitrarily small error probability observed at the receiver.

3.3.4 Non-ergodic fading channels

There is another type of fading, namely *non-ergodic* fading. In this type of fading channels, the time-invariable channel gain matrix $\mathbf{H}$ are randomly distributed but chosen before the start of channel use. Such channel fading is also known as quasi-static fading. This fading condition is practical. Consider a static wireless environment with rich multipath. Because there is no (or rare) movement in such an environment, the channel gains can be regarded as pre-fixed during all the channel use. Rich multipath introduces the fluctuation in the received signal strength over adequately long time period. If the number of propagation path is large enough, the magnitude of the channel gain displays the Rayleigh distribution.

In non-ergodic fading channels, there is always a non-zero probability that the channel is unable to support the transmitted information no matter how long the code length is. In this case, outage occurs, i.e., the channel fails to carry the error-free information at the target data rate R. The *outage probability*, P_{out}, is used to measure the percentage of a fading channel being in outage, which can be computed from

$$P_{out}(R, SNR) = \Pr\left[\log_2\left(\mathbf{I}_M + \frac{SNR}{N}\mathbf{H}\mathbf{H}^*\right) < R\right]. \tag{3.33}$$

Assuming $M = N = 1$, P_{out} in (3.33) becomes

$$P_{out}(R, SNR) = \Pr\left[|\alpha|^2 < \frac{2^R - 1}{SNR}\right] = 1 - \exp\left(-\frac{2^R - 1}{SNR\sigma^2}\right), \tag{3.34}$$

where the magnitude of the channel gain, $|\alpha|$, is assumed to be Rayleigh-distributed. The outage probability is also suitable for calculating the error probability of each channel realization in the block fading channel condition.

3.3.5 Notes on channel capacity and mutual information

Either (3.17) or (3.18) suggests that the Shannon capacity is an average concept based on the average SNR observed by the receiver. In AWGN or other types of noise channels, the channel capacity can be achieved with arbitrarily small error probability when the Gaussian coded information is sent by the transmitter. In ergodic fading channels, the time average of the channel gain is equal to the ensemble average of the channel gain so that the randomness of the channel gain can be averaged out (removed) over time. Therefore, the Shannon capacity is achievable in ergodic channels. In the block fading channels and non-ergodic fading channels, however, the channel capacity is non-existent as there are always chances that the wireless fading channel fails to deliver the transmitter's information at the target data rate, due to the randomness of the channel gain. In this case, the channel performance is measured by mutual information and outage probability.

3.4 Diversity-multiplexing trade-off

A communication system can achieve *diversity gain* when the same information is transmitted multiple times. This can occur in time domain, frequency domain and/or space domain. The probability of error occurring at the receiver can thus be reduced. In other words, more diversity gain leads to lower error probability. When the SNR is high, the transmitter may sacrifice some diversity gain by sending out information faster. In this case, higher *multiplexing gain* is achieved, i.e., during the same time period more new information has been sent to the receiver. There is, however, one drawback that the error probability will increase at the receiver. This is the so-called *diversity-multiplexing trade-off*, the fundamental trade-off of communications. In [46, 47], the multiplexing gain r of a coding scheme is defined as

$$r = \lim_{SNR \to \infty} \frac{R(SNR)}{\log_2 SNR}, \tag{3.35}$$

and the diversity gain d is defined as

$$d = -\lim_{SNR\to\infty} \frac{\log_2 P_e(SNR)}{\log_2 SNR}, \tag{3.36}$$

where $P_e(SNR)$ is the error probability of the coding scheme as the function of SNR and $R(SNR)$ is the transmit rate as the function of SNR. When the coding block length is long enough, such as $L \geq M+N-1$, the error probability is dominated by the outage probability, i.e., $P_e(SNR) = P_{out}(SNR, R)$. Define $d^*(r)$ as the *supremum*[1] of the diversity gain, d, achieved over all coding schemes. Therefore, $d^*(r) = d_{out}(r)$, where $d_{out}(r)$ is the diversity gain found through outage probability. The remaining of the problem is how to work out the outage probability of an $M\times N$ MIMO system, which can start at finding the joint PDF of the ordered nonzero eigenvalues of $\mathbf{H}^*\mathbf{H}$.

Assuming that the entries of the $M\times N$ channel matrix $\mathbf{H}$ are i.i.d complex Gaussian variables with zero mean and unit variance in block fading channels and without loss of generality $M \geq N$, the joint PDF of the ordered nonzero eigenvalues of $\mathbf{H}^*\mathbf{H}$, $\lambda_1 \leq \lambda_2 \leq \ldots \leq \lambda_n$, is [46]

$$p(\lambda_1,\cdots,\lambda_n) = K_{M,N}^{-1} \prod_{i=1}^{N} \lambda_i^{M-N} \prod_{i<j} (\lambda_i - \lambda_j)^2 e^{-\sum_i \lambda_i} \tag{3.37}$$

where $K_{M,N}$ is a normalizing constant. Defining

$$\alpha_i = -\log_2 \lambda_i / \log_2 SNR \tag{3.38}$$

(thus, $\alpha_i \leq \alpha_j$, $i < j$) or alternatively $\lambda_i = SNR^{-\alpha_i}$, the joint PDF of $\boldsymbol{\alpha} = [\alpha_1, \ldots, \alpha_n]$ can be found as

$$p(\boldsymbol{\alpha}) = K_{M,N}^{-1} (\log_2 SNR)^N \prod_{i=1}^{N} SNR^{-(M-N+1)\alpha_i} \prod_{i<j} \left(SNR^{-\alpha_i} - SNR^{-\alpha_j} \right)^2 \exp\left(-\sum_{i=1}^{N} SNR^{-\alpha_i} \right). \tag{3.39}$$

[1] Given a subset S of a partially ordered set T, the supremum (sup) of S, if it exists, is the least element of T that is greater than or equal to each element of S. Consequently, the supremum is also referred to as the least upper bound (lub or LUB). If the supremum exists, it may or may not belong to S and it is unique. For example, $\sup\{x \in \Re : 0 < x < 1\} = \sup\{x \in \Re : 0 \leq x \leq 1\} = 1$.

For high SNR, $|SNR^{-\alpha_i}-SNR^{-\alpha_j}|$ is dominated by $SNR^{-\alpha_j}$ and the joint probability in (3.39) can be simplified to

$$p(\boldsymbol{\alpha}) = \prod_{i=1}^{N} SNR^{-(2i-1+M-N)\alpha_i}. \tag{3.40}$$

Denoting $f(a) \doteq a^{-b}$ for

$$-\lim_{a\to\infty} \frac{\log_2 f(a)}{\log_2 a} = b, \tag{3.41}$$

where b is known as the *exponential order* of $f(a)$, and recalling (3.28), the outage probability of a MIMO system at target data rate $R = r\log_2 SNR$ in high SNR regime can be found as

$$P_{out}(R) \doteq P\left[\prod_{i=1}^{N}(1+SNR\lambda_i) < SNR^r\right]. \tag{3.42}$$

Using (3.38), (3.42) can also be expressed as

$$P_{out}(R) \doteq P\left[\prod_{i=1}^{N} SNR^{(1-\alpha_i)^+} < SNR^r\right] = P\left[\sum_{i=1}^{N}(1-\alpha_i)^+ < r\right], \tag{3.43}$$

where $(1+SNR\lambda_i) \doteq SNR^{(1-\alpha_i)^+}$. The random vector $\boldsymbol{\alpha}$ indicates the level of singularity of $\mathbf{H}$. The larger α_i's are, the more singular $\mathbf{H}$ is. Then, the outage probability of $\mathbf{H}$ in the outage event $A = \{\alpha: \Sigma_i(1-\alpha_i)^+ < r\}$ can be computed as [46]

$$P_{out}(r\log_2 SNR) \doteq \int_A p(\boldsymbol{\alpha})d\boldsymbol{\alpha} = \int_{A'}\prod_{i=1}^{N} SNR^{-(2i-1+M-N)\alpha_i}\, d\boldsymbol{\alpha} \doteq SNR^{-d_{out}(r)}, \tag{3.44}$$

where the last step uses Laplace's method,

$$d_{out}(r) = \inf_{\boldsymbol{\alpha}\in A'} \sum_{i=1}^{\min\{M,N\}}(2i-1+|M-N|)\alpha_i \tag{3.45}$$

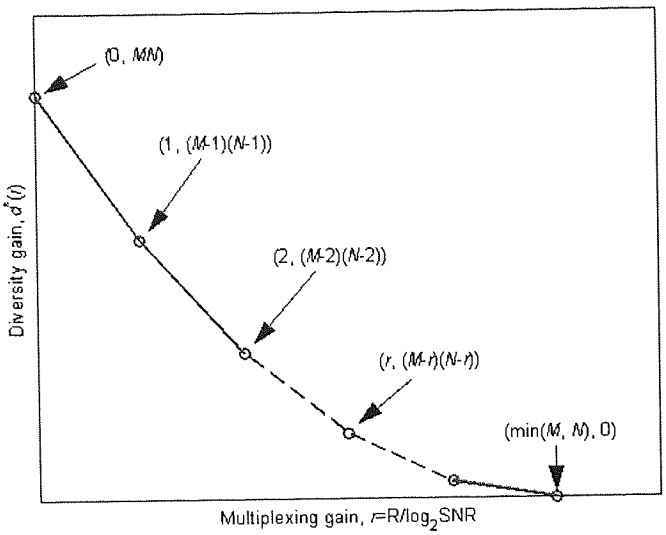

Figure 3-1 The diversity-multiplexing trade-off curve.

and $$A^{+}=\left\{\alpha\in\Re^{\min\{M,N\}+}\middle|\alpha_1\geq\cdots\geq\alpha_{\min\{M,N\}}\geq 0 \text{ and } \sum_i(1-\alpha_i)^{+}<r\right\} \tag{3.46}$$

In (3.46), $\Re^{\min\{M, N\}+}$ is the set of real $\min\{M, N\}$-vectors with nonnegative elements. Comparing (3.44) with (3.39), one important fact can be revealed that the diversity gain of $CN(0, 1)$-faded channels is equal to the exponential order of the SNR component in the joint PDF presented by (3.39) for high SNR.

Then the optimal trade-off curve $d^*(r)$, which is equal to $d_{out}(r)$ and shown in Figure 3-1, can be explicitly computed as [46]

$$d^*(r)=(M-r)(N-r), \quad \text{for } l\geq M+N-1, \tag{3.47}$$

where $d^*_{max} = MN$ and $r_{max} = \min\{M, N\}$. This result stands when the channels are considered uncorrelated.

3.5 MIMO channel models

This section demonstrates how to model MIMO channels in different scattering environments, using ray-tracing and stochastic modelling techniques. The models

visited in this section are applied to the macrocellular scenario. Some of these models will be extended in Chapter 5.

3.5.1 Green field model

As suggested by the name of the model, there is no obstacle between the transmitter and the receiver in the green field model. Figure 3-2 shows the geometry of the model. The signal radiated by the pth transmit antenna impinges as a plane wave on the receive antenna array at the angle of θ_p. Denote D_p the distance between the pth transmit antenna and the first receive antenna. The transmit and receive antenna spacing is d_t and d_r, respectively. Thus, the normalised green-field channel model can be expressed as $\mathbf{H} = [\mathbf{H}_1\ \mathbf{H}_2\ \ldots\ \mathbf{H}_N]$ where the channel propagation vector induced by the pth transmit antenna can be denoted as [9]

$$\mathbf{H}_p = e^{-j\frac{2\pi}{\lambda}D_p}\left[1 \quad e^{-j\frac{2\pi}{\lambda}d_r\sin\theta_p} \quad \cdots \quad e^{-j\frac{2\pi}{\lambda}(M-1)d_r\sin\theta_p}\right]^T \qquad p = 1,\cdots,N, \tag{3.48}$$

where λ is the carrier wavelength, M is the number of the receive antennas and ^{T} stands for transpose. As the item $e^{-j2\pi D_p/\lambda}$ has no contribution to the channel capacity [9], (3.48) can be simplified to [9]

$$\mathbf{H}_p = \left[1 \quad e^{-j\frac{2\pi}{\lambda}d_r\sin\theta_p} \quad \cdots \quad e^{-j\frac{2\pi}{\lambda}(M-1)d_r\sin\theta_p}\right]^T. \tag{3.49}$$

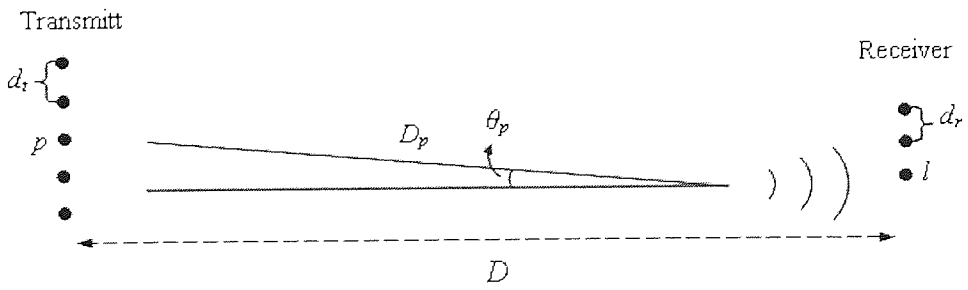

Figure 3-2 The green field model.

When the transmitter-receiver distance D is large, θ_p approaches zero and $\mathbf{H}$ becomes an all-ones matrix, i.e., the *rank*[1] of $\mathbf{H}$ is one. This suggests that if θ_p can be increased, despite of large D, to make the elements in $\mathbf{H}_p$ more distinguishable, the rank of $\mathbf{H}$ will increase, leading to higher channel capacity. The presence of scatterers can accomplish the mission. This is the major reason why many MIMO systems exploit multipath fading environments.

To achieve high capacity, the full orthogonality between the columns of $\mathbf{H}$ is intended. If the transmit antenna array is assumed to be linear-uniform, the orthogonality between any adjacent columns, i.e., adjacent transmit antennas, is adequate to assure the full orthogonality in $\mathbf{H}$. The orthogonality between two adjacent columns in $\mathbf{H}$ can be presented as [9]

$$\left\langle \mathbf{H}_p, \mathbf{H}_{p+1} \right\rangle = \sum_{p=0}^{M-1} e^{j\frac{2\pi d_r}{\lambda} l\left(\sin\theta_{p+1} - \sin\theta_p\right)} = 0. \tag{3.50}$$

Usually, D is much larger than d_t and d_r. Therefore, it is reasonable to set $\sin\theta_p \approx (p-1)d_t/D$. As a result, (3.50) can be rewritten as [9]

$$\left\langle \mathbf{H}_p, \mathbf{H}_{p+1} \right\rangle = \sum_{l=0}^{M-1} e^{j\frac{2\pi d_t d_r}{\lambda D} l} = 0, \tag{3.51}$$

which implies that

$$\frac{d_t d_r}{D} \geq \frac{\lambda}{M}. \tag{3.52}$$

Eq. (3.52) is, however, insufficient to achieve exact orthogonality [9]. This inequality can be presented as

[1] The rank of a $M \times N$ matrix $\mathbf{A}$ is equal to either the column rank or the row rank, since the column rank and the row rank are always equal. The column/row rank of $\mathbf{A}$ is the maximal number of linearly independent columns/rows of $\mathbf{A}$. The maximal rank of $\mathbf{A}$ is $\min(M, N)$. $\mathbf{A}$ is said to have full rank when its rank is as large as possible. Otherwise, $\mathbf{A}$ is rank deficient.

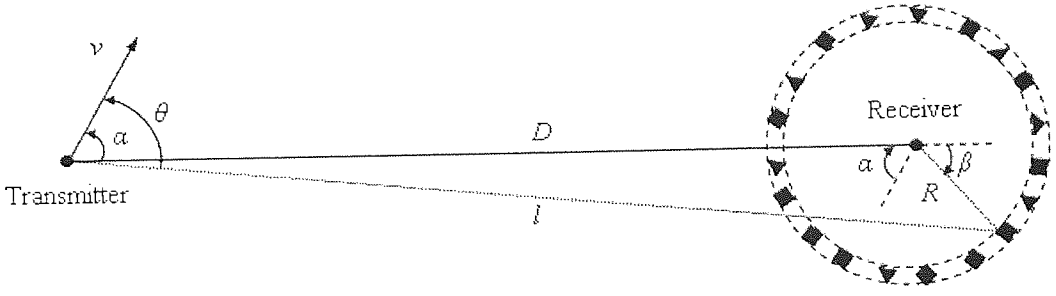

Figure 3-3 The "one-ring" scattering model.

$$\frac{d_l}{D} \geq \frac{\lambda}{Md_r}, \tag{3.53}$$

which can be interpreted as that the angular resolution of the receive antenna array should be below the angular separation of the adjacent transmit antennas [9].

3.5.2 "One-ring" model

The scattering model shown in Figure 3-3 was first introduced in [48] for the SISO communication. Since the scatterers surrounding the receiver is assumed to be uniformly distributed on a ring, the model is better known as "one-ring" model. In this model, the transmitter moves with the constant speed v at an angle of α as indicated in the scattering model. It is also assumed that the transmitter-receiver distance D is so large that θ changes insignificantly during the observation time of interest, i.e., the distance covered by the transmitter's movement is small, compared to D. Then, the normalised received baseband signal can be presented as [48]

$$r(t) = \frac{1}{\sqrt{S}} \left\{ \sum_{s=1}^{S/2-1} \left[e^{i(\omega_m t \cos\alpha_s + \phi_s)} + e^{-i(\omega_m t \cos\alpha_s + \phi_{-s})} \right] + e^{i(\omega_m t + \phi_S)} + e^{-i(\omega_m t + \phi_{-S})} \right\}, \tag{3.54}$$

where S is the total number of the scatterers and assumed to be odd[1]; $\omega_m = 2\pi f_m$; $f_m \cos\alpha_s$ is the Doppler shift associated with the sth scatterer, where $\alpha_s = 2\pi s/S$ for the uniform distribution and for the definition of Doppler shift $f_m = f_c v/c$ in (2.19); and ϕ_s

[1] This is a reasonable assumption when S is large enough.

represents the dielectric property and the radial displacement from the scatterer ring of the actual scatterer. If S is large enough, the *central limit theorem* [29] may be used to conclude that $r(t)$ is approximately a complex Gaussian process, i.e., $|r(t)|$ is Rayleigh distributed. The approximation is rather good for $S \geq 6$ with deviations from the Rayleigh distribution confined mostly to the extreme peaks, following the work in [49, 50].

The "one-ring" model was later slightly modified by Shiu, et al. [7] to fit their interest in evaluating the MIMO fading channels, as shown in Figure 3-4. In the figure, the antenna arrays are linearly and uniformly distributed; Θ is the AOD of the transmitter; Δ is the *angular spread* of the transmitter; $S(\theta)$ represents a scatterer indexed by θ; D is the transmitter-receiver distance; and R is the radius of the scatterer ring. The normalised channel coefficient $\mathbf{H}_{l,p}$ between the pth transmit antenna and the lth receive antenna is found as [7]

$$\mathbf{H}_{l,p} = \frac{1}{\sqrt{2\pi}} \int_0^{2\pi} \frac{1}{\sqrt{S}} \sum_{s=1}^{S} \delta(\theta - \theta_s) \exp\left\{ -j \frac{2\pi}{\lambda} \left(D_{TA_p \to S(\theta)} + D_{S(\theta) \to RA_l} \right) + j\phi(\theta) \right\} d\theta, \quad (3.55)$$

where S can be any positive number; $\phi(\theta)$ indicates the same effect as ϕ_n in (3.54); and $D_{\bullet}$ is the distance between the subscripted objects. By the central limit theorem, $\mathbf{H}_{l,p}$ is $CN(0, 1)$ when S is sufficiently large. The covariance (found to characterise $\mathbf{H}$ according to (3.6) and (3.7)) between $\mathbf{H}_{l,p}$ and $\mathbf{H}_{m,q}$ is given by [7]

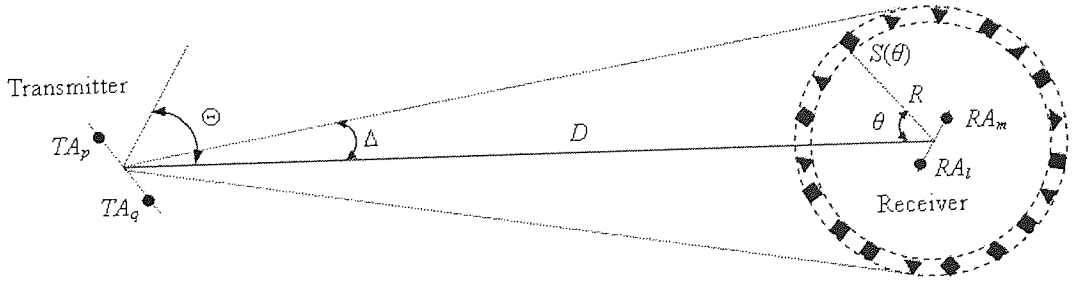

Figure 3-4 The "one-ring" scattering model for MIMO channels.

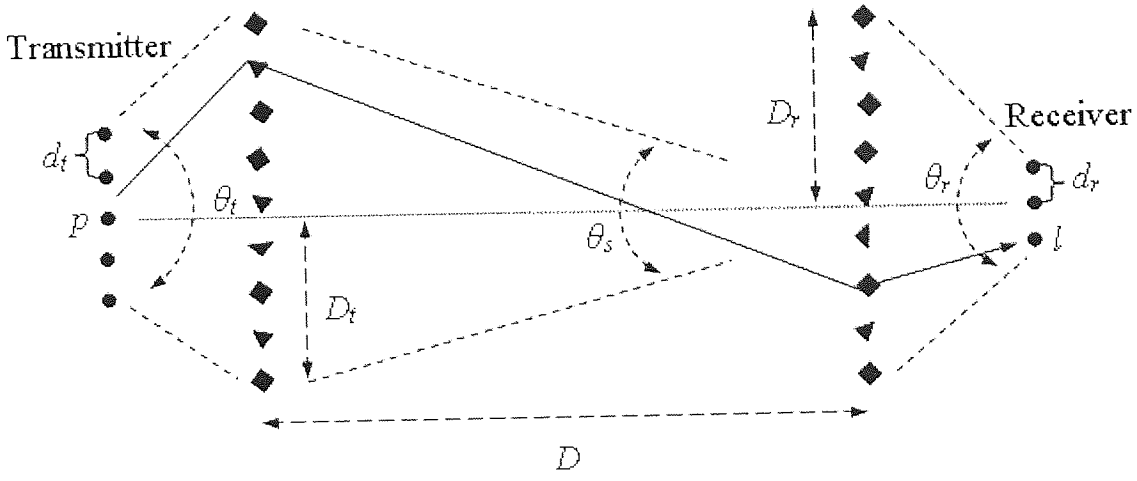

Figure 3-5 The uniform-scatterer model.

$$\mathrm{E}\left[\mathbf{H}_{l,p}\mathbf{H}^{*}_{m,q}\right]=\frac{1}{2\pi}\int_0^{2\pi}\exp\left\{-j\frac{2\pi}{\lambda}\left(D_{TA_p\to S(\theta)}-D_{TA_q\to S(\theta)}+D_{S(\theta)\to RA_l}-D_{S(\theta)\to RA_m}\right)\right\}d\theta, \quad (3.56)$$

where the PDF of the uniform distribution is $p(\theta) = 1/2\pi$. It is shown in [7] that the angular spread Δ is a key parameter. As Δ decreases, the correlation between individual channels will rise and consequently this leads to decreasing the mutual information of the multiple-antenna channel. The direction of the transmit antenna array is also crucial for achieving high mutual information. When the AOD is known, it is recommended to deploy a broadside ($\Theta = 0^{\circ}$) linear antenna array with large antenna spacing at the transmitter. If the signals propagate omnidirectionally, the transmit antenna array is better to have a symmetric shape, for example, hexagon. A more generalised channel model and its correlation model can be found in [8], where a LOS path is considered and the receiver is moving at the speed v.

3.5.3 Uniform-scatterer model

It is commonly considered that the wireless signals scattered twice are still recognizable by the receiver. So the "one-ring" model is insufficient to illustrate signal propagation in some multipath environments. To investigate the wireless channel behaviour in double-scattering environments, a heuristic uniform-scatterer model is proposed in [9]. Figure 3-5 shows the geometry of the uniform-scatterer model, where

all the scatterers are assumed to be ideal reflectors and only local scatterers of the transmitter and the receiver are considered, since the remote scatterers are assumed to have limit influence on the overall channel condition due to path loss for the very large transmitter-receiver distance. In addition, the scatterers should be sufficiently far away from the antenna arrays so that the assumption of plane-wave holds. Assuming that omnidirectional antenna arrays are deployed at both the transmitter and the receiver sides, the angular spread θ_t and θ_r of the transmitter and the receiver are determined by the radii of local scatterers, D_t and D_r, respectively. Moreover, S scatterers are assumed on each side, where S should be large enough for random fading to occur (refer to Subsection 3.5.2).

Treating the receiver-side scatterers as the virtual receive antennas, the channel gain vector between the nth transmit antenna and these scatterers can be modelled as [9]

$$\mathbf{Y}_n = \mathbf{\Phi}_{\theta_S,d_S}^{1/2} \mathbf{H}_{w,t|n}, \tag{3.57}$$

which is similar to (3.6) and where $\mathbf{H}_{w,t|n} \sim CN(0, \mathbf{I}_S)$ and $[\mathbf{\Phi}_{\theta_S,d_S}]_{S\times S}$ is the channel correlation matrix, which can be constructed using the following model for uniformly distributed arrays [51]

$$\left[\mathbf{\Phi}_{\theta_S,d_S}\right]_{l,p} = \frac{1}{S} \sum_{i=-(S-1)/2}^{(S-1)/2} e^{-j2\pi(p-l)\cos\left(\pi/2+\theta_{S,i}\right)d_S/\lambda}, \tag{3.58}$$

where $d_s = 2D_r/S$; S is assumed to be odd; $\theta_{s,i}$ is the AOA of the ith transmitter-side scatterer and in the range $[-\theta_s/2, \theta_s/2]$. For the uncorrelated transmit antenna array, the channel gain $\mathbf{Y} = [\mathbf{Y}_1\ \mathbf{Y}_2\ \ldots\ \mathbf{Y}_N]$ can be found as [9]

$$\mathbf{Y} = \mathbf{\Phi}_{\theta_S,d_S}^{1/2} \mathbf{H}_{w,t}. \tag{3.59}$$

If the correlation is considered between the transmit antennas, $\mathbf{Y}$ is found as [9]

$$\mathbf{Y} = \mathbf{\Phi}_{\theta_S,d_S}^{1/2} \mathbf{H}_{w,t} \mathbf{\Phi}_{\theta_t,d_t}^{1/2}, \tag{3.60}$$

where $\mathbf{\Phi}_{\theta_t,d_t}$ can be found through (3.58) with d_t replacing d_s.

Let $D_{s,m}$ represent the distance between the sth receiver-side scatterer and the mth receive antenna. The steering matrix of the receive antenna array can then be constructed as [9]

$$\Im = \begin{bmatrix} e^{-j2\pi d_{1,1}/\lambda} & \cdots & e^{-j2\pi d_{S,1}/\lambda} \\ \vdots & & \vdots \\ e^{-j2\pi d_{1,M}/\lambda} & \cdots & e^{-j2\pi d_{S,M}/\lambda} \end{bmatrix}. \tag{3.61}$$

Thus, the channel gain between the transmitter and the receiver is found as [9]

$$\mathbf{H} = \Im\mathbf{Y}. \tag{3.62}$$

It is proved in [9] that $\mathbf{H}$ is statistically equivalent to $\mathbf{\Phi}_{\theta_r,d_r}^{1/2}\mathbf{H}_{w,r}\mathbf{Y}$, where $\mathbf{H}_{w,r} \sim CN(0, 1)$. Then, the normalised channel gain $\mathbf{H}$ is modelled as

$$\mathbf{H} = \frac{1}{\sqrt{S}}\mathbf{\Phi}_{\theta_r,d_r}^{1/2}\mathbf{H}_{w,r}\mathbf{\Phi}_{\theta_s,d_s}^{1/2}\mathbf{H}_{w,t}\mathbf{\Phi}_{\theta_t,d_t}^{1/2}. \tag{3.63}$$

The correlation model in (3.58) indicates that the fading correlation in a MIMO channel can be governed by the antenna spacing, the scatterer spacing, the carrier wavelength, the radius of the scatterers and the respective angular spread/beamwidth of the transmitter and the receiver. The existence of fading correlation in the channel reduces the rank of the channel, resulting in lower mutual information/capacity of the channel. The presence of $\mathbf{\Phi}_{\theta_s,d_s}$ in (3.63) shows more insight of the effect of scatterers on the MIMO channel. Even when $\mathbf{\Phi}_{\theta_r,d_r} = \mathbf{\Phi}_{\theta_t,d_t} = \mathbf{I}$ (i.e., no correlation at both sides), the MIMO channel may still lose rank. This occurs when the rank of $\mathbf{\Phi}_{\theta_s,d_s}$ drops due to, such as, large D, or small D_t or D_r, or both. The extreme case is when $\mathbf{\Phi}_{\theta_s,d_s}^{1/2}$ is an all-one matrix. This kind of channel is the so-called *pinhole* channel, i.e., the scattered signals travel through a very thin air pipe, causing the channel rank to remain low. When $\mathbf{\Phi}_{\theta_s,d_s} = \mathbf{I}$, (3.63) is the same as (3.7), implying that (3.63) is a more accurate

model. Figure 3-6 illustrates the outage probability of the mutual information of this model computed using (3.23). In the settings of the plot, the angular spreads, θ_t and θ_r, are set to $\pi/2$; the antenna spacing $d_t = d_r = \lambda/2$; in "Pinhole" scenario, $D_t = D_r = 30$ m and $D = 1000$ km; in "Moderate correlation" scenario, $D_t = D_r = 500$ m and $D = 50$ km; in "Low correlation" scenario, $D_t = D_r = 100$ m and $D = 50$ m.

3.5.4 Con-focal-ellipses model

Each MIMO channel can be thought to consist of several SISO channels of the pairs of the transmit and the receive antennas. Since the antennas on the either side are closely located, characterising any of the SISO channels is adequate to present the MIMO channel. Considering an N-tapped power delay profile of one SISO channel [41], the uniformly distributed scatterers contributing to the nth tap are situated on the nth scatterer ellipse with $n \leq N$, where the foci of the N con-focal ellipses are the transmitter and the receiver, respectively. Therefore, the amplitude of each tap can be presented as, assuming omnidirectional antennas at both sides [41]

$$\alpha_n = \alpha_{n0} + \alpha_{n1} = \alpha_{n0} + \sqrt{\frac{G_{tx}G_{rx}}{d_n^{\gamma}}}\frac{\lambda}{4\pi}\sum_{s=1}^{S_n}\Gamma_{ns}\exp(j\phi_{ns}), \tag{3.64}$$

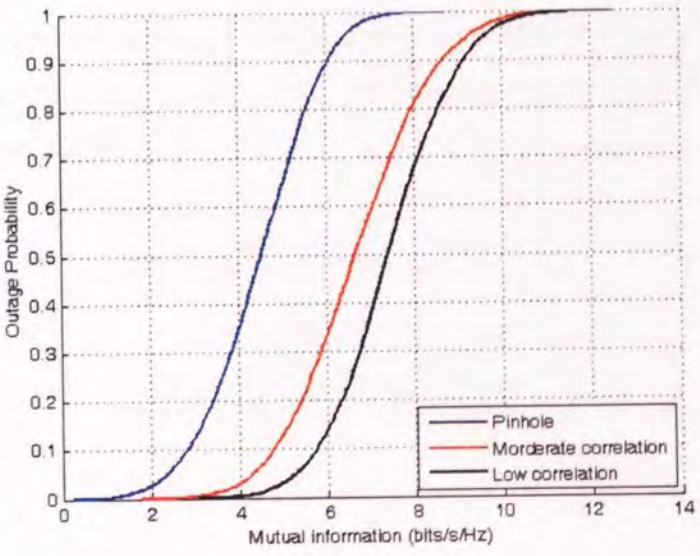

Figure 3-6 Outage probability of the mutual information in the uniform-scatterer model.

where G_{tx} and G_{rx} are the antenna gains of the transmit and the receive antennas; d_n is the path length associated with the nth ellipse, which can be calculated as $d_n = c\tau_n + d_0$ (c is the velocity of carrier; τ_n is the delay of the nth tap; and d_0 is the path length related to the first tap); γ is the path-loss exponent; λ is the wavelength; S_n is the number of scatterers on the nth scatterer ellipse; $\Gamma_{ns}\exp(j\phi_{ns})$ is the complex reflection coefficient of the sth scatterer on the nth ellipse; α_{n0} represents the amplitude of the LOS or the quasi LOS links in Ricean fading channels,

$$\alpha_{n0} = \begin{cases} \sqrt{\dfrac{G_{tx}G_{rx}}{d_0^{\gamma}}}\dfrac{\lambda}{4\pi}, & n = 1 \\ 0, & n > 1 \text{ or Rayleigh fading} \end{cases}$$

As given in Subsection 2.4.2, the K-factor in Ricean fading channel can be defined as

$$K = \frac{|\alpha_{10}|^2}{\mathrm{E}\left[|\alpha_{11}|^2\right]}. \tag{3.65}$$

For the scenario of macrocellular communication concerned in this model, there is a scatterer-free area in the vicinity of the transmitter and a scatterer ring with uniformly distributed scatterers surrounding the receiver. The scatterers in this scatterer ring are assumed to be taken from among the scatterers on the first ellipse near the receiver side. Therefore, the complete geometry model can be revealed in Figure 3-7. Using ray-tracing method as described in Section 2.1, the channel matrix of the con-focal-ellipses model can be expressed as [41]

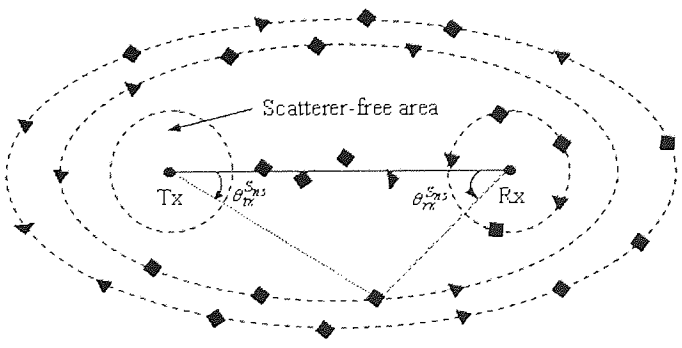

Figure 3-7 The con-focal-ellipses scattering model.

$$\mathbf{H}_{l,p}(\omega) = \mathbf{H}_{l,p}^{LOS}(\omega) + \sum_{n=1}^{N}\sum_{s=1}^{S_n}\frac{\lambda}{4\pi}\sqrt{\frac{G_{tx}^{p}\left(\theta_{tx}^{S_{ns}} - \psi_{tx}\right)G_{rx}^{l}\left(\theta_{rx}^{S_{ns}} - \psi_{rx}\right)}{\left(d_{p,S_{ns}} + d_{l,S_{ns}}\right)^{\gamma}}} \times \Gamma_{ns}\exp(-j\phi_{ns})\exp\left(-j\frac{\omega}{c}\left(d_{p,S_{ns}} + d_{l,S_{ns}}\right)\right), \tag{3.66}$$

where the LOS component can be calculated as [41]

$$\mathbf{H}_{l,p}^{LOS}(\omega) = \frac{\lambda}{4\pi}\sqrt{\frac{G_{tx}^{p}\left(\theta_{tx}^{l} - \psi_{tx}\right)G_{rx}^{l}\left(\theta_{rx}^{p} - \psi_{rx}\right)}{\left(d_{p,l}\right)^{\gamma}}}\exp\left(-j\frac{\omega}{c}d_{p,l}\right); \tag{3.67}$$

$G_{tx}^{p}\left(\theta_{tx}^{S_{ns}} - \psi_{tx}\right)$ and $G_{rx}^{l}\left(\theta_{rx}^{S_{ns}} - \psi_{rx}\right)$ are respectively the gains of the pth transmit antenna and the lth receive antenna, associated with the angle of the sth scatterer on the nth ellipse and the corresponding pointing angle of the transmitter and the receiver, respectively; $d_{p,Sns}+ d_{l,Sns}$ is the path length between the pth transmit antenna and the lth receive antenna via the sth scatterer on the nth ellipse. The channel gain, $H_{l,p}(\omega)$, presented in channel model in (3.66) is for the frequency-selective fading, while it reduces to scalar $H_{l,p}$ for flat-fading channels.

In this model, the Ricean K-factor and RMS delay spread are strongly dependent on the range of the transmitter-receiver distance and that of the scatterers. The antenna beamwidth of the receiver affects the channel performance sensitively. More specifically, wider beamwidth reduces the value of K-factor and the correlation between the receive antennas, but increases RMS delay spread. Also, the scatterer density, η[1], and the scatterer coefficient, $\Gamma\exp(j\phi)$ have insignificant effects on the channel performance, while the total number of scatterers is fixed.

[1] The scatterer density in the con-focal-ellipses model is defined as

$$\eta = \frac{S}{\frac{\pi}{4}d_N\sqrt{d_N^2 - d_0^2}},$$

where S is the total number of scatterers and d_N is the range related to the largest ellipse.

3.6 Summary

The MIMO systems, including the performance evaluation tools, channel capacity of different fading types and diversity-multiplexing trade-off, are discussed in this chapter. These tools will be frequently used in the later chapters to assess the performance of various systems. The MIMO channels can be modelled using either ray-tracing or stochastic method, where the latter is based on the former. The models presented in Section 3.5 demonstrate the practical exercises of these methods and also show the connection between the two modelling methods. The models discussed are developed for different scattering environments. These models will be extended in Chapter 5 for investigating the performance of MIMO systems in a more realistic propagation environment.

4 Cooperative Communication Systems

For CC systems to function well, cooperative protocols on the medium access control (MAC) layer have been defined for operations in the relay nodes. These protocols tell the relay nodes when and how to participate in cooperation depending on the information collected from the physical (PHY) layer. For the half-duplex systems, i.e., the relay nodes are unable to transmit and receive at the same time, cooperative protocols are designed to ensure orthogonality between the transmit nodes (the source and the relay nodes). Because of this, the spectral efficiency of a half-duplex CC system is usually significantly lower than that of a non-cooperative one. The destination, however, receives more reliable data, due to the diversity gains achieved. The issue of low spectral efficiency may be avoided by using a full-duplex antenna on each relay node.

The cooperative protocols, such as amplify-forward (AF), decode-forward (DF) and compress-forward (CF), were first proposed in [15]. The development of these protocols has attracted many research efforts [16, 52-67]. Each cooperative protocol is used in conjunction with one of the following relaying algorithms: fixed relaying, selection relaying, incremental relaying, non-orthogonal relaying, dynamic relaying, opportunistic relaying and clustered relaying.

Fixed relaying means that the relay node is always involved in transmission. In selection relaying, the relay node works only when the quality of the source-relay channel is above an expected level. In incremental relaying, a feedback channel between the source and the destination nodes is needed to inform the source node and the relay nodes of the status of the source-destination channel. If the channel is good enough, the relay node remains silent; otherwise, it performs relaying. In non-orthogonal relaying, one of the relay nodes can amplify and forward previously received source information, when the source node is transmitting new information. The relay node should use a different codebook that is known to all the nodes in the network. Dynamic relaying is particularly proposed for the DF protocol. In dynamic relaying, the relay nodes keep receiving the source information until the mutual information between the source and the relay nodes is large enough for them to

successfully decode the source information. Therefore, the time length for the relay nodes to help the source node is dynamic, depending on the channel condition. In opportunistic relaying, only the best relay node, in terms of its associated channel quality, forwards the source information. In clustered relaying, the relay nodes are clustered with either the source node or the destination node, or both, in order to ideally achieve the best diversity gain or multiplexing gain offered by a CC system.

According to the functionality of relay nodes, CC systems can be divided into three types: multihop relaying, cooperative relaying and cooperative diversity. In multihop relaying [68], the source information is sent out to a particular relay node rather than directly to the destination node. This relay node will forward the processed source information to either the next relay node or the destination node. The forwarding continues until the source information reaches the destination node.

In both cooperative relaying and cooperative diversity the source information can reach the destination node via the relay nodes, as well as via the direct transmission channel. There is, however, one significant difference between cooperative relaying and cooperative diversity. In the former, only one transmit node is the source node that sends out original information and all the others are the relay nodes dedicated to performing relaying if required. In cooperative diversity, all the transmit nodes can act as the source nodes as well as the relay nodes, to provide help to each other.

The protocols discussed in this section are designed for both cooperative relaying and cooperative diversity. Unless specified, the relay nodes are in half-duplex (HD) mode, i.e., the relay nodes are unable to transmit and receive simultaneously. Also, all the nodes concerned are equipped with only one antenna. All the wireless channels in this chapter are assumed to be slow- and flat- faded. Some of the protocols discussed in this chapter will be used later in Chapter 6 for investigating the effect of fading correlation on CC systems.

4.1 Direct transmission

The maximum mutual information of the non-cooperation or direct transmission system can be found as

$$I_D = \log_2\left(1 + SNR_{s,d}\left|\alpha_{s,d}\right|^2\right), \tag{4.1}$$

where subscript $_{s,d}$ indicates the source-destination channel; thus $SNR_{s,d}$ and $\alpha_{s,d}$ are the SNR and the channel gain of the source-destination channel, respectively. Then the outage probability of direct transmission is found as

$$P_D^{out}(SNR, R) := \Pr[I_D < R] = \Pr\left[\left|\alpha_{s,d}\right|^2 < \frac{2^R - 1}{SNR}\right] = 1 - \exp\left(-\frac{2^R - 1}{SNR\sigma_{s,d}^2}\right) \sim \frac{1}{\sigma_{s,d}^2}\frac{2^R - 1}{SNR}, \tag{4.2}$$

where := is the operator standing for definition, $e^x = \sum_{n=0}^{\infty} \frac{x^n}{n!}$ has been applied for the third equation, R is the target data rate, $\sigma_{s,d}$ is the standard deviation of the AWGN on the source-destination channel, and from which the optimal diversity-multiplexing trade-off, defined in (3.35) to (3.47), of direct transmission can be presented as

$$d_D^*(r) = (1 - r)^+. \tag{4.3}$$

4.2 Amplify-forward protocols

In the AF protocols, the source signals are scaled up in power at the relay nodes before being forwarded to the destination node. Thus, sometimes they are referred as analogue protocols. The original AF protocol is proposed in [16]. Later, this protocol is optimised in [52, 60, 61, 63, 67].

4.2.1 Fixed relaying

In fixed relaying, a relay node is always involved in the transmission of the source information regardless the quality of the source information received. Such relaying algorithm makes the structure of the relay nodes simple but has a side effect that the forwarded source information from the relay nodes can be corrupted and can be treated as noise at the destinations. In this case, energy consumed at the relay nodes for cooperation has little performance improvement for return.

Figure 4-1 illustrates a CC system, where two source nodes ($s_{(i)}$, $i = 1, 2$) help each other to deliver information to different destination nodes ($d_{(i)}$). When time division multiple access (TDMA) is required for radio access, the half-duplex nature of these nodes needs to be taken into account. One example of such a scheme is shown in Figure 4-2, where T is the duration for one transmission period and Tx and Rx stand for transmission and reception, respectively. The original AF protocol is built based on the orthogonal time division, i.e., (b) and (c) in this figure.

In AF protocols, each source node amplifies the received information along with the noise before re-transmitting the information to the destination. Thus, the received information at the destination regarding either of the source nodes can be modelled as [16]

$$\underbrace{\begin{bmatrix} y_d(t) \\ y_d(t+T/4) \end{bmatrix}}_{\mathbf{Y}_d(t)} = \underbrace{\begin{bmatrix} \alpha_{s,d} \\ \alpha_{r,d}\upsilon\alpha_{s,r} \end{bmatrix}}_{\mathbf{A}} \mathbf{X}_s(t) + \underbrace{\begin{bmatrix} 0 & 1 & 0 \\ \alpha_{r,d}\upsilon & 0 & 1 \end{bmatrix}}_{\mathbf{B}} \underbrace{\begin{bmatrix} z_r(t) \\ z_d(t) \\ z_d(t+T/4) \end{bmatrix}}_{\mathbf{Z}(t)}, \tag{4.4}$$

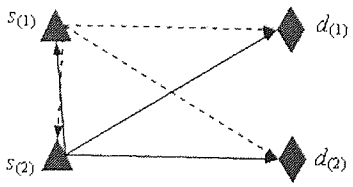

Figure 4-1 A cooperative system with two source and two destination nodes.

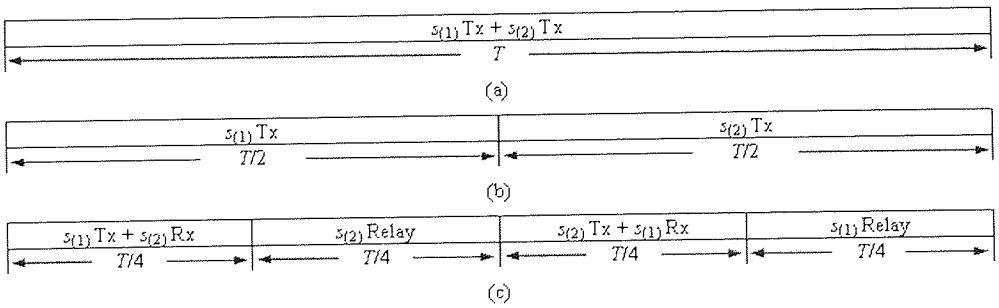

Figure 4-2 An example of TDMA schemes. (a) Direct transmission with interference; (b) Orthogonal direct transmission; (c) Orthogonal cooperation/cooperative system.

where $\mathbf{Y}_d(t)$ is the vector of the received signals at the destination; $\mathbf{A}$ is the vector of channel gains; $\mathbf{B}$ is the amplification matrix for noise; $\mathbf{Z}(t)$ is the vector of received noise at the destination; $\alpha_{i,j}$, $i \in \{s, r\}$, $j \in \{r, d\}$, $\sim CN(0, \sigma_{i,j}^2)$; z_j are AWGN, $\sim CN(0, \sigma_j^2)$; υ is the so-called amplification factor and has an upper bound [16]

$$\upsilon \le \sqrt{\frac{P_r}{\left|\alpha_{s,r}\right|^2 P_s + \sigma_r^2}}, \tag{4.5}$$

where P_s and P_r are the transmitted power of the source node and the relay node, respectively. Thus, for the memoryless channels, the mutual information of the AF protocol for one source-destination pair, can be found as [16]

$$I_{AF} \le I(\mathbf{X}_s; \mathbf{Y}_d) \le \frac{1}{2}\log_2\left[\det\left(\mathbf{I} + \left(P_s \mathbf{A}\mathbf{A}^*\right)\left(\mathbf{B}\boldsymbol{\Psi}_{\mathbf{Z}}\mathbf{B}^*\right)^{-1}\right)\right], \tag{4.6}$$

where $\boldsymbol{\Psi}_{\mathbf{Z}} = \mathrm{diag}(\sigma_r^2, \sigma_d^2, \sigma_d^2)$. Then, the maximum mutual information, achieved with a Gaussian input and the maximal υ, can be expressed as [16]

$$\begin{aligned} I_{AF} &= \frac{1}{2}\log_2\left(1 + \frac{P_s\left|\alpha_{s,d}\right|^2}{\sigma_d^2} + \frac{P_s\left|\alpha_{r,d}\upsilon\alpha_{s,r}\right|^2}{\left(\left|\alpha_{r,d}\upsilon\right|^2\sigma_r^2 + \sigma_d^2\right)}\right) \\ &= \frac{1}{2}\log_2\left(1 + SNR_{s,d}\left|\alpha_{s,d}\right|^2 + f\left(SNR_{s,r}\left|\alpha_{s,r}\right|^2, SNR_{s,r}\left|\alpha_{s,r}\right|^2\right)\right), \end{aligned} \tag{4.7}$$

where $f(a, b) = ab/(a+b+1)$. Eq. (4.7) is equivalent to the maximal mutual information of the fixed AF (FAF) protocol. Assuming that SNRs in this section are the same, the asymptotic outage probability of FAF can thus be calculated as [16]

$$P_{FAF}^{out}(SNR, R) = \Pr\left[I_{AF} < R\right] \sim \left(\frac{1}{2\sigma_{s,d}^2}\frac{\sigma_{s,r}^2 + \sigma_{r,d}^2}{\sigma_{s,r}^2\sigma_{r,d}^2}\right)\left(\frac{2^{2R} - 1}{SNR}\right)^2. \tag{4.8}$$

Then the optimal diversity-multiplexing trade-off of FAF is

$$d^*_{FAF}(r) = 2(1-2r)^+. \tag{4.9}$$

4.2.2 Selection relaying

In selection relaying, each relay node is able to decide on their own whether or not they should forward the source information to the destination node. The decision criterion is based on the quality of the source-relay channels and the transmit power of the source node. The drawback of this relaying algorithm is the hardware complexity of the relay nodes.

For the selection AF (SAF) protocol, the maximum mutual information is

$$I_{SAF} = \begin{cases} \frac{1}{2}\log_2\left(1+2SNR\left|\alpha_{s,d}\right|^2\right), & \left|\alpha_{s,r}\right|^2 \le g(SNR) \\ I_{AF}, & \left|\alpha_{s,r}\right|^2 \ge g(SNR) \end{cases} \tag{4.10}$$

where $g(SNR) = (2^{2R}-1)/SNR$. The calculation of the outage probability of SAF is similar to that of the selection DF (SDF) protocol in Subsection 4.3.2.

4.2.3 Incremental relaying

Comparing with the fixed relaying and the selection relaying algorithms, incremental relaying is claimed to offer the highest spectral efficiency. In this strategy, the source and the relay nodes are informed by the destination node through a 1-bit feedback about whether the transmission on the source-destination channel is successful or failed. If failed, the relay nodes should re-transmit the source information; otherwise, the source node can continuously send out new information. The feedback channels from the destination to the relay nodes are critical to the implementation of this relaying algorithm.

For the incremental AF (IAF) protocol, the maximum mutual information is

$$I_{IAF} = \begin{cases} I_D, & \left|\alpha_{s,d}\right|^2 \ge g'(SNR) \\ I_{AF}, & \left|\alpha_{s,d}\right|^2 \le g'(SNR) \end{cases} \tag{4.11}$$

where $g'(SNR) = (2^R-1)/SNR$. The outage behaviour of IAF can be found as [16]

$$\begin{aligned} P_{IAF}^{out}(SNR,R) &= \Pr[I_D < R]\Pr[I_{AF} < R/2 | I_D < R] \\ &= \Pr[I_D < R]\frac{\Pr[I_{AF} < R/2, I_D < R]}{\Pr[I_D < R]} \\ &= \Pr[I_{AF} < R/2], \end{aligned} \tag{4.12}$$

where $\Pr[I_{AF} < R/2,\ I_D < R] = \Pr[I_{AF} < R/2]$ is because the outage event of relaying taking place includes that of the direct transmission. In IAF, the expected spectral efficiency is a mean value as [16]

$$\begin{aligned} \overline{R} &= R\Pr\left[|\alpha_{s,d}|^2 \geq g'(SNR)\right] + \frac{R}{2}\Pr\left[|\alpha_{s,d}|^2 < g'(SNR)\right] \\ &= \frac{R}{2}\left[1+\exp\left(-\frac{2^R-1}{SNR}\right)\right] \\ &:= q(R,SNR). \end{aligned} \tag{4.13}$$

Define $\tilde{q}^{-1}(\overline{R},SNR) := \min q^{-1}(\overline{R},SNR)$ to be the smallest R required to reduce the outage probability in (4.12) as well as to retain the expected spectral efficiency in (4.11). Thus, the asymptotic outage probability of IAF can be computed from [16]

$$P_{IAF}^{out}\left(SNR,\tilde{q}^{-1}(\overline{R},SNR)\right) \sim \left(\frac{1}{2\sigma_{s,d}^2}\frac{\sigma_{s,r}^2+\sigma_{r,d}^2}{\sigma_{s,r}^2\sigma_{r,d}^2}\right)\left(\frac{2^{\overline{R}}-1}{SNR}\right)^2. \tag{4.14}$$

Then the optimal diversity-multiplexing trade-off of IAF can be found as

$$d_{IAF}^*(r) = 2(1-r)^+. \tag{4.15}$$

4.2.4 Non-orthogonal relaying

For the AF protocols with a single relay node in fixed or selection relaying algorithms, the maximum mutual information can be generalised to [52]

$$\mathbf{Y} = \begin{bmatrix} \alpha_{s,d}\mathbf{A}_1 & 0 \\ \alpha_{r,d}\alpha_{s,r}\mathbf{B}\mathbf{A}_1 & \alpha_{s,d}\mathbf{A}_2 \end{bmatrix}\mathbf{X} + \begin{bmatrix} 0 \\ \alpha_{r,d}\mathbf{B} \end{bmatrix}\mathbf{Z}_r + \mathbf{Z}_d, \tag{4.16}$$

where $[\mathbf{X}]_L$ and $[\mathbf{Y}]_L$ (L is the length of the original source information) are the information sent by the source node and received by the destination node, respectively; $[\mathbf{A}_1]_{L'\times L'}$ and $[\mathbf{A}_2]_{(L-L')\times(L-L')}$ (L' is the length of the source information that is sent out by the relay node) are diagonal matrices; $[\mathbf{B}]_{(L-L')\times L'}$ can be considered as the amplification matrix at the relay node; $[\mathbf{Z}_r]_{L'}$ and $[\mathbf{Z}_d]_L$ are the vectors of AWGN observed by the relay and the destination nodes, respectively. In this generalization, the source node is allowed to continue transmitting new information during the second phase which is assigned for the relay node only in the original AF protocol. The relay node uses a different codebook[1] known by all the nodes in the network. It also suggests that no more diversity gain can be achieved when more than one relay node forward the same source information *simultaneously* in Phase II. This is because multiple relay nodes only lead to $\alpha_{r,d}\alpha_{s,r}\mathbf{B}\mathbf{A}_1$ being replaced by $\Sigma_r\alpha_{r,d}\alpha_{s,r}\mathbf{B}\mathbf{A}_1$ and $\alpha_{r,d}\mathbf{B}$ by $\Sigma_r\alpha_{r,d}\mathbf{B}$, where neither achieves additional diversity gain. By letting $L' = L/2$, $\mathbf{A}_1 = \mathbf{I}_{L'}$, $\mathbf{A}_2 = 0$ and $\mathbf{B} = \upsilon\mathbf{I}_{L'}$, (4.16) is identical to (4.4). The maximum mutual information for large SNR of this generalised AF (GAF) protocol is found as [52]

$$\lim_{SNR\to\infty}\frac{\max_{\Psi_\mathbf{X}} I_{GAF}(\mathbf{X};\mathbf{Y})}{\log_2(SNR)} = (L-2l')(1-v_{s,d})^+ + l'(\max\{2(1-v_{s,d}),1-(v_{r,d}+v_{s,r})\})^+, \quad (4.17)$$

where $l' \le \min(L', L-L')$; $\Psi_\mathbf{X}$ is the covariance matrix of the input $\mathbf{X}$; $v_{s,d}$, $v_{r,d}$ and $v_{s,r}$ are the exponential orders of $|\alpha_{s,d}|^2$, $|\alpha_{r,d}|^2$ and $|\alpha_{s,r}|^2$, respectively. Then the outage probability becomes [52]

$$P_{GAF}^{out}(SNR,R) = \Pr\{(L-2c)(1-v_{s,d})^+ + c(\max\{2(1-v_{s,d}),1-(v_{r,d}+v_{s,r})\})^+ < LR\} \quad (4.18)$$

By using Lemma 5 in [46], the upper bound of the optimal diversity-multiplexing trade-off can be found [52]

[1] The different codebook should be uncorrelated to the codebooks used by other transmitters. As claimed in information theory, Gaussian codebooks are recommended for maximum mutual information between the source and the destination nodes.

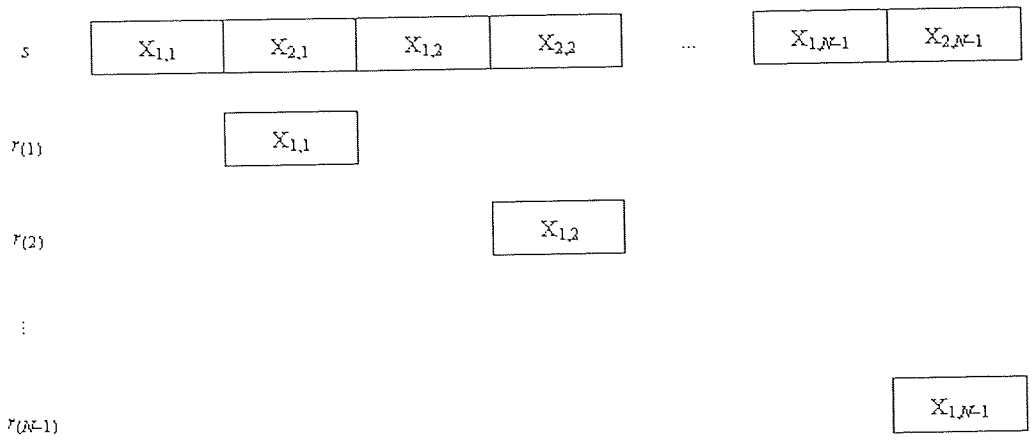

Figure 4-3 The TDMA scheme for NAF with N–1 relay nodes.

$$d^{*}_{GAF}(r) \le d_{out}(r) = (1-r) + (1-2r)^{+}. \tag{4.19}$$

The upper bound is achieved when $c = L' = L/2$, $\mathbf{A}_1 = \mathbf{A}_2 = \mathbf{I}_{L/2}$ and $\mathbf{B} = \upsilon\mathbf{I}_{L/2}$. In this case, the source node can transmit new information in Phase II during which the relay node repeats its observation of the source information in Phase I. This protocol is named as non-orthogonal AF (NAF). For this protocol to work properly, the destination node needs to know $\mathbf{B}$ and all the channel gains. The most significant advantage of this protocol is the enhancements in both spectral efficiency and diversity gain, i.e., data rate enhancement via continuous transmission on the source-destination channel and diversity enhancement via cooperation.

The single-relay-node NAF protocol can be easily extended to the case with N–1 relay nodes as shown in Figure 4-3. In this case, each relay node *in turn* forwards the source information it observed in Phase I. Correspondingly, the optimal diversity-multiplexing trade-off for this generalised case can be presented as [52]

$$d^{*}_{NAF}(r) = (1-r) + (N-1)(1-2r)^{+}. \tag{4.20}$$

4.2.5 Opportunistic relaying

In this type of relaying algorithm proposed in [67], a *best* relay node is said to be chosen as the forwarding node among the N relay nodes, when the channel condition associated with it meets the criterion, i.e.,

$$\min\left(\left|\alpha_{s,r}\right|^2,\left|\alpha_{r,d}\right|^2\right)=\max\left\{\min\left(\left|\alpha_{s,r(1)}\right|^2,\left|\alpha_{r(1),d}\right|^2\right),\ldots,\min\left(\left|\alpha_{s,r(N)}\right|^2,\left|\alpha_{r(N),d}\right|^2\right)\right\}. \quad (4.21)$$

The poorer channel associated with the best relay node is surely stronger than the poorer channels associated with other relay nodes, increasing the probability of successful relaying. Thus, the outage probability of the opportunistic AF (OAF) protocol can be computed as [67]

$$\begin{aligned}
&P_{OAF}^{out}(SNR,R)\\
&=\Pr\left[I_{AF}(\mathbf{X}_s;\mathbf{Y}_d)<R=r\log_2 SNR\right]\\
&=\Pr\left[1+SNR\left|\alpha_{s,d}\right|^2+f\left(SNR\left|\alpha_{s,r}\right|^2,SNR\left|\alpha_{r,d}\right|^2\right)<SNR^{2r}\right]\\
&\le\Pr\left[\left|\alpha_{s,d}\right|^2<SNR^{2r-1},f\left(SNR\left|\alpha_{s,r}\right|^2,SNR\left|\alpha_{r,d}\right|^2\right)<SNR^{2r}\right]\\
&\le\Pr\left[\left|\alpha_{s,d}\right|^2<SNR^{2r-1},\min\left(\left|\alpha_{s,r}\right|^2,\left|\alpha_{r,d}\right|^2\right)<SNR^{2r-1}+SNR^{r-1}\sqrt{1+SNR^{2r}}\right]\\
&\doteq SNR^{2r-1}SNR^{N(2r-1)}\\
&=SNR^{(N+1)(2r-1)},
\end{aligned} \quad (4.22)$$

where $f(a, b)$ is the same as that in (4.7). Thus, the optimal diversity-multiplexing trade-off of OAF, that is, the exponential order of SNR, can be found as

$$d_{OAF}^{*}(r)\le(N+1)(1-2r)^{+}. \quad (4.23)$$

Later, it will be revealed that OAF can achieve the upper bound of selection (distributed) space-time-coding-based DF in Section 4.3.2. This has been claimed as the most significant advantage of opportunistic relaying, i.e., the simpler relay node structure can achieve the same performance as that of a more complex relay node structure.

4.2.6 Clustered relaying

How to maximise the diversity gain is always an open and critical issue for CC systems. One of the many possible answers to the question may be found in [60, 61],

regarding the location of relay nodes. The following is focused on how the clusters are formed to maximise the diversity gain in CC systems.

Consider a relaying system with one source node (s), two relay nodes ($r_{(1)}$ and $r_{(2)}$) and one destination node (d). Number these nodes from 1 to 4. When the relay nodes are located closely to either the source node or the destination node, they are either in the AWGN area or in the Rayleigh fading area.

First, assuming that both relay nodes are in the Rayleigh fading area and no CSI known to the transmitters, the achievable rate R for a coding scheme C is upper-bounded by, given the channel gain matrix $\mathbf{H}$, and using max-flow min-cut theorem [69],

$$R(\mathbf{H}) \le \min\{I(X_1; Y_2, Y_3, Y_4 | X_2, X_3, \mathbf{H}), I(X_1, X_2; Y_3, Y_4 | X_3, \mathbf{H}), I(X_1, X_3; Y_2, Y_4 | X_2, \mathbf{H}), I(X_1, X_2, X_3; Y_4 | \mathbf{H})\}, \tag{4.24}$$

for some $p(x_1, x_2, x_3)$. In (4.24), the ith mutual information term represents the ith cut set CS_i, i.e., $CS_1 = \{s\}$, $CS_2 = \{s, r_{(1)}\}$, $CS_3 = \{s, r_{(2)}\}$ and $CS_4 = \{s, r_{(1)}, r_{(2)}\}$. For all i [60],

$$P(R(\mathbf{H}) < R) \ge P(I_i < R) \ge \min_{p(x_1,x_2,x_3)} P(I_i < R) = P_{out,CS_i}, \tag{4.25}$$

where P_{out, CS_i} is the outage probability of the ith cut set. Since $P(R(\mathbf{H}) < R) \ge \max_i P_{out, CS_i}$, the outage probability of the system using any coding scheme can be found as [60]

$$P_{out} = \min_{\text{any } C} P(R(\mathbf{H}) < R) \ge \max_i P_{out,CS_i}, \tag{4.26}$$

which suggests that the largest outage of the cut set terms provides the lower bound of the outage probability of this CC system.

The four mutual information terms in (4.24) can be considered to represent three equivalent multiple-antenna systems at the high SNR regime, i.e., one 1×3 single-input multiple-output (SIMO) system for CS_1, one 3×1 multiple-input single-output (MISO) system for CS_4 and two 2×2 MIMO systems for CS_2 and CS_3. For the SIMO and MISO systems, the maximum achievable diversity gain is 3. For the MIMO systems, it is 4. Using the FAF protocol, the diversity gain at 3 can be achieved, regardless the location

of the relay nodes when they are in the Rayleigh fading area. However, the diversity gain at 4 is only achievable when one relay node is clustered with the source node and the other one with the destination node and both relay nodes are in the AWGN area, forming a virtual MIMO system.

4.3 Decode-forward protocols

In the DF protocols, the source information is first decoded by the relay nodes. Then, the relay nodes will re-encode the source information, using either same or different (uncorrelated from the one used by the source node) codebook. In this protocol family, the relay node decodes the source information fully or symbol-by-symbol.

4.3.1 Fixed relaying

For the TDMA scheme shown in Figure 4-2, the maximum mutual information of fixed DF (FDF) is found to be [16]

$$I_{FDF} = \frac{1}{2}\min\left\{\log_2\left(1+SNR\left|\alpha_{s,r}\right|^2\right), \log_2\left(1+SNR\left|\alpha_{s,d}\right|^2+SNR\left|\alpha_{r,d}\right|^2\right)\right\}, \tag{4.27}$$

which is established according to the max-flow min-cut theorem. The first term in (4.27) represents the maximum rate at which the relay node can reliably decode the source information, while the second term shows the maximum rate at which the destination node can reliably decode the source information transmitted from the source and the relay nodes, respectively. The mutual information of FDF is achieved when both the relay node and the destination node decode the entire information without error. The outage probability of FDF is expressed as [16]

$$\begin{aligned} P_{FDF}^{out}(SNR,R) &= \Pr[I_{FDF} < R] \\ &= \Pr\left[\left|\alpha_{s,r}\right|^2 < g(SNR)\right] \\ &\quad + \Pr\left[\left|\alpha_{s,r}\right|^2 \geq g(SNR)\right]\Pr\left[\left|\alpha_{s,d}\right|^2+\left|\alpha_{r,d}\right|^2 < g(SNR)\right] \\ &\sim \frac{1}{\sigma_{s,r}^2}\frac{2^{2R}-1}{SNR}. \end{aligned} \tag{4.28}$$

Thus, the optimal diversity-multiplexing trade-off of FDF can be found as

$$d_{FDF}^{*}(r)=(1-2r)^{+}. \tag{4.29}$$

4.3.2 Selection relaying

If the relay nodes are allowed to forward the source information selectively, the maximum mutual information of the system can be derived from [16]

$$I_{SDF}=\begin{cases}\frac{1}{2}\log_2\left(1+2SNR\left|\alpha_{s,d}\right|^2\right), & \left|\alpha_{s,r}\right|^2<g(SNR)\\ \frac{1}{2}\log_2\left(1+SNR\left|\alpha_{s,d}\right|^2+SNR\left|\alpha_{r,d}\right|^2\right), & \left|\alpha_{s,r}\right|^2\geq g(SNR)\end{cases} \tag{4.30}$$

where a relay node will inform the source node of its decision and the source node is responsible for repeating the information it has just sent out, when the relay node decides to stay silent. Consequently, the outage probability is [16]

$$\begin{aligned}P_{SDF}^{out}(SNR,R)&=\Pr[I_{SDF}<R]\\&=\Pr\left[\left|\alpha_{s,r}\right|^2<g(SNR)\right]\Pr\left[2\left|\alpha_{s,d}\right|^2<g(SNR)\right]\\&\quad+\Pr\left[\left|\alpha_{s,r}\right|^2\geq g(SNR)\right]\Pr\left[\left|\alpha_{s,d}\right|^2+\left|\alpha_{r,d}\right|^2<g(SNR)\right]\\&\sim\left(\frac{1}{2\sigma_{s,d}^2}\frac{\sigma_{s,r}^2+\sigma_{r,d}^2}{\sigma_{s,r}^2\sigma_{r,d}^2}\right)\left(\frac{2^{2R}-1}{SNR}\right)^2.\end{aligned} \tag{4.31}$$

Thus, the optimal diversity-multiplexing trade-off of SDF can be found as

$$d_{SDF}^{*}(r)=2(1-2r)^{+}. \tag{4.32}$$

For the cooperation among more than two source nodes, the maximum mutual information of selection repetition-based DF (S-R-DF) as shown in Figure 4-4 (b) can be expressed as [59]

$$I_{S-R-DF}=\frac{1}{N}\log\left(1+SNR\left|\alpha_{s,d(s)}\right|^2+SNR\sum_{r\in D(s)}\left|\alpha_{r,d(s)}\right|^2\right), \tag{4.33}$$

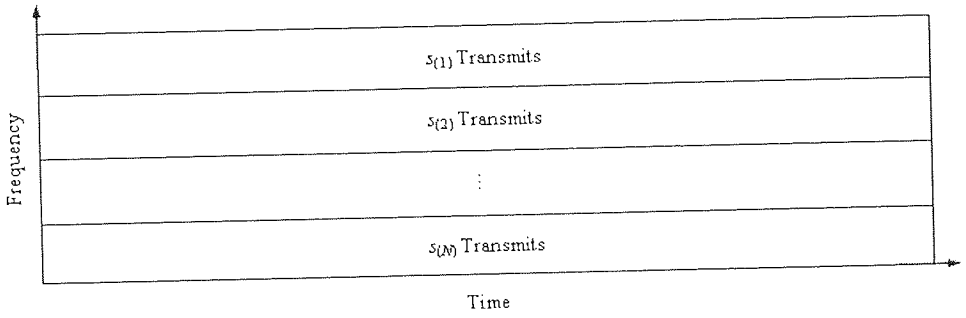

(a)

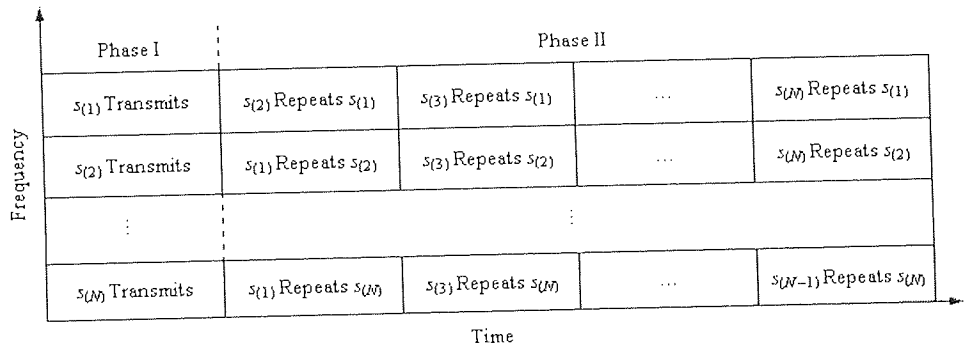

(b)

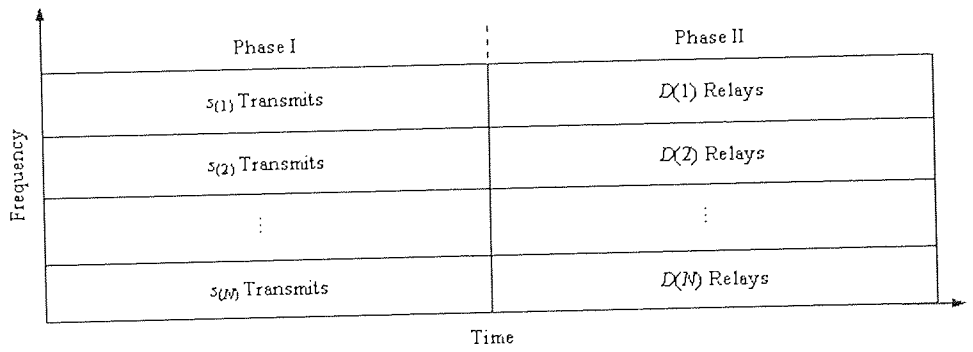

(c)

Figure 4-4 The medium access control for N source nodes in selection cooperative systems. (a) Non-cooperative; (b) Repetition-based; (c) Space-time-coding-based.

where $d(s)$ represents the destination node associated with one particular source node; $D(s)$ is the set of the decoding relay nodes that are able to fully decode the source information. Thus, the outage probability can be computed from [59]

$$P_{S-R-DF}^{out}(SNR,R)=\Pr[I_{S-R-DF}<R]=\sum_{D(s)}\Pr[D(s)]\Pr[I_{S-R-DF}<R|D(s)]$$
$$\sim\left[\frac{2^{NR}-1}{SNR}\right]^{N}\sum_{D(s)}\lambda_{s,d(s)}\prod_{r\in D(s)}\lambda_{r,d(s)}\prod_{r\notin D(s)}\lambda_{s,r}\frac{1}{(|D(s)|+1)!}, \qquad (4.34)$$

where λ is the parameter of the exponential distribution under the assumption that all the wireless channels suffer from the Rayleigh fading.

When the selection (distributed) space-time-coding-based DF (S-STC-DF) protocol is applied in CC systems, the spectral efficiency can be enhanced dramatically as illustrated in Figure 4-4 (c). The maximum mutual information of this protocol is given in [59]

$$I_{S-STC-DF}=\frac{1}{2}\log\left(1+\frac{2}{N}SNR\left|\alpha_{s,d(s)}\right|^{2}\right)+\frac{1}{2}\log\left(1+\frac{2}{N}SNR\sum_{r\in D(s)}\left|\alpha_{r,d(s)}\right|^{2}\right). \qquad (4.35)$$

where $2/N$ is used because each source node transmits in half of the available degree of freedom in S-STC-DF instead of $1/N$ in S-R-DF, and therefore, the power constraint $P_{\text{S-STC\_DF}} = (2/N)P_{\text{S-R-DF}}$. Based on (4.35), the outage probability of S-STC-DF can be found as [59]

$$P_{S-STC-DF}^{out}(SNR,R)=\Pr[I_{S-STC-DF}<R]=\sum_{D(s)}\Pr[D(s)]\Pr[I_{S-STC-DF}<R|D(s)]$$
$$\sim\left[\frac{2^{2R}-1}{2SNR/N}\right]^{N}\sum_{D(s)}\lambda_{s,d(s)}\prod_{r\in D(s)}\lambda_{r,d(s)}\prod_{r\notin D(s)}\lambda_{s,r}\times A_{|D(s)|}\left(2^{2R}-1\right), \qquad (4.36)$$

where $A_n(t)=\frac{1}{(n-1)!}\int_0^1\frac{w^{n-1}(1-w)}{1+tw}dw,\quad n>0$. Using the convenient bounds of (4.34) and (4.36), the optimal diversity-multiplexing trade-off of S-R-DF and S-STC-DF can be found as, respectively,

$$d^*_{S-R-DF}(r) = N(1-Nr)^+ \tag{4.37}$$

and
$$(N-2Nr-2r)^+ \le d^*_{S-STC-DF}(r) \le N(1-2r)^+. \tag{4.38}$$

For both S-STC-DF and S-R-DF, a relay node is said to be involved in Phase II, if

$$|\alpha_{s,r}|^2 > \frac{\left(2^{NR}-1\right)}{SNR}. \tag{4.39}$$

4.3.3 Incremental relaying

When incremental relaying is employed, the maximum mutual information of the DF cooperative system can be expressed as

$$I_{IDF} = \begin{cases} I_D, & |\alpha_{s,d}|^2 \ge g'(SNR) \\ \frac{1}{2}\log_2\left(1+SNR|\alpha_{s,d}|^2+SNR|\alpha_{r,d}|^2\right), & |\alpha_{s,d}|^2 \le g'(SNR) \end{cases} \tag{4.40}$$

The outage events of IDF are the same as those of IAF as given in (4.12). Thus, the outage probability of IDF can be found in a similar way.

4.3.4 Dynamic relaying

In this protocol proposed in [52], abbreviated as DDF, the relay node keeps listening to the source information until it has gained enough mutual information to successfully decode the source information. Therefore, the time length for the relay node to cooperate is dynamic, depending on the channel condition. When the relay node re-encodes the source information, it can use a different and independent codebook. Denote L as the number of the consecutive symbols in the source information and L' as the number of the symbols that the relay node needs to listen to for successful decoding. Thus, the minimum mutual information required at the relay node is LR and L' can be found to meet [52]

$$L' = \min\left\{L, \left\lceil \frac{LR}{\log_2\left(1 + SNR\left|\alpha_{s,r}\right|^2 \sigma_d^2/\sigma_r^2\right)} \right\rceil\right\}. \tag{4.41}$$

Then, the received signals at the destination node can be presented as [52]

$$\mathbf{Y}_i = \begin{cases} \alpha_{s,d}\mathbf{X}_i + \mathbf{Z}_{d|i}, & 1 \le i \le L' \\ \alpha_{s,d}\mathbf{X}_i + \alpha_{r,d}\tilde{\mathbf{X}}_i + \mathbf{Z}_{d|i}, & L' \le i \le L \end{cases} \tag{4.42}$$

where $\tilde{\mathbf{X}}_i$ represents the signal is sent from the relay node. In DDF, the destination node needs to learn L', $\alpha_{s,d}$ and $\alpha_{r,d}$. Then, the optimal diversity-multiplexing trade-off is given by [52]

$$d^*_{DDF}(r) = \begin{cases} 2(1-r), & 0 \le r \le \frac{1}{2} \\ (1-r)/r, & \frac{1}{2} \le r \le 1 \end{cases} \tag{4.43}$$

The single-relay DDF protocol can also be generalised to the case of multiple relay nodes. In the generalised protocol, the source node still transmits new information continuously and each relay node listens until the mutual information received from the source node and other relay nodes exceeds LR. Once a relay node can successfully decode source information, it will forward the re-encoded source information during $(L-L')/R$. The optimal diversity-multiplexing trade-off of DDF with $N-1$ relay nodes can be computed as [52]

$$d^*_{N-DDF}(r) = \begin{cases} N(1-r), & 0 \le r \le 1/N \\ 1 + (N-1)(1-2r)/(1-r), & 1/N \le r \le 0.5 \\ (1-r)/r, & 0.5 \le r \le 1 \end{cases} \tag{4.44}$$

4.3.5 Opportunistic relaying

Opportunistic relaying can also be applied to repetition based DF, abbreviated O-R-DF. Denote O as the event that the best relay node can successfully decode the source

information and O^C as the complimentary event of O. Thus, the outage probability of O-R-DF is found as

$$\begin{aligned}
&P_{O-R-DF}^{out}(SNR,R)\\
&=\Pr\left[I_{S-R-DF}<r\log_2 SNR|O\right]\Pr(O)+\Pr\left[I_{S-R-DF}<r\log_2 SNR|O^C\right]\Pr\left(O^C\right)\\
&=\Pr\left[1+SNR\left(|\alpha_{s,d}|^2+|\alpha_{r,d}|^2\right)<SNR^{2r}\right]\Pr(O)+\Pr\left[1+SNR|\alpha_{s,d}|^2<SNR^{2r}\right]\Pr\left(O^C\right)\\
&\le\Pr\left[1+SNR\left(|\alpha_{s,d}|^2+|\alpha_{r,d}|^2\right)<SNR^{2r}\right]\\
&\quad+\Pr\left[1+SNR|\alpha_{s,d}|^2<SNR^{2r}\right]\Pr\left[1+SNR|\alpha_{s,r}|^2<SNR^{2r}\right]\\
&\le\Pr\left[|\alpha_{s,d}|^2+|\alpha_{r,d}|^2<SNR^{2r-1}\right]+\Pr\left[|\alpha_{s,d}|^2<SNR^{2r-1}\right]\Pr\left[|\alpha_{s,r}|^2<SNR^{2r-1}\right]\\
&\le\Pr\left[|\alpha_{s,d}|^2<SNR^{2r-1}\right]\Pr\left[|\alpha_{r,d}|^2<SNR^{2r-1}\right]\\
&\quad+\Pr\left[|\alpha_{s,d}|^2<SNR^{2r-1}\right]\Pr\left[|\alpha_{s,r}|^2<SNR^{2r-1}\right]\\
&\doteq SNR^{(N+1)(2r-1)},
\end{aligned}\tag{4.45}$$

where the proof can be found in [67]. Thus, the optimal diversity-multiplexing trade-off of O-R-DF is

$$d_{O-R-DF}^{*}(r)\le(N+1)(1-2r)^{+},\tag{4.46}$$

which is the same as (4.23) of OAF and also achieves the upper bound of S-STC-DF with simpler relay nodes in structure.

4.3.6 Clustered relaying

An encoding-decoding strategy will first be discussed and followed by the performance of clustered relaying for the DF protocol.

Consider a single source-destination cooperative relaying system with one full-duplex relay node, as shown in Figure 4-5. Thus, the achievable data rate of the DF protocol is up to [15]

$$R_{DF}=\max_{p(x_1,x_2)}\min\left\{I(X_1;Y_2|X_2),I(X_1X_2;Y_3)\right\},\tag{4.47}$$

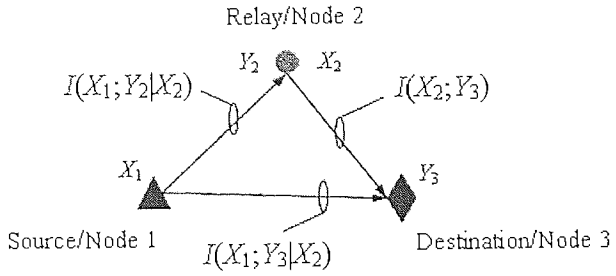

Figure 4-5 The information transfer for a three-node cooperative relaying system.

where $I(X_1;Y_2|X_2)$ is the mutual information observed by the relay node (shown in Figure 4-5) and $I(X_1X_2;Y_3)$ by the destination node.

A regular encoding approach [54, 70, 71] is employed at the transmitters, i.e., the source and the relay nodes. The message w is divided into B blocks w_1, w_2, ..., w_B of nR bits each. The coding approach is illustrated in Figure 4-6 for $B = 3$. The codeword $x_1(i, j)$ and $x_2(i)$ of length n are transmitted in $B+1$ durations, where i, j are between 1 and $2nR$. Therefore, the number of message bits $B_w = BnR$, the number of channel uses $N = n(B+1)$, and the overall rate $R_w = R \times B/(B+1)$. One can achieve the overall rate as close to R as targeted by having large B.

For the relay node to decode the source message, it can use either the maximum-likelihood or typical sequence decoder. By random coding arguments, the relay node can be guaranteed to decode the source message as long as n is large and [15]

$$R < I(X_1;Y_2|X_2) \tag{4.48}$$

Suppose that the relay node can decode $x_1(1, w_1)$ to correctly obtain w_1 in Duration 1. It will then transmit $x_2(w_1)$ in Duration 2, using either the same or different codebook that is used by the source node. This continues until the last block is transmitted.

Suppose that at the destination node, all the transmitted blocks have been received. Thus, the node can apply two different decoding techniques. First, it is the *backward decoding* [71]. Let y_{3b} be the bth received block at the destination node. In backward decoding technique, the first decoded block is the last block w_B from $y_{3(B+1)}$. Since $y_{3(B+1)}$ depends on $x_1(w_B, 1)$ and $x_2(w_B)$, w_B can be correctly decoded as long as n is large and [15]

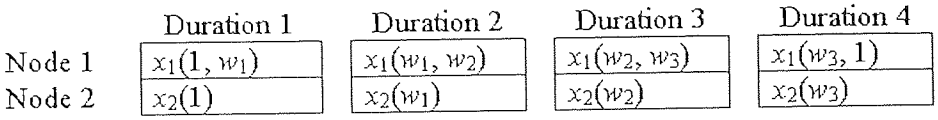

Figure 4-6 Regular encoding at the transmitters for $B = 3$.

$$R < I(X_1 X_2; Y_3). \tag{4.49}$$

Once the destination node correctly decodes w_B, it can then decode w_{B-1}. The process continues until w_1 is decoded.

The major disadvantage of backward decoding is the decoding delay as the last block is decoded first and the delay increases as B enlarges. This problem can be solved by another decoding technique – the *sliding-window* decoding technique, proposed by Carleial in [70]. The transmitted codeword remains the same as in Figure 4-6, but the destination node can decode w_1 first after Block 2 by using a sliding window of the past two received blocks from different transmitters y_{31} and y_{32}, i.e., $x_1(1, w_1)$ and $x_2(w_1)$. The destination node can correctly decode the source message as long as n is large and [15]

$$R < \underbrace{I(X_2; Y_3)}_{\text{from } y_{32}} + \underbrace{I(X_1; Y_3 | X_2)}_{\text{from } y_{31}} = I(X_1 X_2; Y_3). \tag{4.50}$$

The process continues until the last block w_B is decoded. The wireless channels between nodes s and t can be as [15]

$$\mathbf{Y}_t = \sum_{s \neq t} \frac{\mathbf{H}_{t,s}}{\sqrt{d_{s,t}^{\gamma}}} \mathbf{X}_s + \mathbf{Z}_t, \tag{4.51}$$

where $d_{s,t}$ is the normalised distance between the source and any other nodes, relative to the source-destination distance, as in (2.17); γ is the path loss exponent; $\mathbf{H}_{t,s}$ is the matrix of channel gains and $\mathbf{X}_s$, $\mathbf{Y}_t$ and $\mathbf{Z}_t$ are the vectors of the source information, the received information at the destination node and the destination noise, respectively. There is a power constraint on the transmitted codeword, i.e., $\mathrm{E}[\mathbf{X}_s \mathbf{X}_s^*] \leq P_s$. The data rate of full-duplex DF for several fading conditions is discussed in [54], which is summarised below.

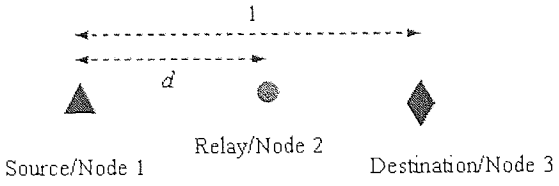

Figure 4-7 An example of node distribution.

- No fading: the entries of $\mathbf{H}_{t,s}$ are constants and known to all nodes. For one relay node, the best data rate in (4.47) can be found as [15]

$$R_{DF} = \max_{0\le|\Phi|\le 1} \min\left\{\log_2\left(1+\frac{P_1}{d_{1,2}^{\gamma}}\left(1-|\Phi|^2\right)\right), \log_2\left(1+\frac{P_1}{d_{1,3}^{\gamma}}+\frac{P_2}{d_{2,3}^{\gamma}}+\frac{2|\Phi|\sqrt{P_1P_2}}{\sqrt{d_{1,3}^{\gamma}d_{2,3}^{\gamma}}}\right)\right\}, \quad (4.52)$$

where Φ is the complex correlation coefficient between $\mathbf{X}_1$ and $\mathbf{X}_2$, defined in (3.1); P_1 and P_2 are the transmit power of the source node (Node 1) and the relay node (Node 2), respectively. Consider an example of the geographical distribution of the nodes as in Figure 4-7. Thus, when the relay node moves toward the source node, i.e., $d_{1,2} \to 0$ and $d_{2,3} \to 1$, and note $d_{1,3} = 1$, the DF data rate in (4.52) becomes [15]

$$R_{DF} = \log_2\left(1+P_1+P_2+2\sqrt{P_1P_2}\right) \quad (4.53)$$

On the other hand, when the relay node moves toward the destination node, i.e., $d_{1,2} \to 1$ and $d_{2,3} \to 0$, and note $d_{1,3} = 1$, the DF data rate is [15]

$$R_{DF} = \log_2\left(1+P_1\right) \quad (4.54)$$

Comparing (4.53) and (4.54), it can be remarked that the DF protocol performs better when the relay node is clustered with the source node.

For a network with N relay nodes, the best data rate for the DF protocol is [15]

$$R_{DF} = \log_2\left(1+\left[\sum_{t=1}^{N+1}\sqrt{P_t}\right]^2\right), \quad (4.55)$$

which is achieved when the relay nodes are clustered with the source node.

- Phase fading: the amplitude of the fading coefficients in $\mathbf{H}_{t,s}$ is assumed to be 1 and the phase experiences fading, i.e., $\mathbf{H}_{t,s}(i, j) = e^{j\theta_{t,s}(i, j)}$, where $\theta_{t,s}(i, j)$ is independently uniformly distributed over $[0, 2\pi)$. Thus, for networks with one relay node, the best data rate for the DF protocol in phase fading channel condition is [15]

$$R_{DF} = \log_2\left(1 + \frac{P_1}{d_{1,3}^{\gamma}} + \frac{P_2}{d_{2,3}^{\gamma}}\right), \tag{4.56}$$

as long as

$$\frac{P_1}{d_{1,3}^{\gamma}} + \frac{P_2}{d_{2,3}^{\gamma}} \le \frac{P_1}{d_{1,2}^{\gamma}}. \tag{4.57}$$

The condition defined in (4.57) implies that the relay nodes should be near the source node. This result can be generalised to Rayleigh fading, and to other random processes in which the phase varies uniformly over time and $[0, 2\pi)$.

For a network with N relay nodes, the best rate of DF protocol is found as [15]

$$R_{DF} = \log_2\left(1 + \sum_{t=1}^{N+1} \frac{P_t}{d_{t,N+2}^{\gamma}}\right), \tag{4.58}$$

as long as

$$\sum_{t=1}^{N+1} \frac{P_t}{d_{t,N+2}^{\gamma}} \le \max_{P(\bullet)} \min_{1 \le s \le N} \sum_{t \in P(1:s)} \frac{P_t}{d_{t,P(s+1)}^{\gamma}}, \tag{4.59}$$

where $P(\bullet)$ is a permutation on $\{1, 2, \ldots, N\}$ with $P(1) = 1$ and $P(N) = N$, and $P(i{:}j) = \{P(i), P(i+1), \ldots, P(j)\}$.

- Fading with directions, single-bounce fading and quasi-static fading: Similar conclusion can be drawn in these types of fading conditions that the relay

node(s) should be close to or clustered with the source node to offer the better performance for the full-duplex DF protocols.

4.4 Compress-forward protocols

CF protocols allow the relay nodes forward a quantised and compressed (estimated) version of the source information to the destination [15, 54].

Consider the same network topology[1] as in Figure 4-5. Thus, the highest achievable data rate of CF is [15]

$$R_{CF} = I\left(\mathbf{X}_1; \hat{\mathbf{Y}}_2 \mathbf{Y}_3 | \mathbf{X}_2\right), \tag{4.60}$$

where $\hat{\mathbf{Y}}_2$ is the estimate of $\mathbf{Y}_2$, the received source information at the relay node; the compression rate at the relay node must satisfy [15]

$$I\left(\hat{\mathbf{Y}}_2; \mathbf{Y}_2 | \mathbf{Y}_3 \mathbf{X}_2\right) \leq I\left(\mathbf{X}_2; \mathbf{Y}_3\right), \tag{4.61}$$

and the joint probability distribution of the random variables follows [15]

$$p(x_1)p(x_2)p\left(\hat{y}_2 | x_2, y_2\right)p\left(y_2, y_3 | x_1, x_2\right) \tag{4.62}$$

The compression techniques are developed by Wyner and Ziv in [72], where the received information at the destination node, $\mathbf{Y}_3$, is exploited by the relay node through a feedback channel.

For wireless channels with no fading, the best achievable data rate of the CF protocol for one relay node can be found as [15]

$$R_{CF} = \log_2\left(1 + P_1 + P_2\right), \tag{4.63}$$

[1] The relay node is also at full-duplex mode.

where P_1 and P_2 are respectively the transmit power of node 1 and 2, the relay node is moving toward the source node, $d_{1,2} \to 1$, and the nodes are located the same as in Figure 4-7. When the relay node is getting closer to the destination node, the data rate becomes [15]

$$R_{CF} = \log_2(1 + 2P_1). \tag{4.64}$$

Comparing (4.63) and (4.64), it can be drawn that the best achievable data rate of CF depends on both the location and the transmit power of the relay node. If $P_1 > P_2$, the relay node should be clustered with the destination node. If $P_1 < P_2$, it should be on the source node side. If $P_1 = P_2$, it can stay with either the source or the destination node.

4.5 Performance comparison

The diversity-multiplexing trade-off of various protocols discussed in the previous two sections is summarised in Figure 4-8 and Figure 4-9 for single relay node and multiple relay nodes cases, respectively.

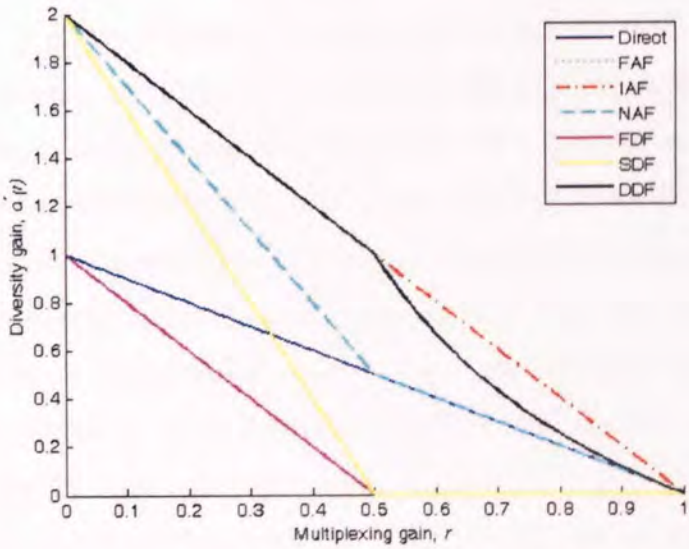

Figure 4-8 The diversity-multiplexing trade-off curves of the protocols with one relay node.

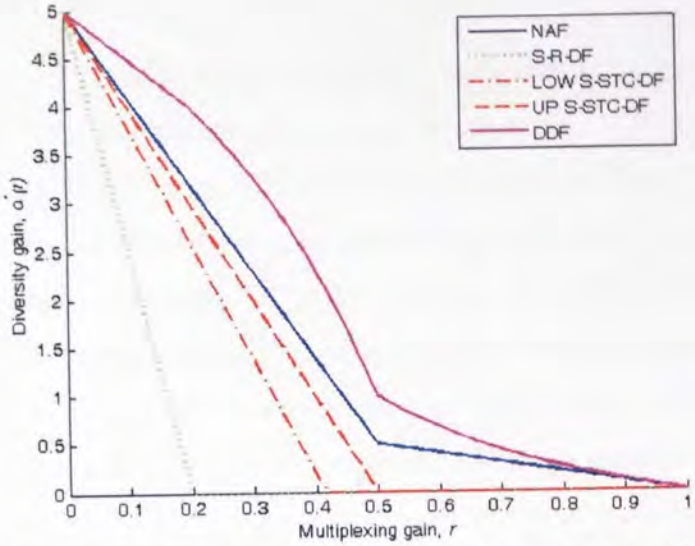

Figure 4-9 The diversity-multiplexing trade-off curves of the protocols with four relay nodes.

In the single-relay case, FAF and SDF have the same performance. They both outperform the direct transmission when the multiplexing gain, r, is lower than 0.35. They are also better than FDF. The best performance is offered by IAF, which proves the importance of the extra feedback channel from the destination node to the source node. The second best protocol is DDF. The deficit of diversity gain in this protocol compared to IAF for $r > 0.5$ is due to the fact that on the average the relay node is involved for transmitting only a fraction of the source information. For NAF, the half-duplex constraint on the antennas makes its performance identical to that of the direct transmission, when $r > 0.5$. In this regime, the information on the relay-destination channel is different from that on the source-destination channel and thus, is treated as interference by the destination node. Therefore, the relay-destination channel is unable to support achieving the multiplexing gain, as also suggested by $(1-2r)^+$ in (4.19).

In the multiple-relay case, the later proposed NAF and DDF are clearly the better protocols than the original S-R-DF and S-STC-DF, as shown in Figure 4-9. For $r > 0.5$ regime, the performance of the multi-node NAF is still identical to that of the direct transmission, for the same reason as in the single-node NAF. The performance of the opportunistic protocols overlaps with that of S-STC-DF, thus omitted in the graph. It is unclear why the performance of DDF drops so sharply when r is between 0 and 0.5. It may be subject to either the half-duplex constraint or the suboptimality of DDF [52].

4.6 Summary

The protocols and the algorithms for CC systems seek maximising the diversity gain with as little multiplexing gain compromised as possible. Different protocols are designed for the relay nodes to cope with different system conditions. The performance of these CC systems is evaluated through channel capacity and diversity-multiplexing trade-off. In the single-relay case, FAF and SDF have the same performance and are better than FDF. The best performance is offered by IAF which requires 1-bit feedback from the destination node to the source node. The second best protocol is DDF. For NAF, the half-duplex constraint on the antennas makes its performance identical to that of the direct transmission, when $r > 0.5$. In the multiple-relay case, the later proposed NAF and DDF are clearly the better protocols than the original S-R-DF and S-STC-DF. The performance of the opportunistic protocols overlaps with that of S-STC-DF. Later in Chapter 6, some of the protocols will be re-evaluated with the fading correlation taken into account. In Chapter 7, fixed and selection decode-forward protocols will be implemented using wireless sensor transceivers.

5 MIMO Channels in Scattered Fading Channels

The performance of MIMO channels in different propagation environments is subject to the conditions of scatterers such as their physical properties and density. The scatterers that the transmitted signals encounter in wireless propagation channels can be any obstacles, such as trees, cars, buildings, pedestrians and so on. Therefore, modelling scattering environment is crucial for characterising MIMO propagation channels and evaluating their performances. It is important to understand the extent of the impacts of scattering environments on channel performances. Such impacts can be investigated through examining the channel matrix of a MIMO system with respect to antenna correlation, matrix's condition number and mutual information/capacity. The chapter is focused on the investigation of how these MIMO channel performances are affected by the scatterer density in flat and frequency-selective fading channels.

It has been shown that formalising an appropriate scattering model in a particular channel environment plays significant roles in performance evaluation for MIMO channels. The traditional "one-ring" and "two-ring" scattering models have been extensively investigated in [7, 8, 42, 73] and [74, 75], respectively, for deriving the MIMO channel models and determining mutual information/capacity and correlation in such channels. The structure of scatterers is one of the key factors in channel modelling in both outdoor [9, 41, 76, 77] and indoor [11, 78] environments. Most channel models reported are constructed using the ray-tracing method, based on the scattering environment involved.

The purposes of the work in this chapter are to extend the previous work [9, 41] to a more realistic propagation environment and to investigate the effect of scatterer density on channel performances in a double-scattering environment featuring both remote and local scatterers. The investigation considers both flat fading and frequency-selective fading channels. The effect of scatterer density has been investigated by a few researchers in double-scattering environments. For example, in the MIMO scattering model given in Subsection 3.5.3 and [9], the radii of the scatterer zones (which are related to the scatterer density) govern the performances of the channel. This is because they affect the angular spread of both the transmitter and the receiver. In

another channel model given in Subsection 3.5.4 and [41], however, the scatterer density is found to have a marginal impact on channel performances when the total number of scatterers is fixed. The parameters used for defining scatterer density are slightly different in [41] and [9], i.e., the radius and the area of the scatterer zone are respectively used in the definition of scatterer density. Given the different scatterer structures that lead to different observations in [41] and [9] on the effect of scatterer density, the effect of scatterer density in a double-scattering environment is investigated, which is a combination of the scattering models of [41] and [9]. It is intended to discover the conditions that would lead to different conclusions over the impact of scatterer density that is defined as the ratio of the number of scatterers to the area covered by the scatterers, similar to that defined in [41] except for the shape of the scattering zones defined.

The double-scattering model concerned in this chapter features the linearly distributed scatterers for the remote scattering zone and the circularly and uniformly distributed scatterers for the local scattering zone of the receiver. This structure collectively represents the features from those in [41] and [9], but allowing more variations in parameters for investigating the impact of scatterer density. This scattering model may also be regarded as a "two-ring" model[1], assuming that the radius of the scatterer ring at the transmitter side is large enough to treat the concerned remote scatterers residing linearly. The scattering model is suitable for macrocellular wireless systems.

5.1 Double-scattering model and channel propagation model

In this section, the double-scattering model adopted is presented and the relevant channel propagation model is constructed. The abstract double-scattering model, as shown in Figure 5-1, describes a macrocellular environment, which is appropriate for certain urban areas, such as city squares, and suburban areas. The scattering model can be viewed as a "two-ring" model, where the scatterer ring at the transmitter side covers

[1] In the "two-ring" model, the transmitter is also surrounded by a scatterer ring, in additional to the receiver-side scattering ring in the "one-ring" model.

a larger area so that the remote scatterers of interest can be modelled as linearly distributed. The propagation model constructed by means of the ray-tracing method captures critical transmission parameters in wireless channels, such as free space loss, antenna settings, AOA at the receiver side and AOD at the transmitter side.

5.1.1 Double-scattering model

Figure 5-1 shows the structure of the double-scattering model for macrocellular propagation. In this macro-cell, the transmitter is elevated above the top roof of the highest building in the cell, where the transmitter is scatterer-free nearby. In the wireless channel, both local and remote scatterers introduce the multipath effect. The discrete linearly-distributed remote scatterers are closer to the local scatterers of the receiver than to the transmitter. The local scatterers surrounding the receiver are circularly and uniformly distributed within a ring of equal width, which implies that the signals impinging on the receive antennas arrive from all directions after bouncing off the local scatterers. Multipath signals are considered to bounce only once in each scatterer zone, with each of them being reflected by scatterers with a phase shift. It is also assumed that there is no LOS or quasi-LOS channel between the transmitter and the receiver.

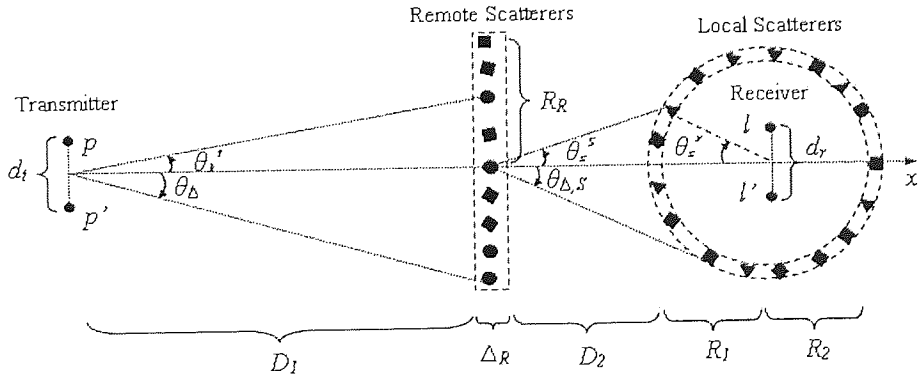

Figure 5-1 The double-scattering MIMO scattering environment.

5.1.2 Channel propagation model

A MIMO channel matrix is obtained from a channel propagation model that is composed of the elements characterising the propagation of the individual channels between transmit-receive antenna pairs. Each element incorporates the physical parameters in each individual propagation channel, such as the free space loss, antenna settings, AOA, AOD, and phase shifts caused by signal delay and the surface properties of the obstacles in the channel. A MIMO channel model can be described by an $M \times N$ matrix $\mathbf{H}(\omega)$, where $\mathbf{H}_{l,p}(\omega)$ is the channel gain from the pth transmit antenna to the lth receive antenna ($l = 1, \ldots, M$, $p = 1, \ldots, N$). The frequency-selective fading channel is represented by $n_r \times n_t$ channel gains, $\mathbf{H}_{l,p}(\omega)$, which reduces to MN scalar values $\mathbf{H}_{l,p}$ for a flat fading channel.

On the propagation channel between the pth transmit antenna and the lth receive antenna in the double-scattering model, the channel gain of one of the signal paths with respect to the specific angle of arrival and angle of departure can be modelled as, using the ray-tracing method, [79]

$$\mathbf{H}_{l,p|k,s}(\omega) = e^{-j\frac{\omega}{c}\left(D_{p,k}+D_{k,s}+D_{s,l}\right)+j\left(\phi_1\left(\theta_k^t\right)+\phi_2\left(\theta_s^r\right)\right)}, \tag{5.1}$$

where K and S denote the numbers of the remote and the local scatterers, respectively; $D_{p,k}+D_{k,s}+D_{s,l}$ calculates the path length between the pth transmit antenna and the lth receive antenna via the kth remote and the sth local scatterers; c is the velocity of carrier; and $\phi_1(\theta_k^t)$ and $\phi_2(\theta_s^r)$ are the phase shifts of the remote and the local scatterers, respectively. These phase shifts are associated with the individual scatterers and uniformly distributed in $[-\pi, \pi)$.

In this double-scattering model, the antenna pattern[1] at the receiver is assumed omnidirectional since the receiver locates at the centre of the scatterer ring, while at the transmitter the directional antennas are deployed for better signal strength. Denote $G_p^t(\theta_k^t)$ as the complex array antenna pattern for the pth transmit antenna, which can be represented as [11]

[1] Antenna pattern is a graphical representation in three dimensions of the radiation of the antenna as a function of the angular direction.

$$G_p^t(\theta_k^t) = g_p^t(\theta_k^t)\exp(j\Phi_p^t(\theta_k^t)) \tag{5.2}$$

where $g_p^t(\theta_k^t)$ is the real-valued antenna pattern as a function of the angular direction and $\Phi_p^t(\theta_k^t) = 2\pi x_p^t sin(\theta_k^t)$ is the phase shift in which x_p^t is the spacing between the pth antenna and the centre of the antenna array. For simplicity, the uniform antenna arrays are perpendicular to the x-axis, as shown in Figure 5-1. The phase shift in (5.7) can then be simplified to

$$\Phi_p^t(\theta_k^t) = 2\pi\left(p - \frac{n_t + 1}{2}\right)d_t \sin\theta_k^t. \tag{5.3}$$

During propagation, the free space loss in (2.4) is considered, where the path length of the signal rays can be determined through the AOD of the transmitter, θ_k^t, and the AOA of the receiver, θ_s^r, respectively. Thus, the free space loss model is presented as $L_f(\omega;\theta_k^t, \theta_s^r)$ here.

For all the signal paths between the two antennas, the channel gain of the channel between the pth transmit antenna and the lth receive antenna can be constructed as [79]

$$\mathbf{H}_{l,p}(\omega) = \frac{1}{\sqrt{KS}}\sum_{k=1}^{K}\sum_{s=1}^{S}\frac{G_p^t(\theta_k^t)}{\sqrt{L_f(\omega;\theta_k^t,\theta_s^r)}}H_{l,p|k,s}(\omega). \tag{5.4}$$

5.2 Performances in flat fading channels

This subsection demonstrates the relation between the scatterer density and the correlation, matrix condition number and mutual information of a flat fading channel modelled in the previous section, through Monte-Carlo simulations. The simulations are confined in the slow fading channels. The mutual information evaluated is normalized to the channel bandwidth, i.e., it is in unit of bits/s/Hz. The scatterer density of the remote/local scatterer zone is defined in each scatterer zone as the ratio of the number of the remote/local scatterers to the area covered by these scatterers. Therefore, the scatterer density can change in two ways: by varying the number of

scatterers but with the fixed area or by varying the area but with the fixed number of scatterers. Let η_R and η_L be the scatterer densities for the remote and the local scatterer zones, respectively. Then [79],

$$\eta_R = \frac{K}{2R_R\Delta_R} \text{ and } \eta_L = \frac{S}{\pi\left(R_1^2 - R_2^2\right)}, \tag{5.5}$$

where R_1 is the radius of the outer circle of the local scatterer zone, R_2 is the radius of the inner circle of the local scatterer zone, and K and S are the numbers of remote and local scatterers, respectively. For the simulations, it is assumed that both remote and local scatterers distribute geometrically within a range of 1 *unit* wide, i.e., $(R_1-R_2) = 1$ *unit*. All other distances/ranges are normalised with respect to the width of both scatterer zones.

The simulation parameters are given in Table 5-1 and Table 5-2. The horizontal beamwidth in Conds. 1 ~ 5 is associated with the radius of the remote scatterer zone, R_R, and the distance between the transmitter and the remote scatterers, D_1 (Cond refers to Condition). Conds. 1 ~ 3 feature the fixed scatterer area but with the changeable number of scatterers, while in Conds. 1, 4 & 5 different values of the area of scattering zones with a fixed number of scatterers are specified. The simulation results shown in Figure 5-2 ~ Figure 5-5 include the mean mutual information, outage capacity, condition number and correlation, with respect to the ways the scatterer density is changed for flat fading channels.

The spatial degree of freedom and diversity are adopted as the evaluation tools for analysing the effects of scatterer density. The spatial degree of freedom is the minimum number of non-correlated spatial fading channels in a multiple-antenna channel, and diversity indicates the degree of connectivity between the transmitter and the receiver. Both of them ultimately determine the performance of a MIMO channel. The change of the scatterer density can be caused by varying either the area of the scatterer zone or the number of the scatterers in the zone. Fixing the number of the scatterers leads to constant diversity, while varying the area of a scatterer zone implies the change of spatial degree of freedom. The spatial degree of freedom at the

transmitter side can be evaluated through the transmit beamforming. For example, for the kth remote scatterer, the corresponding transmit beamforming can be obtained by [47]

$$e_t\left(\theta_k^t\right)=\frac{1}{\sqrt{n_t}}\begin{bmatrix}1\\ \exp\left(-j\frac{2\pi}{\lambda}\left(2-\frac{n_t-1}{2}\right)d_t\sin\theta_k^t\right)\\ \vdots\\ \exp\left(-j\frac{2\pi}{\lambda}\left(n_t-\frac{n_t-1}{2}\right)d_t\sin\theta_k^t\right)\end{bmatrix}; \tag{5.6}$$

and the overall transmit beamforming with K remote scatterers is [47],

$$\varepsilon_t\left(\theta^t\right)=\left[e_t\left(\theta_1^t\right)\ \cdots\ e_t\left(\theta_K^t\right)\right]^T, \tag{5.7}$$

where ^{T} stands for transpose. More differences between the rows in (5.7) will result in higher spatial degree of freedom. Note that (5.6) and (5.7) are suitable for all scattering models. At the receiver side, the angular resolvability of the receiver influences the spatial degree of freedom, which indicates the capability of the receive antenna array to resolve the incoming signals [47]. Angular resolvability is subject to the number of the angular bins of an antenna array. More bins imply higher resolvability. Given the normalised length[1] and the number of antennas, each receive antenna array has a fixed number of angular bins. Each bin represents one resolvable path. The receive antenna array with higher resolvability can provide higher spatial degree of freedom.

The mutual information of the MIMO channel in flat fading channels is calculated by (3.23) with equal transmit power at the transmitter.

5.2.1 Fixed area of scatterer zones

Figure 5-2 demonstrates the mean mutual information for the MIMO channels in the double-scattering environment under Conds. 1 ~ 3 in Table 5-1, respectively, where the variation of the scatterer densities is caused only by the number of the scatterers.

[1] For the uniform linear antenna array, it is defined as the physical array length divided by the carrier wavelength.

The condition number and the correlation of the channels under these conditions can be found in Figure 5-4 and Figure 5-5, respectively. It can be observed that when the correlation and the condition number vary within a limit range, the mean mutual information curves of the double-scattering model overlap with each other in the entire range of *SNR* in simulations. It demonstrates that when the area of both scatterer zones is fixed, the scatterer density has a marginal effect on channel performances.

Table 5-1 The channel conditions I

	Cond. 1	Cond. 2	Cond. 3
Antenna Numbers	4×4		
Antenna Spacing (m)	0.5λ		
Horizontal Beam Azimuth ($^{\circ}$)	22.6		
Antenna Gain (dBi)	17.5		
Distance (D_1, D_2)	500, 50		
Scatterer Number (K, S)	80, 100	20, 100	20, 200
Scatterer Area (S_R, S_L)	200, 311.01		
Scatterer Density (η_R, η_L)	0.4, 0.32	0.1, 0.32	0.1, 0.64
Carrier Frequency (GHz)	2.000		

"$_R$"--- Remote scatterers; "$_L$"--- Local scatterers.

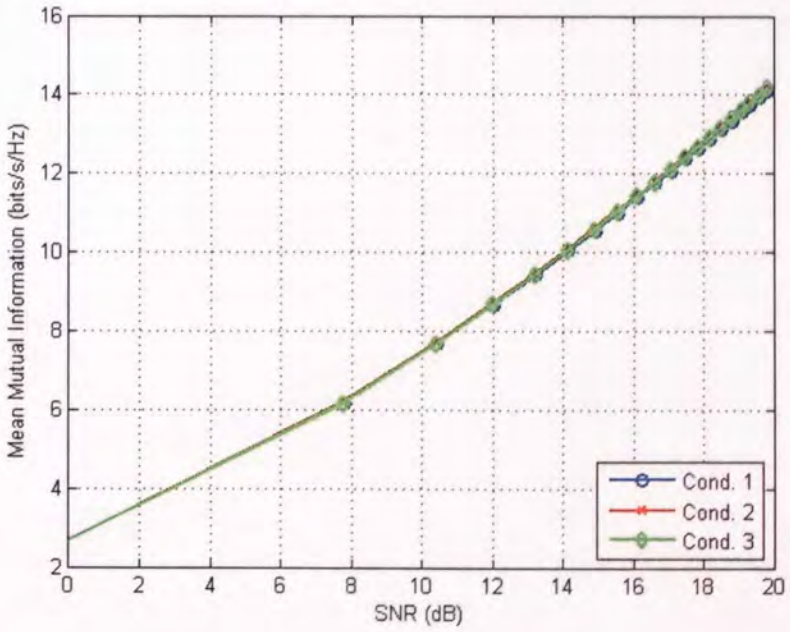

Figure 5-2 The mutual information in flat fading channels, when *SNR* is varying (Cond. 1 ~ 3).

The fixed area of the remote scatterer zone freezes the angular spread of the transmit antenna array. Therefore, the increased number of remote scatterers will reduce the differences between the rows in (5.7), offsetting the potential increase in diversity brought by the increased number of remote scatterers. If the number of remote scatterers decreases, the improved spatial degree of freedom due to more independent signal components available will be sacrificed by the reduced amount of diversity. From the receiver's point of view, the varied number of surrounding scatterers has a minor effect on the angular resolvability of the receiver. Since each angular bin of an antenna array represents one resolvable path, not all of the actual signal paths can be resolved according to the simulation conditions. The varied number of local scatterers contributes little to the resolution of the receive antenna array. There is one exception when the number of local scatterers is smaller than that of angular bins. Similarly, within the channel between the two scatterer zones, varying scatterer density through changing the number of scatterers has little effect on channel performances as the impacts from the spatial degree of freedom and the diversity of this part of channel are conversed and balanced out by each other.

Overall, if the scatterer density is changed only by the numbers of the scatterers, the variation of channel performance is negligible in flat fading channels, as shown by the performance results.

Table 5-2 The channel conditions II

	Cond. 1	Cond. 4	Cond. 5
Antenna Numbers	4×4		
Antenna Spacing (m)	0.5λ		
Horizontal Beam Azimuth ($^{\circ}$)	22.6	11.4	6.9
Antenna Gain (dBi)	17.5		
Distance (D_1, D_2)	500, 50	500, 50	500, 75
Scatterer Number (K, S)	80, 100		
Scatterer Area (S_R, S_L)	200, 311.01	100 , 311.01	100, 153.94
Scatterer Density (η_R, η_L)	0.4, 0.32	0.8, 0.32	0.8, 0.65
Carrier Frequency (GHz)	2.000		

"$_R$"--- Remote scatterers; "$_L$"--- Local scatterers.

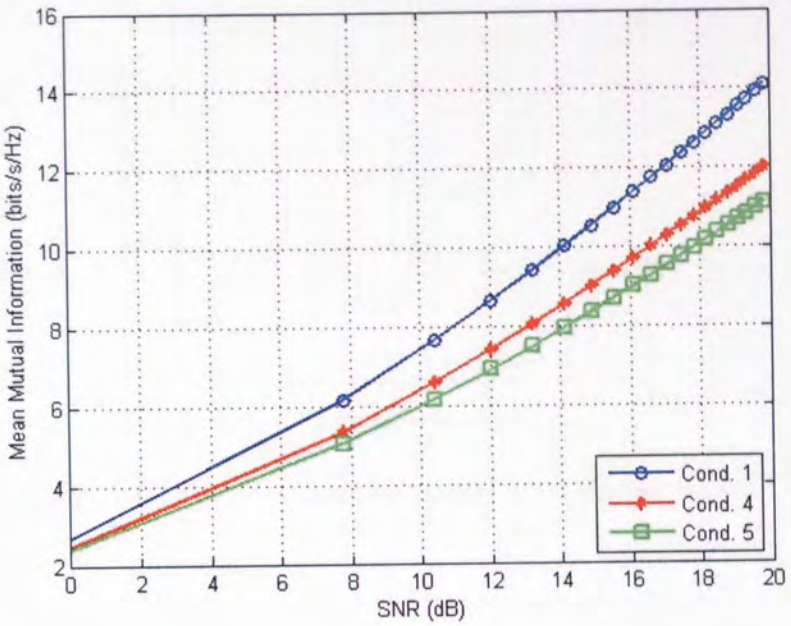

(a)

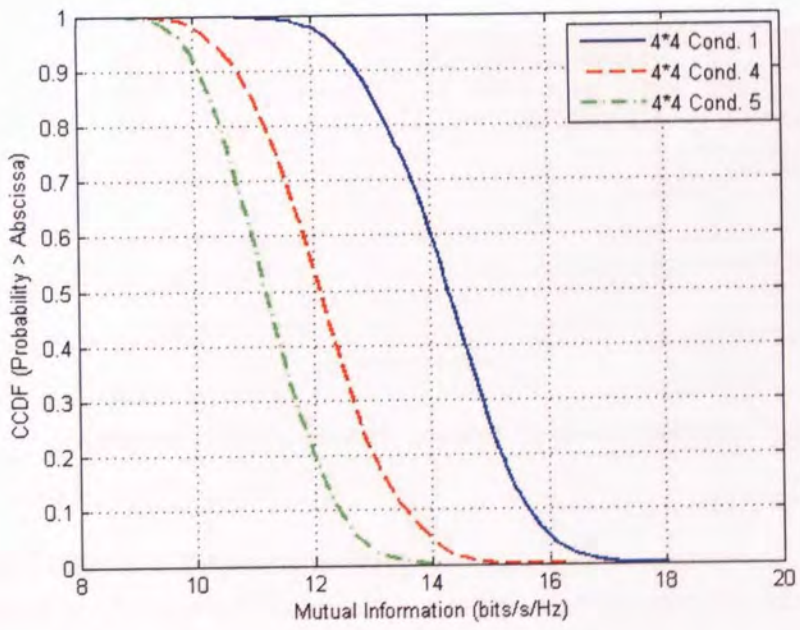

(b)

Figure 5-3 The mutual information of Cond. 1, 4, & 5 in flat fading channels. (a) Mean mutual information vs. SNR; (b) Outage probability (SNR = 20 dB).

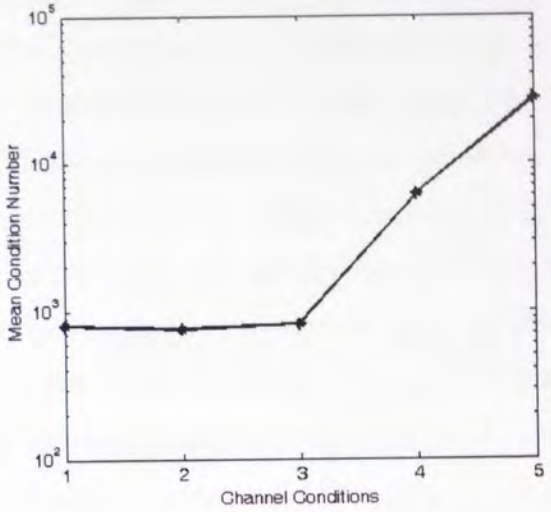

Figure 5-4 The mean condition number of the channel matrix.

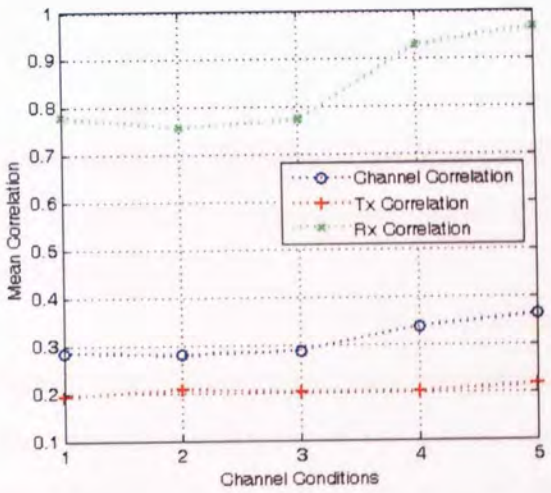

Figure 5-5 The mean correlation of the channel matrix.

5.2.2 Fixed numbers of scatterers

In this subsection, the scatterer densities, η_R and η_L, are changed by allowing the area of the two scatterer zones to vary but with the fixed number of scatterers, as described in Conds. 1, 4, & 5 in Table 5-2. In these conditions, Cond. 1 sets up the simulated channel with the lowest scatterer densities, while both scatterer zones have the highest density in Cond. 5. Figure 5-3 shows the comparison in capacity, in terms of both mean mutual information and outage capacity. It can be seen in the figure that the

channel mutual information deteriorates with the increased η_R and η_L. The corresponding correlation coefficient and condition number are shown to increase when η_R and η_L enlarge, as shown in Figure 5-4 and Figure 5-5, respectively.

With the increase of scatterer densities, η_R and η_L, the differences between the rows of transmit beamforming in (5.7) will reduce, resulting in lower spatial degree of freedom. At the receiver, varying the density, η_L, of local scatterers makes little contribution to angular resolvability of the receiver. With the fixed number of the local scatterers, the number of the arrival signals in each angular bin remains unchanged, no matter the area is large or small. Thus, the area of the local scatterer ring has a minor impact on channel performance. Between the two scatterer zones, any increase of the scatterer density by reducing the area of the two scatterer zones will lead to the reduced spatial degree of freedom in this part of the channel and vice versa.

In summary, increasing the scatterer densities, η_R and η_L, by reducing the area of the scatterer zones will only cost some of the spatial degree of freedom, which can be visualised in Figure 5-3 ~ Figure 5-5. The way the scatterer density, η_R, varies described in this subsection can be interpreted as the change of antenna beamwidth at the base station, which is the key parameter that causes the variation of channel performances in flat fading channels.

The results shown in this section also suggest that the correlation and the condition number can be used to predict the variation of the mutual information of a MIMO channel. When they both increase, the mutual information of this MIMO channel will reduce accordingly; otherwise, this MIMO channel is able to support delivering more information with arbitrarily small error probability to the receiver.

5.3 Performances in frequency-selective fading channels

The channel capacity performance is shown in this section, in frequency-selective fading channels. The simulations are considered in the slow fading channel. The simulation conditions in the flat fading channel scenario are still applied to the simulations for frequency-selective channels in which the number of delay taps is V.

The transmission is considered over a coding block of length $T > 0$. The channel is assumed to be constant over the block, i.e., the channel coherence time spans T symbols. Therefore, the channel matrix in frequency-selective fading channels can be expressed in the form of block Toeplitz matrix as [80]

$$\mathbf{H} = \begin{bmatrix} \mathbf{H}_0 & 0 & \cdots & 0 \\ \mathbf{H}_1 & \mathbf{H}_0 & \ddots & \vdots \\ \vdots & \mathbf{H}_1 & \ddots & 0 \\ \mathbf{H}_{V-1} & \vdots & \ddots & \mathbf{H}_0 \\ 0 & \mathbf{H}_{V-1} & \vdots & \mathbf{H}_1 \\ \vdots & \ddots & \ddots & \vdots \\ 0 & \cdots & 0 & \mathbf{H}_{V-1} \end{bmatrix}, \tag{5.8}$$

where $\mathbf{H}_v$: $M \times N$, $v = 0, 1, \ldots V-1$, are the channel matrices and the dimensions of $\mathbf{H}$ are $M(T+V-1) \times NT$. Accordingly, the mutual information per symbol period is [80]

$$C_{FS} = \frac{1}{T+V-1} \log_2 \left[\det \left(I_{M(T+V-1)} + \frac{SNR}{N} \mathbf{H}\mathbf{H}^* \right) \right]. \tag{5.9}$$

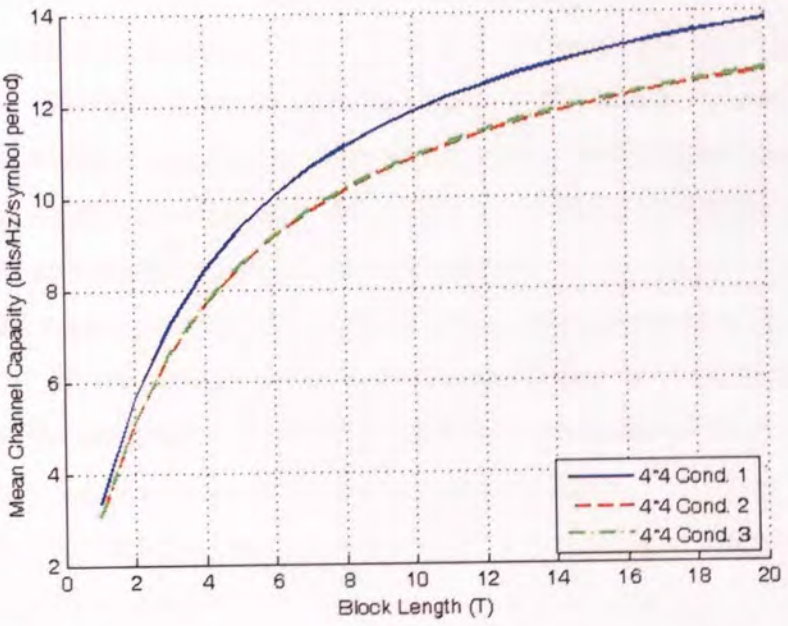

Figure 5-6 The mean channel capacity against the coding block length in frequency-selective fading channels, where the area of scatterer zones are fixed. SNR = 20dB.

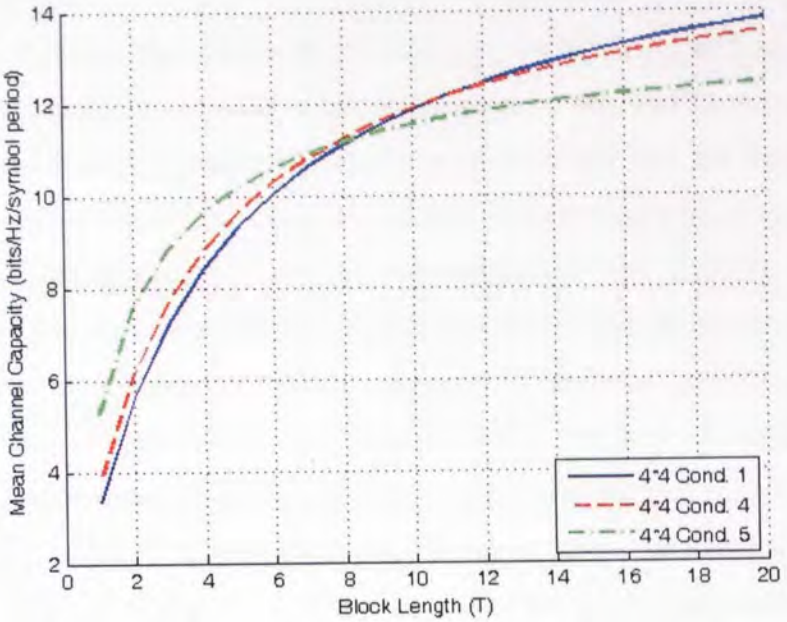

Figure 5-7 The mean channel capacity against the coding block length in frequency-selective fading channels, where the number of scatterers in each scatterer zone is fixed. SNR = 20dB.

Figure 5-6 shows the mean channel capacity against the coding block length T, in the scenario that the scatterer densities in both scatterer zones are varied by the number of scatterers in the zones. It can be observed that once the area of the scatterer zones is fixed, more scatterers in the remote scatterer zone can provide higher channel capacity for all the values of T demonstrated. Moreover, the number of scatterers in the local scatterer zone has a limited effect on channel capacity.

The channel capacity curves illustrated in Figure 5-7 correspond to the scenario that the area of the scatterer zones is the sole affecting parameter in determining scatter density. When the transmitted signals are coded in a comparatively short period, higher channel capacity can be observed in denser scatterer zones. The figure also suggests that higher channel capacity can be achieved with lower scatterer densities and longer coding blocks at the transmitter.

Also, both Figure 5-6 and Figure 5-7 show that longer coding blocks of the transmitted signals can lead to higher channel capacity under all channel conditions.

5.4 Summary

This chapter discusses the effects of the scatterer densities, η_R and η_L, on MIMO channel performances in a double-scattering model in flat and frequency-selective fading channels through theoretical modelling, simulations and the analysis of the spatial degree of freedom and diversity. In flat fading channels, it is shown that changing the scatterer densities only by the numbers of the scatterers in the two scatterer zones has little impact on the performances. Also, when the area of the scatterer zones is unfixed, significant impacts of scatterer density on channel performances can be observed. In the latter scenario, the way of varying scatterer density is equivalent to adjusting the antenna beamwidth of the transmitter.

In frequency-selective fading channels, higher scatterer density in the remote scatterer zone leads to higher channel capacity when the area of the scatterer zones is fixed. When the scatterer density is varied by changing the area but with the fixed number of scatterers, higher channel capacity can be obtained in either of the situations: a) in denser scatterer zones with short coding blocks; and b) in sparser scatterer zones with long coding blocks. Also, longer coding block offers better channel capacity under all channel conditions.

The outcome of this work has extended the results reported in other work such as [41] and [9] and, at the same time, explained why and how the scatterer density has varied impacts on channel performances. This could help to gain better understanding of the behaviours of MIMO channel in different and more realistic propagation environments and to select proper transmitter parameters in order to maximise the system performance.

6 Cooperative Communication in Correlated Fading Channels

So far, CC systems have been studied mainly in the uncorrelated fading channels, and the mutual information between the source and the destination nodes is also obtained based on this assumption. It is therefore essential to find the actual benefits that could be achieved using this technology in a more realistic environment, such as in correlated fading channels. In MIMO systems, the effect of fading correlation on channel capacity is found to be variable, from negligible [81] to nontrivial (negative [82-85] or positive [86]). The question is whether this attribute could also exist in CC via relays, where a virtual array of antennas is formed. The so-called unitary-independent-unitary (UIU) model [87] is adopted to investigate the correlation effect in CC systems, as it covers the case of non-identically distributed fading across different channels. The variances of the uncorrelated fading coefficients can then be extracted from this model containing the elements reflecting the correlation coefficients and the variances of the correlated fading coefficients. The fading correlation is concerned with both FAF and S-STC-DF protocols. Figure 6-1 shows a CC system with three relay nodes.

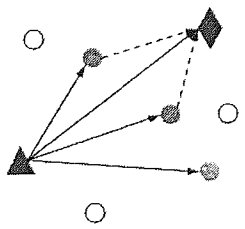

Figure 6-1 A CC system with three relay nodes. The "triangle" represents the source node; the "diamond" the destination node; the greyed "circles" the relay nodes.

6.1 Correlated channel model

The channels of a CC system can be most likely described as non-identically distributed fading, where the variances of fading coefficients appear to be asymmetric.

Thus, the following unitary-independent-unitary (UIU) model can be utilised, which considers a multiple-antenna system with N transmit and M receive antennas [87],

$$\mathbf{H} = \mathbf{U}_r \mathbf{H}_{i.n.d.} \mathbf{U}_t^*, \tag{6.1}$$

where $\mathbf{U}_r$ and $\mathbf{U}_t$ are $M \times M$ and $N \times N$ deterministic unitary matrices; * represents Hermitian transpose; the entries of $\mathbf{H}_{i.n.d.}$ (*i.n.d.* stands for independent and non-identically distributed) are zero mean and independent with arbitrary marginal distributions and variance, constrained only to $\mathrm{E}[\mathrm{trace}(\mathbf{H}_{i.n.d.}\mathbf{H}^*_{i.n.d.})] = MN$. If the *Karhunen–Loève Transform* (KLT) can be factored as in (19) of [87], the columns of $\mathbf{U}_r$ and $\mathbf{U}_t$ correspond to the eigenvectors of $\mathrm{E}[\mathbf{H}\mathbf{H}^*]$ and $\mathrm{E}[\mathbf{H}^*\mathbf{H}]$[1], respectively. Also, the variances of the entries in $\mathbf{H}_{i.n.d.}$ are the eigenvalues of $\mathrm{E}[\mathbf{H}\mathbf{H}^*]$.

Usually, CC systems include two types of channels or two transmission phases: broadcast channel (Phase I) and multiple-access channel (Phase II). The broadcast channel model, $\mathbf{H}_b$, is a vector featuring receive diversity (i.e., $\mathbf{U}_{t|b} = 1$), which can be expressed as [65, 88]

$$\mathbf{H}_b = \mathbf{U}_{r|b} \mathbf{H}_{i.n.d|b}. \tag{6.2}$$

Thus, the mutual information of the channel can be given as [65, 88]

$$\begin{aligned} \mathbf{I}_b(\mathbf{H}_b) &= \eta_b \log_2\left(1 + SNR\mathbf{H}_b^*\mathbf{H}_b\right) \\ &= \eta_b \log_2\left(1 + SNR\mathbf{H}_{i.n.d|b}^*\mathbf{U}_{r|b}^*\mathbf{U}_{r|b}\mathbf{H}_{i.n.d|b}\right) \\ &= \eta_b \log_2\left(1 + SNR\mathbf{H}_{i.n.d|b}^*\mathbf{H}_{i.n.d|b}\right) \end{aligned} \tag{6.3}$$

where η_b is inversely proportional to the number of transmit nodes in the network and SNR is defined as the transmit SNR without fading effect. Similarly, in the multiple-access channel, the channel matrix can be presented as [65, 88]

[1] It can be proved through eigenvalue decomposition as in (3.27).

$$\mathbf{H}_m = \mathbf{H}_{i.n.d|m}\mathbf{U}^*_{t|m}, \tag{6.4}$$

since the destination is the only receiver and thus $\mathbf{U}_{r|m} = 1$. Therefore, the mutual information of the channel can be calculated as [65, 88]

$$\begin{aligned}\mathbf{I}_m(\mathbf{H}_m) &= \eta_m \log_2\left(1 + SNR\mathbf{H}_m\mathbf{H}^*_m\right)\\ &= \eta_m \log_2\left(1 + SNR\mathbf{H}_{i.n.d|m}\mathbf{U}^*_{t|m}\mathbf{U}_{t|m}\mathbf{H}^*_{i.n.d|m}\right)\\ &= \eta_m \log_2\left(1 + SNR\mathbf{H}_{i.n.d|m}\mathbf{H}^*_{i.n.d|m}\right)\end{aligned} \tag{6.5}$$

where η_m is inversely proportional to the number of transmit nodes in this phase. Eqs. (6.3) and (6.5) show the fact that the correlation has no impact on the mutual information of either the broadcast channel or the multiple-access channel, when the two channels are respectively in two unrelated systems. When the two channels are in the same system such as in a CC system, however, the correlation can affect the mutual information of the whole system, as shown in the following.

6.2 Correlated fading coefficients

Assuming that there are only two wireless channels transmitting at the same time in the system, the correlated channel gains $\mathbf{H}$ can be expressed as follows, using the UIU model, [65, 88]

$$\mathbf{H} = \left[\alpha^{cor}_{ch(1)} \quad \alpha^{cor}_{ch(2)}\right]^T = \mathbf{U}_r\left[\alpha_{ch(1)} \quad \alpha_{ch(2)}\right]^T\mathbf{U}^*_t. \tag{6.6}$$

Because $\mathbf{H}$ is a vector, $\mathrm{E}[\mathbf{H}^*\mathbf{H}]$ is a scalar, i.e., $\mathbf{U}_t = 1$ and $\mathrm{E}[\mathbf{H}\mathbf{H}^*]$ is actually the covariance matrix of $\mathbf{H}$, i.e., [65, 88]

$$\mathbf{\Psi} = \mathrm{E}\left[\mathbf{H}\mathbf{H}^*\right] = \begin{bmatrix} {\sigma^{cor}_{ch(1)}}^2 & \sigma^{cor}_{ch(1)}\sigma^{cor}_{ch(2)}\beta e^{j\theta} \\ \sigma^{cor}_{ch(1)}\sigma^{cor}_{ch(2)}\beta e^{-j\theta} & {\sigma^{cor}_{ch(2)}}^2 \end{bmatrix}, \tag{6.7}$$

where σ is the standard deviation for all the channels in both correlation and non-correlation scenarios; β and θ are the magnitude and phase of the complex correlation coefficients between two channels; $\boldsymbol{\Psi}$ must be positive-definite. The eigenvalues of $\boldsymbol{\Psi}$ can be computed through the standard calculation process for eigenvalues as [65, 88]

$$\lambda_{1,2} = \left\{\sigma^2_{ch(1)}, \sigma^2_{ch(2)}\right\} = \frac{\sigma^{cor}_{ch(1)}{}^2 + \sigma^{cor}_{ch(2)}{}^2 \pm \sqrt{\left(\sigma^{cor}_{ch(1)}{}^2 - \sigma^{cor}_{ch(2)}{}^2\right)^2 + 4\beta^2 \sigma^{cor}_{ch(1)}{}^2 \sigma^{cor}_{ch(2)}{}^2}}{2}, \tag{6.8}$$

where $\lambda_{1,2}$ are the variances of the channel gains in the non-correlation scenario with the presence of the variances of fading coefficients in the correlation scenario and the magnitude of correlation coefficient; β should reside in [0, 1) to fulfill $\boldsymbol{\Psi}$'s positive-definite requirement. Eq. (6.8) indicates that θ is irrelevant to influencing the fading coefficients in two-correlated-channels scenario. Correspondingly, $\mathbf{U}_r$ can be found as [65, 88]

$$\mathbf{U}_r = \begin{bmatrix} \dfrac{\left(\sigma^{cor}_{ch(1)}{}^2 - \lambda_1\right)e^{j\theta}}{\sqrt{\Sigma_1}} & \dfrac{\sigma^{cor}_{ch(1)}\sigma^{cor}_{ch(2)}\beta e^{j\theta}}{\sqrt{\Sigma_2}} \\ \dfrac{-\sigma^{cor}_{ch(1)}\sigma^{cor}_{ch(2)}\beta}{\sqrt{\Sigma_1}} & \dfrac{\left(\lambda_2 - \sigma^{cor}_{ch(2)}{}^2\right)}{\sqrt{\Sigma_2}} \end{bmatrix}, \tag{6.9}$$

where $\Sigma_x = \left(\sigma^{cor}_{ch(x)}{}^2 - \lambda_x\right)^2 + \left(\sigma^{cor}_{ch(1)}\sigma^{cor}_{ch(2)}\beta\right)^2$, $x = 1, 2$. For higher dimension matrices, the eigenvalues and eigenvectors can be determined through matrix diagonalization, such as *Schur factorization* $\boldsymbol{\Psi} = \mathbf{U}\boldsymbol{\Lambda}\mathbf{U}^*$, where $\mathbf{U}$ is unitary and $\boldsymbol{\Lambda}$ is a diagonal matrix containing the eigenvalues of $\boldsymbol{\Psi}$ on its diagonal.

From (6.8), the variances of the entries of $\mathbf{H}$, $\sigma^{cor}_{ch(1)}{}^2$ and $\sigma^{cor}_{ch(2)}{}^2$, can be presented in terms of the correlation amplitude, β, and the variances of the entries of $\mathbf{H}_{i.n.d.}$, $\sigma^2_{ch(1)}$ and $\sigma^2_{ch(2)}$, as follows, [65, 88]

$$\left\{\sigma_{ch(1)}^{cor\ 2},\sigma_{ch(2)}^{cor\ 2}\right\}=\frac{\left(\sigma_{ch(1)}^{2}+\sigma_{ch(2)}^{2}\right)}{2}\pm\frac{\sqrt{\left(\sigma_{ch(1)}^{2}+\sigma_{ch(2)}^{2}\right)^{2}-\frac{4\sigma_{ch(1)}^{2}\sigma_{ch(2)}^{2}}{\left(1-\beta^{2}\right)}}}{2}. \tag{6.10}$$

For (6.10) to be real-positive values, the following condition has to be fulfilled that [65, 88]

$$\frac{\max\left(\sigma_{ch(1)}^{2},\sigma_{ch(2)}^{2}\right)}{\min\left(\sigma_{ch(1)}^{2},\sigma_{ch(2)}^{2}\right)}\geq\frac{1+\beta}{1-\beta}. \tag{6.11}$$

Note that if $\sigma_{ch(1)}^{2}=\sigma_{ch(2)}^{2}$, i.e., $\mathbf{H}_{i.n.d.}$ becomes $\mathbf{H}_{i.i.d.}$, β should be zero and $\mathbf{H}$ is also i.i.d.; if the entries of $\mathbf{H}_{i.i.d.}$ are Rayleigh distributed, $\mathbf{H}$ is also Rayleigh distributed. The channel meeting the two conditions is so called the canonical channel referred in [87].

The variances in (6.10) are determined regarding the criterion – if $\sigma_{ch(1)}^{2}>\sigma_{ch(2)}^{2}$, then it follows that $\sigma_{ch(1)}^{2}>\sigma_{ch(1)}^{cor\ 2}>\sigma_{ch(2)}^{cor\ 2}>\sigma_{ch(2)}^{2}$, and vice versa.

6.3 Correlation effect in different protocols

6.3.1 Fixed amplify-forward

In this subsection, the scenario for one relay node is considered. Thus, the correlation is assumed to occur between the source-relay and the source-destination channels in Phase I, where the relay node is closer to the destination node. Rewrite the mutual information of FAF in (4.7) with the correlation taken into account as follows,

$$I_{FAF}^{cor}=\frac{1}{2}\log_{2}\left(1+SNR\left(\left|\alpha_{s,d}^{cor}\right|^{2}+\frac{\left|\alpha_{s,r}^{cor}\right|^{2}\left|\alpha_{r,d}\right|^{2}}{\left|\alpha_{s,r}^{cor}\right|^{2}+\left|\alpha_{r,d}\right|^{2}+\frac{1}{SNR}}\right)\right), \tag{6.12}$$

where υ has been maximised and integrated into the equation; both transmit nodes use the same transmit power and all the AWGN channels are the same as well. Since the correlation has impacts on the source-relay and the source-destination channels symmetrically, (6.12) can be modified to [65]

$$I_{FAF}^{cor} = \frac{1}{2}\log_2\left(1+SNR\left(\left|\alpha_{s,d}\right|^2 \pm \Delta_\alpha + \frac{\left|\alpha_{s,r}\right|^2\left|\alpha_{r,d}\right|^2}{\left|\alpha_{s,r}\right|^2+\left|\alpha_{r,d}\right|^2+\frac{1}{SNR}} \mp \gamma\Delta_\alpha\right)\right)$$
$$= \frac{1}{2}\log_2\left(1+SNR\left(\left|\alpha_{s,d}\right|^2 + \frac{\left|\alpha_{s,r}\right|^2\left|\alpha_{r,d}\right|^2}{\left|\alpha_{s,r}\right|^2+\left|\alpha_{r,d}\right|^2+\frac{1}{SNR}} + \Delta\right)\right), \quad (6.13)$$

where Δ_α is the absolute variation amount of fading coefficients caused by the correlation; γ is a constant between (0, 1); $\Delta = (\pm 1 \mp \gamma)\Delta_\alpha$. Eq. (6.13) stands because, for example, it is true that $(m+\Delta_\alpha)n/(m+\Delta_\alpha+n+1) = mn/(m+n+1)+\gamma\Delta_\alpha$.

When $\sigma_{s,d}^2 > \sigma_{s,r}^2$, the extent of the mutual information variation is subject to $\Delta = (-1+\gamma)\Delta_\alpha$ (degradation). When $\sigma_{s,r}^2 \geq \sigma_{s,d}^2$, the extent depends on $\Delta = (1-\gamma)\Delta_\alpha$ (improvement).

6.3.2 Selection decode-forward

For this protocol, two relay nodes are considered, which are closer to the source node but not clustered. Thus, the source-destination channel is regarded uncorrelated with source-relay channels. For the S-STC-DF protocol in (4.35), the correlation affects the number of involving relay nodes, n, in Phase II[1]. Thus the extent of relay participation in Phase II differs between the correlation and non-correlation scenarios, which cause different system performance in terms of mutual information.

6.4 Simulation results

6.4.1 Fixed amplify-forward

The mutual information of the fixed amplify-forward protocol is illustrated in Figure 6-2 and Figure 6-3, according to the simulation configurations tabulated in Table 6-1. The cooperative system can be simulated by finding the correlated fading coefficients through either (6.6) and (6.9) or (6.10). Here, (6.10) is used. The first set of

[1] For the S-R-DF protocol in (4.33), correlation expresses similar effect as for the S-STC-DF protocol.

configurations, "S-D Better", represents the scenario where the source-relay channel is affected by many signal impairment factors and the source-destination channel is better. The second configuration shows the opposite scenario. In both configurations, the variance of the relay-destination channel is fixed to 0.9. All the wireless channels involved are assumed to be slowly and flatly Rayleigh-faded.

Table 6-1 Simulation configurations for FAF

	$\sigma_{s,r}^2$	$\sigma_{s,d}^2$	$\sigma_{r,d}^2$	β	*SNR* (dB)
S-D Better	0.1	0.6	0.9	0.7	20
S-R Better	0.6	0.1	0.9	0.4	

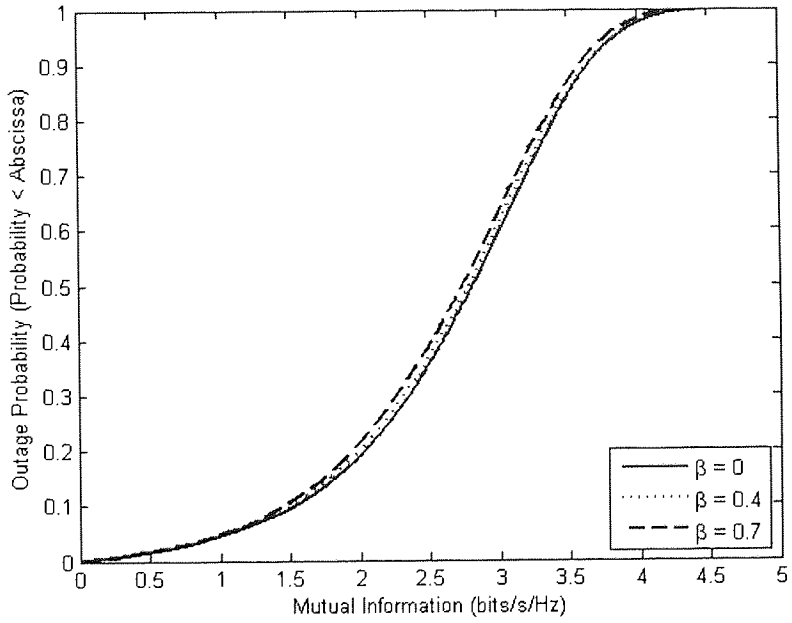

Figure 6-2 Outage probability of FAF when the source-destination channel is better than the source-relay channel.

The differences in mutual information between the uncorrelated and the correlated systems rise along with the increased amplitude of correlation coefficient, β. This is because the variation of the variances caused by the correlation increases when β rises.

In the "S-D Better" scenario, the source-destination channel is degraded with higher correlation, i.e., $\Delta = (-1+\gamma)\Delta_a$. Therefore, the mutual information decreases in line with the increase of correlation, as shown by Figure 6-2. In the "S-R Better" scenario,

performance improvement is observed in Figure 6-3 in association with the correlation. In this protocol, the correlation displays its positive effect over the entire span of mutual information.

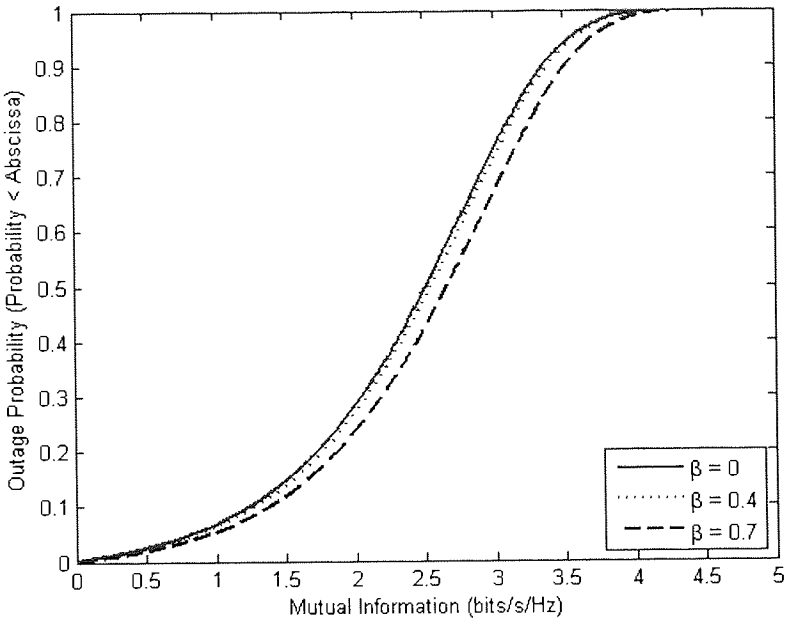

Figure 6-3 Outage probability of FAF when the source-relay channel is better than the source-destination channel.

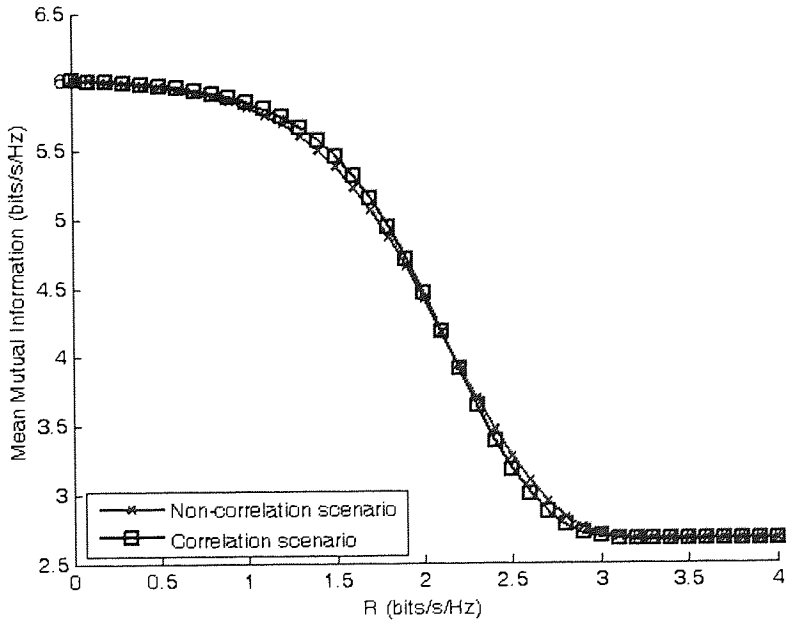

Figure 6-4 Mean mutual information vs. R for S-STC-DF. β and SNR are fixed to 0.5 and 20 dB.

6.4.2 Selection decode-forward

In this subsection, the performance of the two-relay S-STC-DF CC system is simulated, in both correlation and non-correlation scenarios. The variances in the non-correlation scenario are set as follows: $\sigma^2_{s,d} = 1$, $\sigma^2_{s,r(1)} = 1.2$, $\sigma^2_{s,r(2)} = 0.3$, $\sigma^2_{r(1),d} = 1$, and $\sigma^2_{r(2),d} = 1$. All the wireless channels are also assumed to experience slow and flat Rayleigh fading.

Figure 6-4 shows the mean mutual information versus R which determines the threshold in (4.39) for fixed *SNR*. For some values of the threshold given by (4.39), the relay nodes in the correlation scenario tends to participate more in Phase II, while in the non-correlation scenario they are more active for relaying in this phase for some other values. Therefore, in the low regime of R, i.e., low threshold, the relay nodes can help the source node on more occasions to transmit the source data in the correlation scenario. The situation is on the opposite when R is quite large. In general, because of the increasing R and the threshold, the mean mutual information in both scenarios decreases. When R is greater than 3.1 bit/s/Hz, both relay nodes stop cooperating and the source-destination channel is the sole channel available in both correlation and non-correlation scenarios. Thus, the mean mutual information of the system in these two scenarios is the same.

Figure 6-5 and Figure 6-6 illustrate the mean mutual information against β, where the threshold in Figure 6-6 is higher than that in Figure 6-5. Comparing with the non-correlation scenario, the source-relay channels are more similar when the correlation taken into account, in terms of fading variance. For the threshold value used in simulating the channels of Figure 6-5, the relay nodes in the correlation scenario participate more in Phase II, leading to higher mean mutual information. When β increases, the difference of mean mutual information between the two scenarios enlarges. When the threshold (decided by R and *SNR*) is set as high as in the simulation of Figure 6-6, however, the mean mutual information of the non-correlation scenario surpasses that in the correlation scenario.

As illustrated in Figure 6-7, the mean mutual information in the correlation scenario is slightly lower than that in the non-correlation scenario for the low value regime of *SNR*. When *SNR* is between approximately 15 and 25 dB, the system performs better

with the existence of correlation. When *SNR* becomes higher than 25 dB, there is no difference in performance between the correlation and non-correlation scenarios.

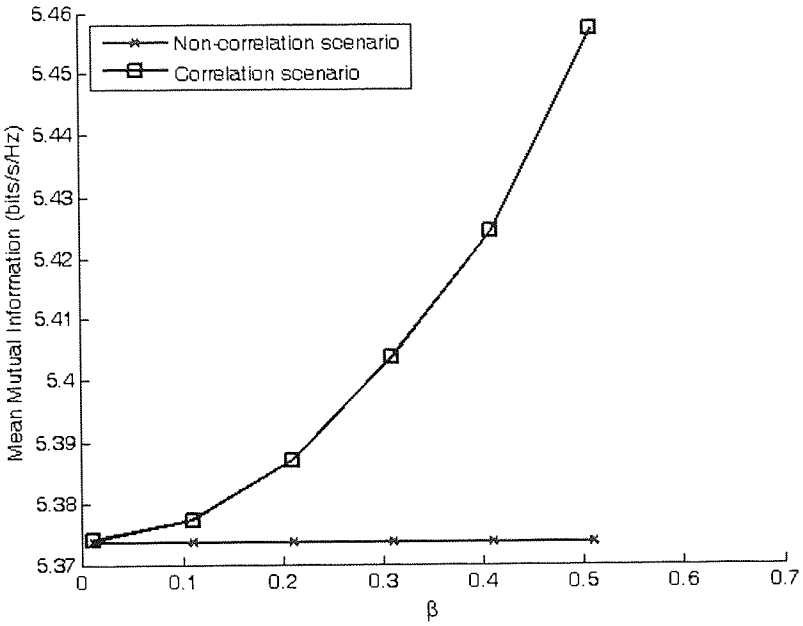

Figure 6-5 Mean mutual information vs. β for S-STC-DF. R and SNR are fixed to 1.5 bit/s/Hz and 20 dB.

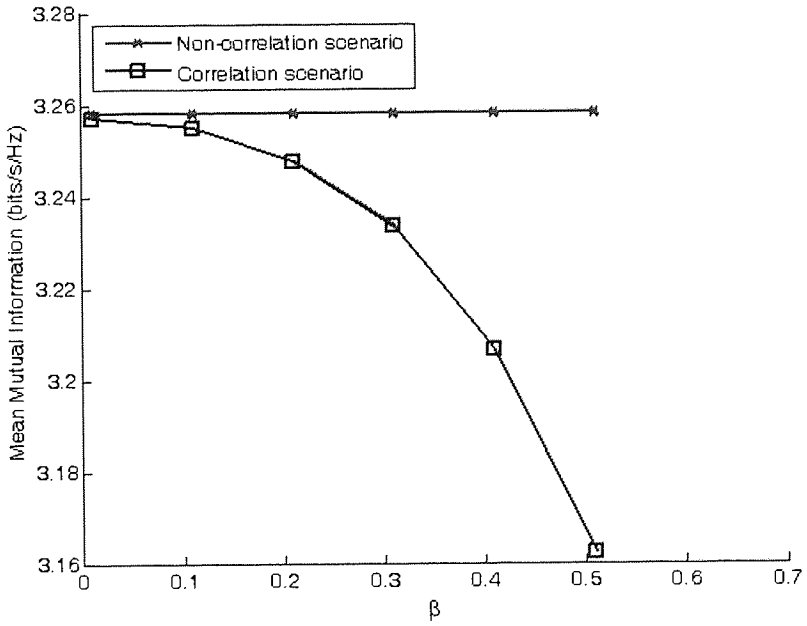

Figure 6-6 Mean mutual information vs. β for S-STC-DF. R and SNR are fixed to 2.5 bit/s/Hz and 20 dB.

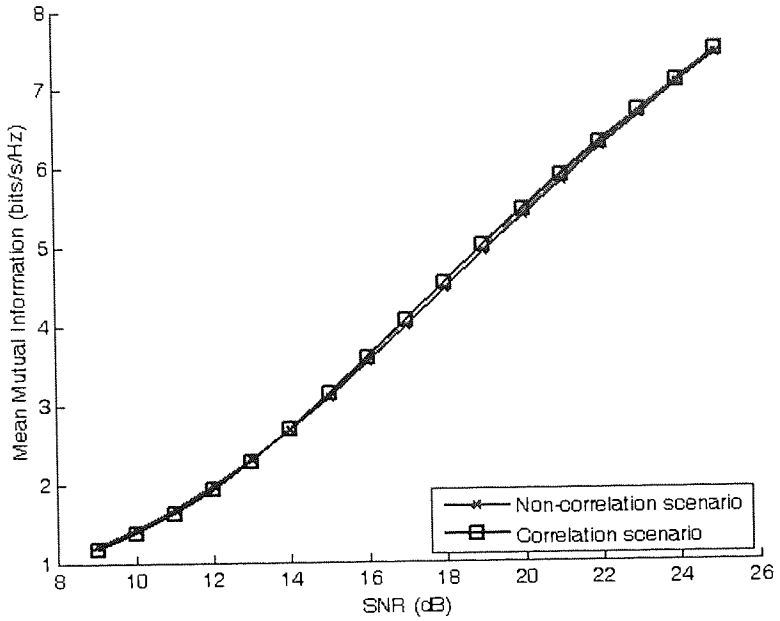

Figure 6-7 Mean mutual information vs. *SNR* for S-STC-DF. β and R are fixed to 0.5 and 1.5 bit/s/Hz.

6.5 Summary

In this chapter, the effects of fading correlation on the performances of FAF and S-STC-DF CC systems are investigated. Since the wireless channels in a CC system are more likely to be asymmetric, in terms of the variances of fading coefficients, the UIU model is used to present the channel model.

For the FAF system, it has been shown that the differences in quality between the source-destination and the source-relay channels can lead to different results of mutual information results in the correlated environment. It can be concluded that a better condition of the source-relay channel than that of the source-destination channel is crucial for obtaining higher mutual information when CC systems operate in correlated fading channel. Otherwise, the mutual information is reduced when the channel conditions are the other way around.

The results for S-STC-DF show that the differences in system performance vary between the correlation and the non-correlation scenarios, with regards to the threshold

set for relay participation in Phase II. Within the different threshold regimes (indicated by either R or SNR, with the other one fixed), the fading correlation introduces different impacts on system performances. In some threshold regimes, the fading correlation should be considered for having more accurate measurements of the system performance while in other regimes the effect of fading correlation may be ignored.

Illustrated by the results of both FAF and S-STC-DF protocols, the correlation can have positive impacts on the system performance.

7 Performance Trade-offs in Cooperative-Relaying Networks

The characteristics of communication through relaying, such as the renowned diversity-multiplexing trade-off, have been reported in [52, 53, 62]. In this chapter, a number of performance parameters are examined to highlight from different angles the fundamental trade-off between reliability (e.g. diversity or loss rate) and efficiency (e.g. throughput or energy efficiency) in the cooperative-relaying network (CRN), a special case of the CC system. This can provide a better understanding of the potential benefits and limitations of this technology, which is vital for system developers or service providers to judge its suitability for future applications. Most researchers draw their trade-off conclusions based on observations at the bit level (PHY layer), which could sometimes overestimate the system performance. The investigation in this chapter will be focused on the performance trade-offs at the packet-level of the CRN.

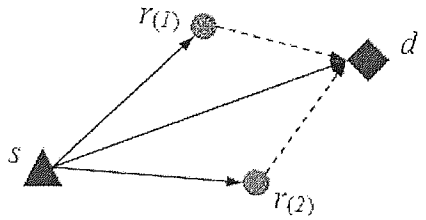

Figure 7-1 Cooperative relaying from the source node (s) to the destination node (d), with the help from two relay nodes ($r_{(1)}$, $r_{(2)}$).

Figure 7-1 shows an example of the possible topologies of a CRN for the investigation, which is comprised of one source node, one destination node and two relay nodes. The number of relay nodes to be deployed can be more than two. The source and the relay nodes are called the transmit nodes when they are in the transmit mode; and the destination and the relay nodes are called the receive nodes when they are in the receive mode. The CRN concerned is considered to be *decentralised* and *asynchronous*, i.e., the relay nodes make their own decisions on whether or not to perform relaying for the source node; and each transmit node sends out packets in their designated time slots. Thus, a TDMA scheme is required to ensure the orthogonality in accessing the wireless media by different nodes. The relaying protocol adopted in this

case is the DF protocol, under which two relaying algorithms, selection relaying and fixed relaying, are utilised. Three coding schemes are employed in the system, namely redundancy-free coding, 1/3 rate and 2/3 rate channel coding, respectively.

The performance of the CRN is studied through simulations as well as experiments. The experimental CRN is realised using wireless sensor transceivers. For the implementation of centralised and synchronous wireless relay networks, please refer to [64, 89]. Challenges in implementing relay networks using commodity hardware can also be found in [64].

7.1 Theoretical background

7.1.1 Direct transmission network

In this scenario, there is no relay node involved. The time slot arrangements for this scheme are shown in the first row of Figure 7-2, where T is the time period for the completion of transmission at one transmit node. The length of T is different between redundancy-free coding and 1/3 rate or 2/3 rate coding, which will be explained later. The mutual information in bits/s/Hz of transmission can be expressed as

$$I_d = \log\left(1 + SNR\left|\alpha_{s,d}\right|^2\right), \tag{7.1}$$

where $\alpha_{s,d}$ is the complex channel gain of the source-destination channel, $\sim CN(0, \sigma^2)$; SNR is the transmit SNR without fading effect. All the wireless channels in this section are assumed to experience slow and flat fading, i.e., the channel gain remains constant over one symbol period.

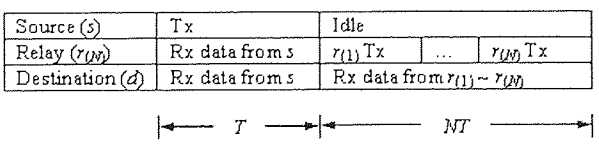

Figure 7-2 The TDMA scheme.

7.1.2 Mutual information, outage probability and diversity gain

During the first time slot T of transmission as shown in Figure 7-2, the source node broadcasts its packets to the network (shown by the solid arrowed lines in Figure 7-1), and the relay and the destination nodes can receive the source packets. Then the relay nodes will decide whether or not to use the subsequent time slots in succession to forward the source packets (shown by the dashed arrowed lines in Figure 7-1) by applying either of the two algorithms: fixed relaying or selection relaying.

The successful decoding criterion in the destination node concerned in this chapter is that as long as there is at least one good packet received for one particular packet number, the destination node declares to have successfully received the packet with this packet number. Thus, the mutual information of the CRN regarding the two relaying algorithms can be respectively presented as follows [90]

$$I_{fix} = \max\left\{\log_2\left(1+SNR\left|\alpha_{s,d}\right|^2\right), \min\left\{\log_2\left(1+SNR\left|\alpha_{s,r(1)}\right|^2\right), \log_2\left(1+SNR\left|\alpha_{r(1),d}\right|^2\right)\right\}, \right.$$
$$\left. \ldots, \min\left\{\log_2\left(1+SNR\left|\alpha_{s,r(N)}\right|^2\right), \log_2\left(1+SNR\left|\alpha_{r(N),d}\right|^2\right)\right\}\right\}, \tag{7.2}$$

$$I_{sel} = \max\left\{\log_2\left(1+SNR\left|\alpha_{s,d}\right|^2\right), \log_2\left(1+SNR\left|\alpha_{r(1),d}\right|^2\right), \ldots, \log_2\left(1+SNR\left|\alpha_{r(n),d}\right|^2\right)\right\}, \tag{7.3}$$

where n is the number of the relay nodes that forward the source packets to the destination node in selection relaying. The wireless channels are assumed to be uncorrelated. For the nodes to perform selection relaying, the following requirement has to be met,

$$\left|\alpha_{r(i),d}\right|^2 \geq g(SNR),$$

where $g(SNR) = (2^R\text{-}1)/SNR$ (R is the source data rate) and $i = 1, 2, \ldots, N$. Comparing (7.2) and (7.3) with (7.1), it can be observed that the mutual information of the relay networks is equal to or greater than that of the direct transmission network, where the source-relay/relay-destination channels are usually better in the received signal quality

than the source-destination channel. Also, mutual information increases with the number of relay nodes.

The outage probability of the networks characterised by the mutual information in (7.1) to (7.3) can be found as follows. For the direct transmission network, the outage probability is [90]

$$P_{out}^{d}(\xi) := \Pr[I_d < R] = \Pr\left[\left|\alpha_{s,d}\right|^2 < g(\xi)\right] = 1 - e^{-\lambda_{s,d} g(\xi)}, \tag{7.4}$$

where λ is the parameter of the exponential distribution, which equals σ^{-2}. For the fixed DF relaying network with one relay node (FixOne), the outage probability is [90]

$$\begin{aligned} P_{out}^{fix,1}(\xi) &:= \Pr[I_{fix} < R] = \Pr\left[\left|\alpha_{s,d}\right|^2 < g(\xi)\right] \Pr\left[\min\left(\left|\alpha_{s,r}\right|^2, \left|\alpha_{r,d}\right|^2\right) < g(\xi)\right] \\ &= \left(1 - e^{-\lambda_{s,d} g(\xi)}\right) \times \left(1 - e^{-(\lambda_{s,r} + \lambda_{r,d}) g(\xi)}\right), \end{aligned} \tag{7.5}$$

where $\min(a_1, \ldots, a_n)$ is also exponentially distributed with parameter $\Sigma_i \lambda_i$, $i = 1, \ldots, n$ for exponentially distributed random variables a_i with parameters λ_i. The outage probability of FixOne found in (7.5) is lower than that of the direct transmission network in (7.4). When there are two relay nodes in the network (FixTwo), the outage probability becomes [90]

$$\begin{aligned} P_{out}^{fix,2}(\xi) &:= \Pr[I_{fix} < R] \\ &= \Pr\left[\left|\alpha_{s,d}\right|^2 < g(\xi)\right] \\ &\times \Pr\left[\min\left(\left|\alpha_{s,r(1)}\right|^2, \left|\alpha_{r(1),d}\right|^2\right) < g(\xi)\right] \Pr\left[\min\left(\left|\alpha_{s,r(2)}\right|^2, \left|\alpha_{r(2),d}\right|^2\right) < g(\xi)\right] \\ &= \left(1 - e^{-\lambda_{s,d} g(\xi)}\right) \times \left(1 - e^{-(\lambda_{s,r(1)} + \lambda_{r(1),d}) g(\xi)}\right) \times \left(1 - e^{-(\lambda_{s,r(2)} + \lambda_{r(2),d}) g(\xi)}\right). \end{aligned} \tag{7.6}$$

Comparing (7.6) with (7.4) and (7.5), it can be observed that the outage probability of FixTwo is the lowest. For the selection DF relaying network, the outage probability can be presented as [90]

$$P_{out}^{sel}(\xi) := \Pr[I_{sel} < R] = \sum_{n} \Pr[n] \Pr[I_{sel} < R|n] \tag{7.7}$$

When there is one relay node in the network (SelOne), it becomes [90]

$$\begin{aligned} & P_{out}^{sel,1}(\xi) \\ &= \Pr\left[|\alpha_{s,d}|^2 < g(\xi)\right] \times \left(\Pr\left[|\alpha_{r,d}|^2 < g(\xi)\right] \Pr\left[|\alpha_{s,r}|^2 > g(\xi)\right] + \Pr\left[|\alpha_{s,r}|^2 < g(\xi)\right] \right) \\ &= \left(1 - e^{-\lambda_{s,d} g(\xi)}\right) \times \left(1 - e^{-(\lambda_{s,r} + \lambda_{r,d}) g(\xi)}\right). \end{aligned} \tag{7.8}$$

When there are two relay nodes in the network (SelTwo), the outage probability is [90]

$$\begin{aligned} & P_{out}^{sel,2}(\xi) \\ &= \Pr\left[|\alpha_{s,d}|^2 < g(\xi)\right] \Pr\left[|\alpha_{s,r(1)}|^2 < g(\xi)\right] \Pr\left[|\alpha_{s,r(2)}|^2 < g(\xi)\right] \\ &+ \Pr\left[|\alpha_{s,d}|^2 < g(\xi)\right] \Pr\left[|\alpha_{r(1),d}|^2 < g(\xi)\right] \Pr\left[|\alpha_{r(2),d}|^2 < g(\xi)\right] \\ &\times \Pr\left[|\alpha_{s,r(1)}|^2 \geq g(\xi)\right] \Pr\left[|\alpha_{s,r(2)}|^2 \geq g(\xi)\right] \\ &+ \Pr\left[|\alpha_{s,d}|^2 < g(\xi)\right] \Pr\left[|\alpha_{r(1),d}|^2 < g(\xi)\right] \Pr\left[|\alpha_{s,r(1)}|^2 \geq g(\xi)\right] \Pr\left[|\alpha_{s,r(2)}|^2 < g(\xi)\right] \\ &+ \Pr\left[|\alpha_{s,d}|^2 < g(\xi)\right] \Pr\left[|\alpha_{r(2),d}|^2 < g(\xi)\right] \Pr\left[|\alpha_{s,r(1)}|^2 < g(\xi)\right] \Pr\left[|\alpha_{s,r(2)}|^2 \geq g(\xi)\right] \\ &= \left(1 - e^{-\lambda_{s,d} g(\xi)}\right) \times \left(1 - e^{-(\lambda_{s,r(1)} + \lambda_{r(1),d}) g(\xi)}\right) \times \left(1 - e^{-(\lambda_{s,r(2)} + \lambda_{r(2),d}) g(\xi)}\right). \end{aligned} \tag{7.9}$$

The outage probability of the selection algorithm is the same as that of the fixed algorithm. There is, however, a disadvantage for the fixed algorithm in energy efficiency, which will be demonstrated later through the simulation and the experimental results.

7.2 Network description

The CRN concerned contains one source node, one destination node and N relay nodes ($N \geq 1$). This section gives the description of the channel coding schemes and the

functions operated at various nodes in the network [90, 91]. All the nodes in the network are aware of which channel coding scheme is being used at the time of transmission.

7.2.1 Channel coding schemes

The channel coding schemes employed are (3, k) coding, where $k = 1, 2, 3$. When $k = 3$, it implies that data are unprotected. In this case, only one data packet is sent out every time a transmit node is active. For $k < 3$, three coded data packets are sent out in a group. When $k = 2$, the first two packets (say A and B) are for original data and the third packet (C) is the parity check or the XOR of the first two packets, i.e., C = A⊕B. When $k = 1$, the original data packet is replicated twice, i.e., three identical data packets are sent out as a repetition code.

For $k = 1$ and 3, the decoding process is rather simple: as long as any of the received data packets passes cyclic redundancy check (CRC), the packet is marked as "successfully received". For $k = 2$, if one of the original data packets fails CRC, it can be recovered from the redundant packet C if C is received successfully. For instant, B is corrupted, but both A and C are intact. Thus, B can be recovered from B = A⊕C.

7.2.2 Node functions

1) The source node is responsible for generating, encoding and transmitting data packets. Each randomly generated data packet is first encoded by one of the coding schemes described above. Then, the coded packet will be further coded using Manchester coding. Frequency shift keying (FSK) is applied as the modulation scheme. The structure of the source node is illustrated in Figure 7-3 and Figure 7-4.

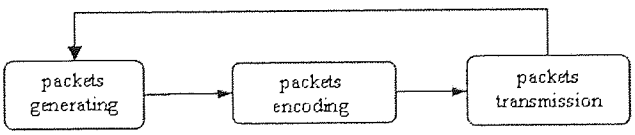

Figure 7-3 The flow chart of the source node.

Source node:

Generating original packets with random data;
Channel coding using one of the (3, *k*) coding schemes;
Manchester coding;
Packets pushed to internal stack waiting for transmission;
FSK modulation.

Figure 7-4 The logical structure of the source node.

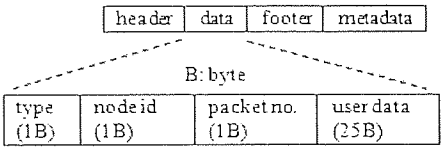

Figure 7-5 The fields of data packets.

Selection relaying node:

FSK demodulation;
Manchester decoding;
CRC checking;
Channel decoding;
If $k = 3$ *and* the packet passes CRC
  Modify "type" and "node id";
  Store the packet;
  Set "engage" to be true;
If $k = 2$
  If both packets pass CRC
    Modify "type" and "node id";
    Store both packets;
    Set "engage" to be true;
  If only one packet passes CRC
    Modify "type" and "node id";
    Store the packet;
    Set "engage" to be true;
    Signal to change to (3, 1) coding scheme;
If $k = 1$ *and* any one of the packets passes CRC
  Modify "type" and "node id";
  Store the packet;
  Set "engage" to be true;
If "engage" *and* signalled to relay
  Channel coding;
  Manchester coding;
  Packets pushed to internal stack waiting for transmission;
  FSK modulation.

Figure 7-6 The logical structure of the relay nodes using selection relaying.

Fixed relaying node:

FSK demodulation;
Manchester decoding;
Channel decoding;
Modify "type" and "node id";
Channel coding;
Manchester coding;
If signalled to relay
  Packets pushed to internal stack waiting for transmission;
  FSK modulation.

Figure 7-7 The logical structure of the relay nodes using fixed relaying.

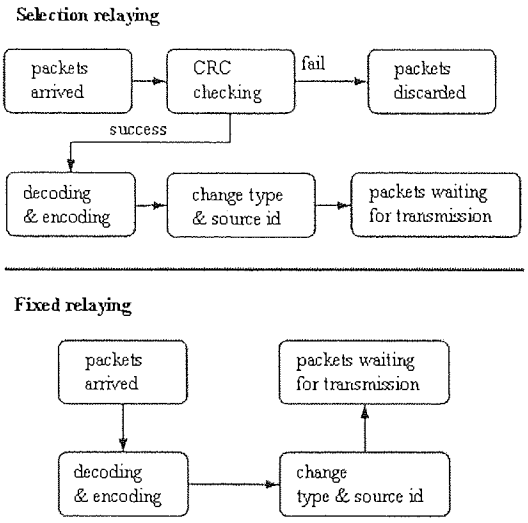

Figure 7-8 The flow charts of the relaying nodes.

2) Two relaying algorithms, selection relaying and fixed relaying, are employed at the relay nodes, respectively. In both algorithms, the relay nodes first carry out FSK demodulation, Manchester decoding and channel decoding. The subsequent operations depend on the relaying algorithm used in the relay nodes.

In selection relaying, the relay nodes need to decide whether or not it should forward the received source data packets, depending on the CRC result of these packets. For k = 1, only one good packet is adequate to "convince" a relay node to forward it. For k = 2, if there is only one successfully received packet, the relay node will apply the (3, 1) coding scheme in forwarding this packet. For k = 3, each packet has to pass CRC before it can be forwarded by the relay node. The forwarded data packets have new values in the data fields, "type" and "node id", indicating that these

are the relayed packets. The structure of a data packet is shown in Figure 7-5. The main purpose of this relaying algorithm is to ensure that the data forwarded by the relay nodes is the same as that sent by the source node. Figure 7-6 shows the logical structure of the relay nodes using selection relaying algorithm.

In the fixed relaying algorithm, the relay nodes skip examining the CRC of each received packet and forward them to the destination node in any circumstances, as shown in Figure 7-7 and Figure 7-8. It is a simpler algorithm but less efficient than selection relaying.

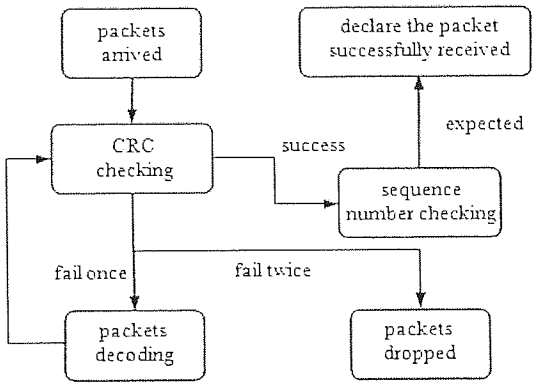

Figure 7-9 The flow chart of the destination node.

Destination node:

FSK demodulation;
Manchester decoding;
Channel decoding;
CRC checking;
If at least one packet passes CRC
  If packet number expected
    Packet of that packet number is "successfully received"
  Else
    Packets "unwanted"

Figure 7-10 The logical structure of the destination node.

3) Figure 7-9 and Figure 7-10 show the flow chart and the logical structure of the destination node. First, the destination node will FSK-demodulate, Manchester-decode and channel-decode the received packets. Then, it will examine the CRC of each packet. A packet with one particular packet number is said to be lost when all of its copies fail CRC checking; otherwise, it is declared as "successfully received". There is

a minor disadvantage of using the CRC result since the result may be incorrect, but the probability of this event is very low.

7.2.3 Time scheduling

To avoid transmission interference or collision between wireless channels, either a TDMA scheme or the Carrier Sense Multiple Access/Collision Avoidance (CSMA/CA) protocol can be used in the multiple access phase (second phase) of the relay network. A TDMA scheme is chosen in the experiments for two reasons. Firstly, TDMA can be easily implemented and is widely employed in many relay networks. Secondly, using TDMA can reduce or eliminate unnecessary delays due to contention operated by CSMA/CA. The simple TDMA scheme applied in the network is shown in Figure 7-2.

7.3 Experimental and initial simulation results

The CRN described in the above section is realised and examined through both experiments and simulations [90, 91].

7.3.1 Experiments

Alongside the simulations on the CRN described in the previous section, an experimental testbed has been built using wireless sensor transceivers for the purpose of collecting field test results and comparing them with those obtained from simulations. The experiments were carried out in the telecommunication laboratory (see Figure 7-11) of the Department of Electronic Engineering at Aston University. The room layout and the location of the sensor nodes are drawn in Figure 7-12. The laboratory is open-spaced and movement was rarely observed during the experiments. The source node (triangle) and the destination node (diamond) were placed at approximately 1 m above the carpeted floor, while 1.2 m for the relay nodes (circles). Up to two relay nodes were used in the experiments. In the case of single relay node, the relay node was placed at the bottom location in Figure 7-12. All the wireless channels were NLOS. The relay nodes were placed with the equal distance to the

source and the destination nodes. The transmit power of all the transmit nodes was set to −5 dBm. For every 66×3 (duration × number of slots) ms, a new data packet was sent out from the source node when $k = 3$. Every 66×3×3 (duration × number of slots × length of code) ms, one or two new packets are generated by the source node when $k =$ 1 or 2 (The $k = 2$ setting applies to simulation only). The structure of data packets is shown in Figure 7-5. Each experiment ran for approximately 15 minutes.

The TDMA is realised in the real network via a so-called small-sized "you-can-relay" (YCR) packet, the structure of which is given in Figure 7-13. Each YCR packet contains the information specifying the identity of the node. The identities of the nodes (except for the destination node) in the network are given as the sequential numbers. Therefore, each relay node can check if the YCR packet received is for itself by adding one to the value of "node id" and verifying if it equals the value of its own identity. Each relay node will also send out a YCR packet to its successive relay node after each time they finish relaying or decide not to relay in selection relaying. The last relay node will not send out any YCR packets. In order for the scheme to work properly, each relay node should reside in the coverage of both its preceding and the source nodes. The test settings are summarised in Table 7-1.

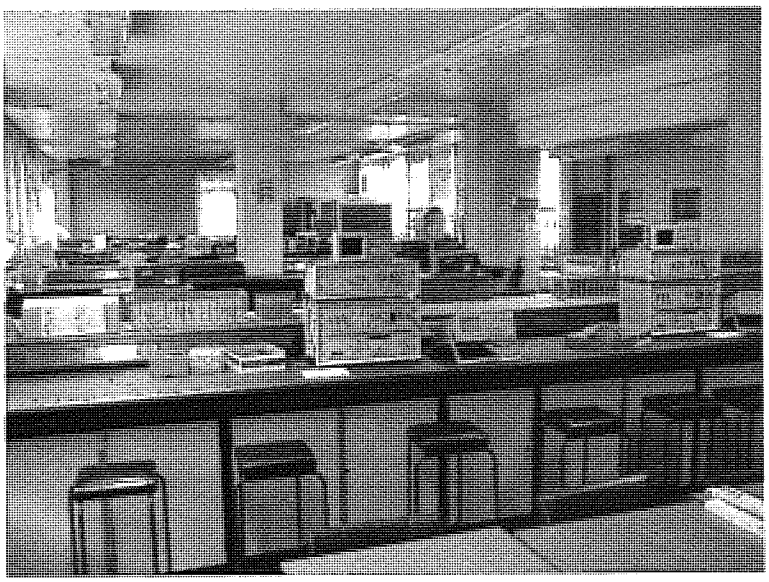

Figure 7-11 The telecommunication laboratory for the tests.

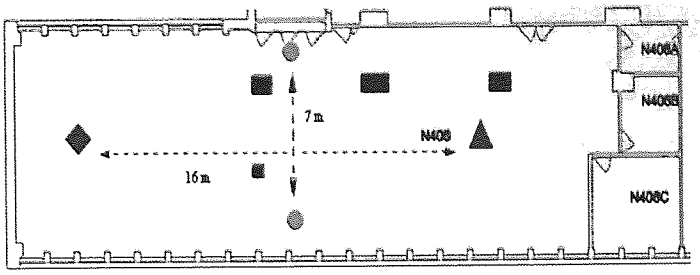

Figure 7-12 The laboratory layout and the location of the sensor nodes.

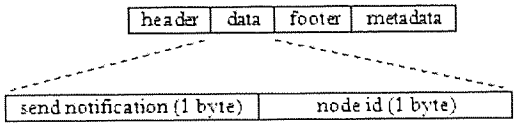

Figure 7-13 The "you-can-relay" packet structure.

Table 7-1 The test settings*

Parameters	Settings
Sensor Nodes	one source node, one or two relay node(s), one destination node
Transmit Power	−5 dBm
Data Rate	$66\times(4-k)\times3$ (k = 1 or 3)
Test Duration	approx. 15 minutes for each test

* applied to both selection and fixed relaying algorithms

Table 7-2 The technical specification of MPR400CB

Parameter	Value
Program Flash Memory	128K bytes
Measurement (Serial) Flash	512K bytes
Serial Communications	UART[a]
Analog to Digital Converter	10 bit ADC
Centre Frequency	433 MHz
Number of Channels	4/50 (programmable, country specific)
Data Rate	38.4 Kbaud (Manchester encoded)
RF Power	-20 to +10 dBm (programmable, typical)
Receive Sensitivity	-98 dBm (typical, analog RSSI[b] at AD Ch. 0)
Outdoor Range	500 ft (1/4 Wave dipole, line of sight)
Current Draw	27 mA (transmit with maximum power); 10 mA (receive); < 1 μA (sleep)

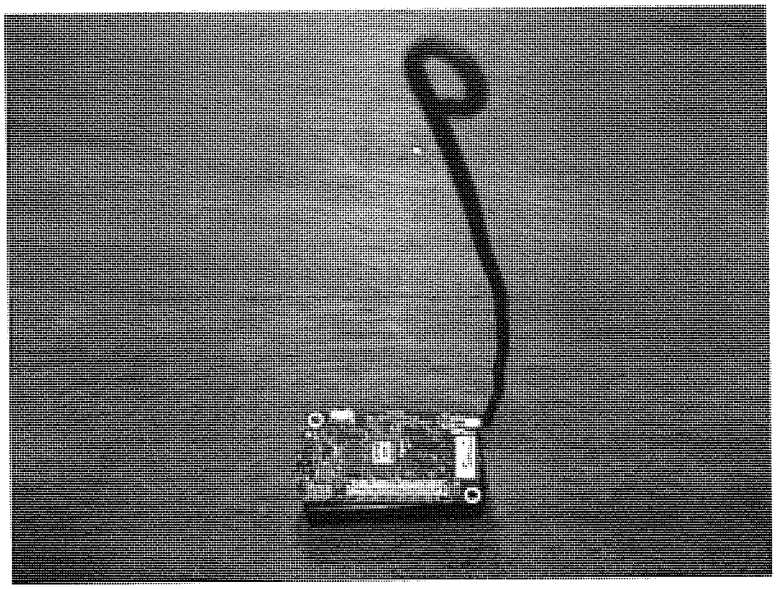

(a)

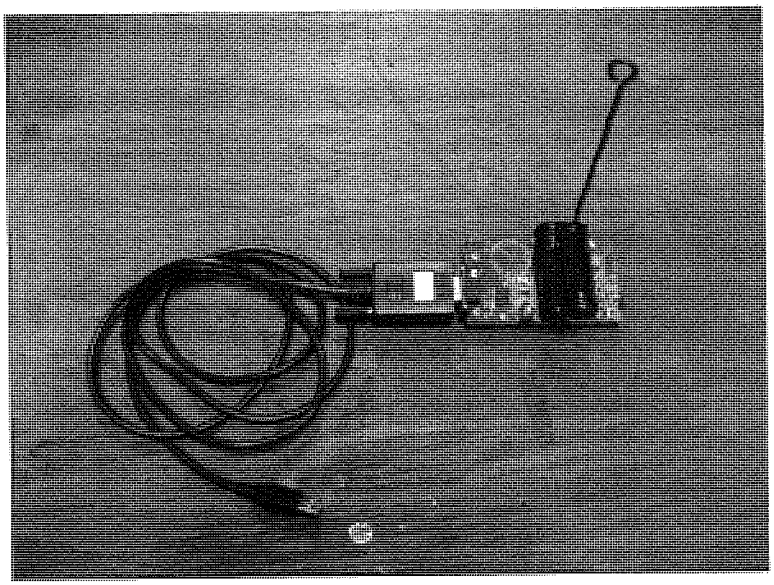

(b)

Figure 7-14 Wireless sensor transceivers used in the testbed. (a) source/relay node; (b) destination node.

The CRN is realised using MPR400CB, a single-antenna radio transceiver operating on 433 MHz and manufactured by Crossbow®. Its major technical specification can be found in Table 7-2 and [92]. Figure 7-14 shows the real sensor transceivers used in the construction of the testbed, where the destination node can be connected to a computer using a serial cable (black in the figure).

7.3.2 Initial simulations

The wireless channels in the simulations are modelled as slow and flat Rayleigh fading channels. The Doppler Shift is 0 Hz and there are two paths between the transmitter and the receiver. The second path is approximately 2.4 m longer than the first path in the source-destination channel and approximately 7.5 m in all the other channels. The path loss is approximately modelled as free space loss in (2.4). Other settings of the initial simulations are identical to those in the experiments.

7.3.3 Performance parameters

1) Data throughput, η, is defined as the ratio of the number of successfully received bits to the time period, T, during which these packets are received,

$$\eta = \frac{N_{suc} L}{T}, \tag{7.10}$$

where N_{suc} is the number of "successfully received" packets and L is the packet length, i.e., 28 bytes or 224 bits here. The data throughput calculates the data rate on the MAC layer (the packet level), which is proportional to the mutual information on the PHY layer (the bit level) but smaller than the latter.

2) Packet loss rate, ρ, is defined as the ratio of the number of the missing source original data packets to the total number of the data packets generated at the source node, N_{gen}, which can be equivalently expressed as

$$\rho = 1 - \frac{N_{suc}}{N_{gen}}. \tag{7.11}$$

The packet loss rate is the error probability computed on the packet basis, which is directly related to the outage probability discussed in Chapter 3 and 4. The former is higher than the latter, since for a corrupted packet only the bad bits contribute to the outage probability but all the bits as a whole in this packet are regarded as loss for the packet loss rate.

3) The SNR without fading effect is the subtraction of the noise floor from the transmit power. The noise floor can be measured using the received signal strength indication (RSSI). The average noise floor for all the experiments is around −62 dBm. Thus, SNR = 57 dB (signal power is −5 dBm).

4) To extract the result for the multiplexing gain under a finite SNR for real data, the following equation is used,

$$r = \frac{R}{\log_2(1+SNR)}, \tag{7.12}$$

which is first proposed in [93] with unity array gain[1]. This multiplexing gain and the following diversity gain are calculated on the packet basis, which gives better practices of performance evaluation than the gains found on the bit basis as in Chapter 3 and 4.

5) Similarly, the diversity gain for real data is modified to,

$$d = -\frac{\log_2 \rho}{\log_2 SNR}. \tag{7.13}$$

There are two types of diversity gain achievable in this network, spatial diversity created by the relay channels and temporal diversity introduced by (3, 1) and (3, 2) coding schemes.

6) Energy efficiency, ε, can be defined as the ratio of the total successfully received bits to the total amount of energy consumed[2],

$$\varepsilon = \frac{\eta}{E} = \frac{\eta}{\sum_{i=1}^{N+1} P_i T_i}, \tag{7.14}$$

[1] In the original definition, SNR is the average received SNR. However, this definition of power is impractical for cooperative systems. Thus, the transmit SNR is used instead, which gives no harm to the analysis in this chapter.

[2] Here, only the transmission energy consumption is concerned as it is the major source of energy consumption in the sensor radio transceivers

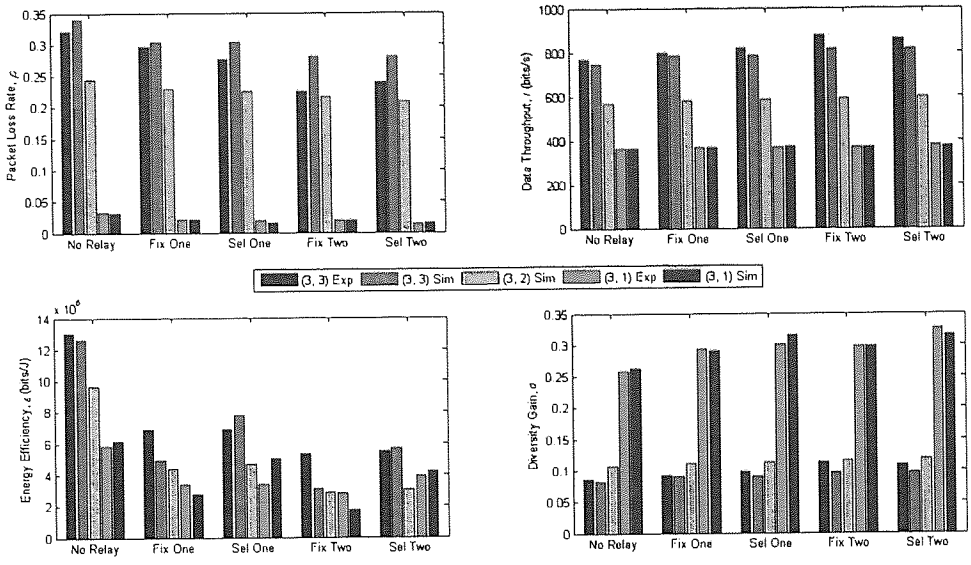

Figure 7-15 The experimental and the initial-simulation results.

where P_i is the transmit power (fixed) at the ith transmit node in Watt, T_i is the total transmission time (including transmission of both data and YCR packets) at the ith transmit node in second.

7.3.4 Results

Figure 7-15 illustrates the experimental and the initial-simulation results of the CRN with different configurations. In the figures, "No Relay" indicates the direct transmission and other captions are in the format of "<Relaying Algorithm> <Number of Relay Nodes>". As the same conclusion drawn through the theoretical analysis in Section 7.1.2, selection relaying and fixed relaying have little difference in reducing errors. This is because when errors occur at the relay nodes after decoding, the erroneous packets are still sent out in fixed relaying but not in selection relaying. In both situations, the transmission quality relies on the source-destination channel. The advantage of fixed relaying is its simplicity, while the selection relaying is better in energy efficiency.

The data throughput of the network implemented is shown in Figure 7-15 when there are no relay nodes (Direct), one relay node (FixOne and DynOne) and two relay nodes (FixTwo and DynTwo), respectively. It is observed that the presence of relay

nodes makes no major difference in throughput for both relaying algorithms, compared to the direct transmission case, when a (3, 1) repetition code is applied in the network. This is due to the added redundancy of the repetition code used even though the loss rate can be reduced in this case. When other coding schemes, (3, 2) and (3, 3), are applied, however, the throughput is improved by the presence of relay nodes. Although the analysis in Section 7.1.2 are confined to the physical layer, the data throughput results obtained from the experiments lead to similar conclusions drawn from the analysis.

As it is expected, the packet loss rate is reduced considerably when the repetition coding is used, which is far lower than that of the networks with other coding schemes applied. The outcomes of the packet loss rate confirm the analytical results of the error probabilities for different network configurations, given in Subsection 7.1.2.

A couple of trade-off pairs can be observed from Figure 7-15. One of them is data throughput vs. packet loss rate (error probability) for the same coding scheme used. Given a coding scheme, more relay nodes help reduce the packet loss rate and improve the data throughput, although for (3, 1) coding the improvement is difficult to spot in the figure. As the packet loss rate can be inversely interpreted by the spatial diversity gain calculated by (7.13), spatial diversity gain is beneficial for data throughput for the same coding schemes and the constant source data rate. There is another type of diversity gain that is involved in this work: temporal diversity gain thanks to the coding schemes employed, which can also be calculated using (7.13). For the same relaying algorithm and with the same number of relay nodes, the coding scheme with more redundancy consequently results in lower data throughput, which forms another trade-off pair, i.e., temporal diversity gain vs. data throughput. This trade-off can lead to a more interesting trade-off pair, i.e., (both spatial and temporal) diversity gain vs. temporal multiplexing gain, shown in Figure 7-16. The linearity of the curves in the figure is because for the SNR value concerned (SNR = 57 dB), $d = -(\log_2\rho/R)\times r$. For each relaying algorithm, the curve is plotted using the following data sets: two nodes under (3, 1) coding scheme (the first set), one node under (3, 2) coding scheme (the second set) and direct transmission under (3, 3) coding scheme (the third set). The first set represents the situation of the highest diversity gain with the lowest temporal

multiplexing gain; the second is for medium diversity gain and medium temporal multiplexing gain; the last shows the lowest diversity gain with the highest temporal multiplexing gain. In Figure 7-16, the gradient values (all negative) indicate that for both relaying schemes the diversity gain is compromised faster when the network configuration switches from the first set to the second set. This is because for the similar amount of spatial diversity gain removed, the temporal diversity gain is more reduced when switching from the first set to the second than from the second to the third.

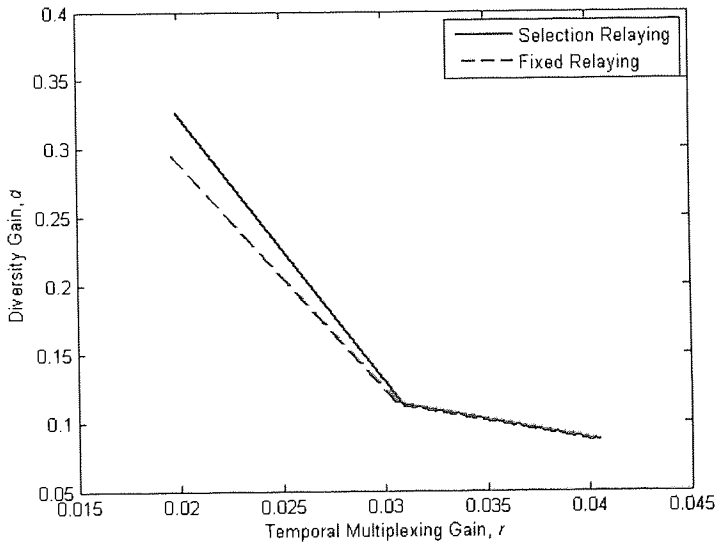

Figure 7-16 Diversity gain vs. Temporal multiplexing gain.

Any gain in diversity and multiplexing is accompanied by higher energy consumption. Therefore, how to choose an appropriate relaying algorithm is really application-dependent. If the application requires high energy efficiency and can tolerate certain level of loss, then one relay or even no relay networks is the better choice. On the contrast, a powerful coding scheme with multiple relay nodes should be employed, when minimizing loss rate is paramount.

The results shown in this section are obtained for the networks with up to two relay nodes. The performance improvement of the networks, especially on data throughput, will be saturated when continuously increasing the number of relay nodes. The theory behind this is rather similar to that of MIMO channels, as explained in [94, 95]. In both papers, the correlation between fading propagation channels has played the main part

for performance saturation. Although in relay networks the correlation is regarded far less severe because of distributed antennas, it will become significant when the field is packed with many relay nodes. Thus, the performance improvement will not remain constant and the energy consumption will be considerably high as the number of relay nodes increases.

The comparison between the experimental and the initial-simulation results shows that they are closely matched, suggesting that the simulation model adopted is appropriate and can be used to investigate the characteristics of the CRN in other propagation environments that are difficult to establish in a laboratory.

7.4 Extended simulation results

The network performances are further investigated through the verified simulations in other propagation environments, where the non-zero Doppler shift is considered and the number of paths increases.

7.4.1 Doppler shift

The Doppler shift is caused by the movement of any object in wireless channels, including the movement of the transmitter and the receiver. Assuming that the symbol length is unchanged, higher Doppler shift causes a wireless channel to become fast fading channel in which the channel gain during a symbol length varies rapidly. This will impair the channel performance. Figure 7-17 shows the impact of Doppler shift on the performance of the CRN, where the Doppler shift is assumed to be the same observed by all the receive nodes. The results for the Doppler shift to be zero are identical to those shown in the previous section.

It can be seen that the Doppler shift has more significant impact on the networks using the (3, 1) coding scheme than those using other two schemes. This is because this scheme exploits temporal diversity to the maximum of what (3, k) schemes can offer. Therefore, once the temporal diversity deteriorates due to the channel becoming fast faded, the networks using a low-rate loss control code such as the (3, 1) code will suffer in performance deterioration faster than those using other higher-rate codes.

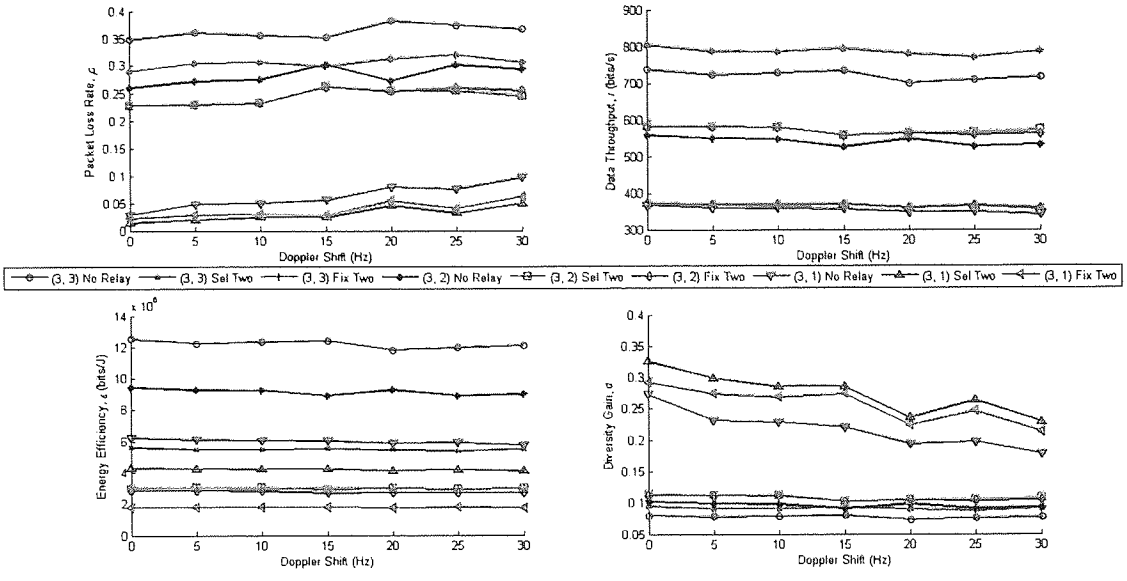

Figure 7-17 The extended simulation results for different Doppler shift values.

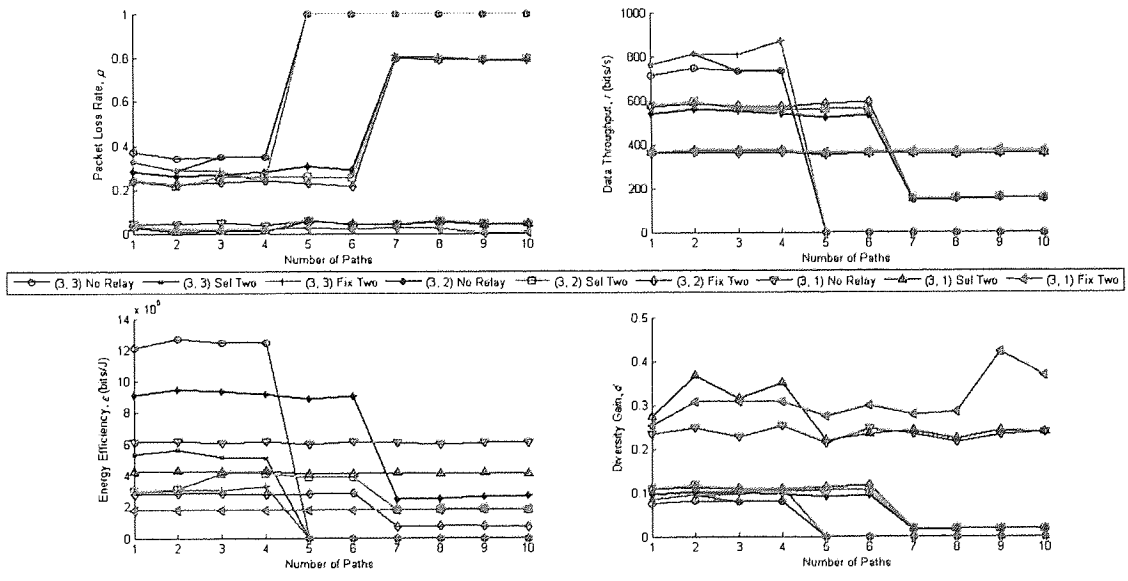

Figure 7-18 The extended simulation results for the multiple paths.

7.4.2 Multipath

In multipath environments, the receivers can observe multiple recognisable signal taps of a transmitted signal. Assuming that the bandwidth of the transmit signal remains the same, more taps tend to cause the channels to be frequency-selective-faded. If no

special frequency multiplexing techniques, such as OFDM, are applied to the transmit signals, the signals can be significantly distorted by such channels. Figure 7-18 shows the network performances against the number of signal paths. It is assumed that the number of observed signal paths by each receiver is the same, and for the source-destination channel the successive path is 2.4 m longer than the preceding one, and for the rest of the links it is 7.5 m. Also, the received signal power of one tap is assumed to be higher than that of its successive tap.

It can be seen that more powerful coding schemes are more resilient in multipath environments. Figure 7-18 suggests a maximum number of paths, with which the (3, 2) and (3, 3) coding schemes can work properly without a significant performance drop. The maximum number of paths for the (3, 1) coding scheme with no performance compromised can be predicted to be above 10 paths. The networks using (3, 2) coding scheme will encounter complete failure before those with (3, 1) coding scheme, if the number of paths continues to increase above 10. One may want to employ nodes with multiple antennas and apply space-time coding on each node in the network to achieve better error performance without using high redundant coding schemes, when the number of signal paths is high.

In a summary, the trade-offs discussed in Section 7.3 still apply to the new propagation environments concerned in this section.

7.5 Summary

In this chapter, the performance trade-offs of the CRN at the packet level are investigated, using both simulations and an experimental testbed. The results obtained have shown the performance trade-offs in the cooperative relaying networks, such as data throughput vs. packet loss rate, temporal diversity gain vs. data throughput, and diversity gain vs. temporal multiplexing gain. They clearly highlight that any technology would have diverse effects on the reliability and efficiency of the same system. In our investigation, for instance, a certain combination of cooperative

relaying algorithms and channel coding schemes can effectively produce diversity and significantly improve the error or loss performance of a wireless network, but at the same time reduce system efficiency in both data delivery and energy consumption.

With large Doppler shifts, the diversity performances offered by more powerful coding schemes are hampered due to the effect of the Doppler shift on the temporal diversity. On the other hand, in multipath-rich environments, powerful coding schemes with more redundancy are recommended in order to maintain the network performance required.

The results presented in this chapter suggest that a proper selection of suitable relaying algorithms and other techniques such as channel coding in the CRNs can meet the requirements for different applications, from energy-efficient environment monitoring to mission-critical content delivery services [96, 97].

8 Conclusions, Contributions and Future Work

Compared with single-antenna systems, multiple-antenna systems – MIMO and CC systems – will be the major technological revolution for air interface and system architect in beyond third generation (B3G) mobile communication systems. They exploit diversity and multiplexing gains in the spatial domain, resulting in dramatic improvements in system performances. This thesis aims to investigate the multiple-antenna systems in a more realistic environment than those reported in previous work, through theoretical analysis and modelling, simulations and experimental investigation. To meet this objective, a MIMO channel model has been developed for a double-scattering propagation environment to examine the effects of the scatterer density on system performances. For CC systems, a correlation model is incorporated to find the mutual information from different protocols that can be delivered to the destination in practical systems. To understand the performance trade-offs in CC systems, a CRN with different configurations has been simulated, the results of which are verified through an experimental testbed.

To carry out the investigations addressed above, some related theories and models are discussed in Chapter 2 – Chapter 4. Large-scale path loss models and small-scale fading models for signal propagating in wireless channels are discussed in Chapter 2. Chapter 3 gives the capacity formulation of wireless MIMO channels and addresses the modelling techniques of multiple-antenna systems. Also in this chapter, the performance evaluation tool, diversity-multiplexing trade-off, is highlighted. Some classic MIMO channel models are re-constructed in Chapter 3, providing better understanding of different MIMO channels and the use of the modelling techniques. Chapter 4 is focused on discussing the protocols for CC systems. Different protocols are designed for the relay nodes to cope with different system conditions.

8.1 Conclusions

Chapter 5 discusses the effects of the scatterer density on MIMO channel performances in a double-scattering (remote and local scatterers) model in flat and

frequency-selective fading channels through theoretical modelling, simulations and the analysis of the spatial degree of freedom and diversity. In flat fading channels, it is shown that changing the scatterer density only by the numbers of the scatterers in the two scatterer zones has little impact on the performances. Also, when the area of the scatterer zones is unfixed, the significant impacts of the scatterer density on channel performances can be observed. In the latter scenario, the way of varying the scatterer density is equivalent to adjusting the antenna beamwidth of the transmitter.

In frequency-selective fading channels, higher scatterer density in the remote scatterer zone leads to higher channel capacity when the area of the scatterer zone is fixed. When the scatterer density is varied by changing the area but with the fixed number of scatterers, higher channel capacity can be obtained in both of the following situations: a) in denser scatterer zones with short coding blocks; and b) in sparser scatterer zones with long coding blocks. Also, longer coding blocks offer better channel capacity under all channel conditions.

The outcome of the work in Chapter 5 has extended the results reported in other work such as [41] and [9] and, at the same time, explained why and how the scatterer density has varied impacts on channel performance. This could help give a better understanding of the behaviours of MIMO channel in different scattering environments and select proper transmitter parameters in order to maximise the system performance.

In Chapter 6, the effects of fading correlation on the performances of the CC systems with FAF and S-STC-DF protocols are investigated. Since the wireless channels in a CC system are more likely to be asymmetric, in terms of the variances of fading coefficients, the UIU model is used to present the channel model.

For the FAF-based CC system, it has been shown that the differences in channel quality between the source-destination and the source-relay channels lead to different mutual information results in the correlated environment. It can be concluded that a better condition of the source-relay channel than that of the source-destination channel is crucial for achieving higher mutual information when CC systems operate in a correlated fading channel. Otherwise, the mutual information is reduced when the channel conditions are the other way around.

The results for S-STC-DF show that the differences in system performance vary between the correlation and non-correlation scenarios, regarding the threshold set for relay participation in the multiple-access phase. Within different threshold regions, the fading correlation introduces different impacts on system performance. In some regions, the fading correlation should be considered for more accurate measurement of system performance, while in other regions the fading correlation may be ignored.

In Chapter 7, several performance trade-offs of the CRN at the packet level are revealed, using both simulations and an experimental testbed. The trade-offs include data throughput vs. packet loss rate, temporal diversity gain vs. data throughput, and diversity gain vs. temporal multiplexing gain. They clearly highlight that any technology has contrasting effects on the reliability and efficiency of the same system. In the investigation, for instance, the combination of cooperative relaying and channel coding can effectively produce diversity and significantly improve the error or loss performance of a wireless network, but at the same time reduce system efficiency in both data delivery and energy consumption.

With large Doppler shifts, the diversity performances offered by more powerful coding schemes are hampered due to the effect of the Doppler shift on the temporal diversity. On the other hand, in multipath-rich environments, powerful coding schemes with more redundancy are recommended to maintain the network performance.

The results presented in Chapter 7 for different scenarios suggest that a proper selection of suitable relaying algorithms and other techniques such as coding in the CRNs can be used to meet the requirements for different applications.

8.2 Contributions

The following contributions have been achieved during the course of this research programme, along with the conclusions summarised in Section 8.1:

- A MIMO channel model has been developed in Chapter 5 for a double-scattering environment in which both remote and local scatterers are considered. The scattering environment adopted is more realistic than those reported

previously. This channel model can be applied in both flat and frequency-selective fading channels. It provides insight into signal propagation in this double-scattering environment and can be conveniently manoeuvred by some important parameters, such as the scatterer density.

- In Chapter 6, the mutual information of different cooperative protocols is re-evaluated in correlated fading channels, using the modified protocol models developed with respect to a general correlated channel model. The analytical results indicates that it is necessary to consider the fading correlation in CC systems for improving the accuracy of performance evaluation, even though the antennas concerned are geometrically apart and at different terminals. Through the explicit analysis of fading correlation in CC systems, the procedure of finding correlated fading coefficients has also been demonstrated.
- A simulation model for CRNs has been built and verified by the results obtained from a real-world testbed in Chapter 7. The testbed is constructed using the contemporary wireless sensor transceivers. The results have revealed the trade-offs between a number of key performance parameters for CC systems in different propagation environments. Both the simulation model and the testbed are ready to be extended to other CC systems, such as cooperative diversity networks.

8.3 Future work

For the benefits of continuing research in the multiple-antenna systems, especially in CC systems, some future work based on the results presented in this thesis is recommended as follows:

- The effect of fading correlation on mutual information in CC systems has been shown in Chapter 6, where the nodes are not clustered. It would be interesting to investigate the effect of fading correlation in the clustered CC systems, which could lead to the modifications to the current cooperative protocols.

- The testbed implemented in Chapter 7 is for cooperative relaying, where the sole task of the relay nodes is to carry out relaying for the source node. The testbed can be extended to operate in a cooperative diversity network, where all the transmit nodes can transmit their own information as well as help each other by relaying other nodes' data. The TDMA scheme applied will be modified accordingly. The destination node should be designed to deal with multiple source data streams. The performance can be evaluated at both network and node levels.

8.4 Publications

1. Guchun Zhang, Xiaohong Peng and Xuanye Gu, "Practical investigation of performance trade-offs in cooperative-relaying wireless networks," in the proceeding of *The 6th ACM International Symposium on Performance Evaluation of Wireless Ad Hoc, Sensor, and Ubiquitous Networks*, Oct. 2009 (PE-WASUN'09).
2. Guchun Zhang, Xiaohong Peng and Xuanye Gu, "Performance analysis of an experimental wireless sensor network," *WILEY Journal of Concurrency and Computation: Practice and Experience -- Special Issue on Advances in Ubiquitous Computing and Networking*.
3. Guchun Zhang, Xiaohong Peng and Xuanye Gu, "Effect of fading correlation on the performance of cooperative systems with multi relay nodes," in the proceeding of *The 5th IEEE International Symposium on Wireless Communication Systems*, Oct. 2008 (ISWCS'08).
4. Guchun Zhang, Xiaohong Peng and Xuanye Gu, "Implementation and performance evaluation of an experimental wireless relay sensor network," in the proceeding of *The 10th IEEE International Conference on High Performance Computing and Communications*, Sept. 2008 (HPCC'08).
5. Guchun Zhang, Xiaohong Peng and Xuanye Gu, "On capacity of cooperative communications in correlated fading channels," in the proceeding of *The 3rd*

IEEE International Conference on Wireless Communications, Networking and Mobile Computing, Sept. 2007 (WiCOM'07).

6. Guchun Zhang, Xuanye Gu and Xiaohong Peng, "An improved urban macrocellular model for MIMO wireless systems," in the proceeding of *First International Conference on Communications and Networking in China*, Oct. 2006 (ChinaCOM'06).
7. Xuanye Gu, Guchun Zhang and Xiaohong Peng, "MIMO systems for broadband wireless communications," *BT Technology Journal*, vol. 24, No. 2, April 2006.

References

[1] "3GPP Release 8," http://www.3gpp.org/Release-8.

[2] "IEEE 802.11n," http://en.wikipedia.org/wiki/IEEE_802.11n.

[3] "WiMAX Forum," http://www.wimaxforum.org/node.

[4] G. J. Foschini, "Layered space-time architecture for wireless communication in a fading environment when using multi-element antennas," *Bell Labs Technical Journal*, vol. 1, pp. 41-59, 1996.

[5] E. Telatar, "Capacity of multi-antenna Gaussian channels," *European Transactions on Telecommunications*, vol. 10, pp. 585-595, 1999.

[6] G. Foschini and M. Gans, "On limits of wireless communication in a fading environment when using multiple antennas," *Wireless Personal Communications*, vol. 6, pp. 311-335, 1998.

[7] D.-S. Shiu, G. J. Foschini, M. J. Gans, and J. M. Kahn, "Fading correlation and its effect on the capacity of multielement antenna systems," *IEEE Transactions on Communications*, vol. 48, pp. 502, 2000.

[8] A. Abdi and M. Kaveh, "A space-time correlation model for multielement antenna systems in mobile fading channels," *IEEE Journal on Selected Areas in Communications*, vol. 20, pp. 550-560, 2002.

[9] D. Gesbert, H. Bolcskei, D. A. Gore, and A. J. Paulraj, "Outdoor MIMO wireless channels: models and performance prediction," *IEEE Transactions on Communications*, vol. 50, pp. 1926-1934, 2002.

[10] V. V. Veeravalli, Y. Liang, and A. M. Sayeed, "Correlated MIMO wireless channels: capacity, optimal signaling, and asymptotics," *IEEE Transactions on Information Theory*, vol. 51, pp. 2058-2072, 2005.

[11] J. W. Wallace and M. A. Jensen, "Modeling the indoor MIMO wireless channel," *IEEE Transactions on Antennas & Propagation*, vol. 50, pp. 591-599, 2002.

[12] E. van der Meulen, "A survey of multi-way channels in information theory: 1961-1976," *IEEE Transactions on Information Theory*, vol. 23, pp. 1-37, 1977.

[13] E. C. van der Meulen, "Transmission of information in a T-terminal discrete memoryless channel," in *Department of Statistics*. Berkeley: University of California, 1968.

[14] E. C. van der Meulen, "Three-terminal communication channels," *Adv. Appl. Probab.*, vol. 3, pp. 120-154, 1971.

[15] T. Cover and A. E. Gamal, "Capacity theorems for the relay channel," *IEEE Transactions on Information Theory*, vol. 25, pp. 572-584, 1979.

[16] J. N. Laneman, D. N. C. Tse, and G. W. Wornell, "Cooperative diversity in wireless networks: efficient protocols and outage behavior," *IEEE Transactions on Information Theory*, vol. 50, pp. 3062-3080, 2004.

[17] S. Berger, M. Kuhn, A. Wittneben, T. Unger, and A. Klein, "Recent advances in amplify-and forward two-hop relaying," *IEEE Communications Magazine*, vol. 47, pp. 50-56, 2009.

[18] A. Goldsmith, *Wireless Communications*. Cambridge: Cambridge University Press, 2005.

[19] T. S. Rappaport, *Wireless Communications : Principles and Practice*, 2nd ed. Upper Saddle River, N.J. ; [Great Britain]: Prentice Hall PTR, 2002.

[20] W. Jakes and D. Cox, *Microwave Mobile Communications*: Wiley-IEEE Press, 1994.

[21] W. C. Y. Lee, *Mobile communications engineering*. New York ; London: McGraw-Hill, 1982.

[22] N. Amitay, "Modeling and computer simulation of wave propagation in lineal line-of-sight microcells," *IEEE Transactions on Vehicular Technology*, vol. 41, pp. 337-342, 1992.

[23] D. Halliday, R. Resnick, and K. S. Krane, *Physics. Vol. 2*, 5th ed. New York ; Chichester: Wiley, 2002.

[24] M. I. Skolnik, *Introduction to radar systems*, 2nd ed. NY: McGraw-Hill, 1980.

[25] S. Y. Seidel, T. S. Rappaport, S. Jain, M. L. Lord, and R. Singh, "Path loss, scattering and multipath delay statistics in four European cities for digital cellular and microcellular radiotelephone," *IEEE Transactions on Vehicular Technology*, vol. 40, pp. 721-730, 1991.

[26] V. Erceg, L. J. Greenstein, S. Y. Tjandra, S. R. Parkoff, A. Gupta, B. Kulic, A. A. Julius, and R. Bianchi, "An empirically based path loss model for wireless channels in suburban environments," *IEEE Journal on Selected Areas in Communications*, vol. 17, pp. 1205-1211, 1999.

[27] J. A. Rice, *Mathematical statistics and data analysis*, 2nd ed. Belmont, Calif: Duxbury Press, 1995.

[28] M. Jankiraman, *Space-time codes and MIMO systems*. Boston ; London: Artech House, 2004.

[29] J. G. Proakis, *Digital communications*, 4th ed. Boston: McGraw-Hill, 2000.

[30] G. L. Stüber, *Principles of mobile communication*, 2nd ed. Boston, Massachusetts; London: Kluwer Academic, 2001.

[31] A. Abdi, C. Tepedelenlioglu, M. Kaveh, and G. Giannakis, "On the estimation of the K parameter for the Rice fading distribution," *IEEE Communications Letters*, vol. 5, pp. 92-94, 2001.

[32] K. Yu, "Modeling of multiple-input multiple-output radio propagation channels," vol. PhD. Stockholm, Sweden: Royal Institute of Technology, 2002.

[33] V. Erceg, "Indoor MIMO WLAN channel models," IEEE 802.11-03/161r2, 2003.

[34] A. Saleh and R. Valenzuela, "A statistical model for indoor multipath propagation," *IEEE Journal on Selected Areas in Communications*, vol. 5, pp. 128-137, 1987.

[35] Q. H. Spencer, B. D. Jeffs, M. A. Jensen, and A. L. Swindlehurst, "Modeling the statistical time and angle of arrival characteristics of an indoor multipath channel," *IEEE Journal on Selected Areas in Communications*, vol. 18, pp. 347-360, 2000.

[36] A. F. Molisch, "A generic model for MIMO wireless propagation channels in macro - and microcells," *IEEE Transactions on Signal Processing*, vol. 52, pp. 61-71, 2004.

[37] J. P. Kermoal, P. E. Mogensen, S. H. Jensen, J. B. Andersen, F. Frederiksen, T. B. Sorensen, and K. I. Pedersen, "Experimental investigation of multipath

richness for multi-element transmit and receive antenna arrays," presented at The 51st IEEE Vehicular Technology Conference Proceedings, Spring 2000.

[38] C. C. Martin, J. H. Winters, and N. R. Sollenberger, "Multiple-input multiple-output (MIMO) radio channel measurements," presented at The 52nd IEEE Vehicular Technology Conference, Fall 2000.

[39] J. Ling, D. Chizhik, P. Wolniansky, R. Valenzuela, N. Costa, and K. Huber, "Multiple transmit multiple receive (MTMR) capacity survey in Manhattan," *Electronics Letters*, vol. 37, pp. 1041-1042, 2001.

[40] P. Soma, D. S. Baum, V. Erceg, R. Krishnamoorthy, and A. J. Paulraj, "Analysis and modeling of multiple-input multiple-output (MIMO) radio channel based on outdoor measurements conducted at 2.5 GHz for fixed BWA applications," presented at The 37th IEEE International Conference on Communications, 2002.

[41] C. Oestges, V. Erceg, and A. J. Paulraj, "A physical scattering model for MIMO macrocellular broadband wireless channels," *IEEE Journal on Selected Areas in Communications*, vol. 21, pp. 721-729, 2003.

[42] S. A.-Q. Fawaz, S. M. Seedahmed, and M. H. Zahir, "A space-time MIMO channel model for macrocell mobile environment," presented at The 12th Asia-Pacific Conference on Communications, 2006.

[43] D. Gesbert, M. Shafi, S. Da-shan, P. J. Smith, and A. Naguib, "From theory to practice: an overview of MIMO space-time coded wireless systems," *IEEE Journal on Selected Areas in Communications*, vol. 21, pp. 281-302, 2003.

[44] T. M. Cover and J. A. Thomas, *Elements of information theory*, 2nd ed. Hoboken, N.J.: Wiley ; Chichester : John Wiley [distributor], 2006.

[45] A. Papoulis, *Probability, random variables and stochastic processes*, 2nd ed. New York ; London: McGraw-Hill, 1984.

[46] L. Zheng and D. N. C. Tse, "Diversity and multiplexing: a fundamental tradeoff in multiple-antenna channels," *IEEE Transactions on Information Theory*, vol. 49, pp. 1073, 2003.

[47] D. Tse and P. Viswanath, *Fundamentals of Wireless Communication*. Cambridge: Cambridge University Press, 2005.

[48] W. C. Jakes, *Microwave mobile communications*. New York ; London: Wiley-Interscience, 1974.

[49] W. R. Bennett, "Distribution of the sum of randomly phased components," *Quartly of Applied Mathematics*, vol. 5, pp. 385-393, 1948.

[50] M. Slack, "The probability of sinusoidal oscillations combined in random phase," *Journal of IEEE*, vol. 93, pp. 76-86, 1946.

[51] D. Asztély, "On antenna arrays in mobile communication systems: fast fading and GSM base station receiver algorithms," Royal Institute of Technology, Stockholm, Sweden IR-S3-SB-9611, March 1996.

[52] K. Azarian, H. E. Gamal, and P. Schniter, "On the achievable diversity -- multiplexing tradeoff in half-duplex cooperative channels," *IEEE Transactions on Information Theory*, vol. 51, pp. 4152-4172, 2005.

[53] Z. Ding, T. Ratnarajah, and C. C. F. Cowan, "On the diversity-multiplexing tradeoff for wireless cooperative multiple access systems," *IEEE Transactions on Antennas and Propagation*, vol. 55, pp. 4627-4638, 2007.

[54] G. Kramer, M. Gastpar, and P. Gupta, "Cooperative strategies and capacity theorems for relay networks," *IEEE Transactions on Information Theory*, vol. 51, pp. 3037-3063, 2005.

[55] H. Ochiai, P. Mitran, and V. Tarokh, "Design and analysis of collaborative diversity protocols for wireless sensor networks," presented at The 60th IEEE Vehicular Technology Conference, Fall 2004.

[56] S. Yang and J.-C. Belfiore, "Towards the optimal amplify-and-forward cooperative diversity scheme," *IEEE Transactions on Information Theory*, vol. 53, pp. 3114-3126, 2007.

[57] S. Yang and J. C. Belfiore, "On slotted amplify-and-forward cooperative diversity schemes," presented at IEEE International Symposium on Information Theory, 2006.

[58] A. Nosratinia, T. E. Hunter, and A. Hedayat, "Cooperative communication in wireless networks," *IEEE Communications Magazine*, vol. 42, pp. 74-80, 2004.

[59] J. N. Laneman and G. W. Wornell, "Distributed space-time-coded protocols for exploiting cooperative diversity in wireless networks," *IEEE Transactions on Information Theory*, vol. 49, pp. 2415-2425, 2003.

[60] M. Yuksel and E. Erkip, "Diversity gains and clustering in wireless relaying," presented at IEEE International Symposium on Information Theory, 2004.

[61] M. Yuksel and E. Erkip, "Diversity in relaying protocols with amplify and forward," presented at IEEE Global Telecommunications Conference, 2003.

[62] M. Yuksel and E. Erkip, "Diversity-multiplexing tradeoff in cooperative wireless systems," presented at 40th Annual Conference on Information Sciences and Systems, 2006.

[63] R. U. Nabar, H. Bolcskei, and F. W. Kneubuhler, "Fading relay channels: performance limits and space-time signal design," *IEEE Journal on Selected Areas in Communications*, vol. 22, pp. 1099-1109, 2004.

[64] A. Bletsas and A. Lippman, "Implementing cooperative diversity antenna arrays with commodity hardware," *IEEE Communications Magazine*, vol. 44, pp. 33-40, 2006.

[65] G.-C. Zhang, X.-H. Peng, and X.-Y. Gu, "On the capacity of cooperative communication in correlated fading channels," presented at The 3rd IEEE International Conference on Wireless Communications, Networking and Mobile Computing, 2007.

[66] L. Sankar, Y. Liang, H. V. Poor, and N. Mandayam, "Opportunistic communications in an orthogonal multiaccess relay channel," presented at IEEE International Symposium on Information Theory, 2007.

[67] A. Bletsas, A. Khisti, D. P. Reed, and A. Lippman, "A simple cooperative diversity method based on network path selection," *IEEE Journal on Selected Areas in Communications*, vol. 24, pp. 659-672, 2006.

[68] P. Gupta and P. R. Kumar, "The capacity of wireless networks," *IEEE Transactions on Information Theory*, vol. 46, pp. 388-404, 2000.

[69] L. R. Ford and D. R. Fulkerson, *Flows in Networks*. Princeton, N.J.: Princeton University Press, 1962.

[70] A. Carleial, "Multiple-access channels with different generalized feedback signals," *IEEE Transactions on Information Theory*, vol. 28, pp. 841-850, 1982.

[71] F. M. J. Willems, "Informationtheoretical results for the discrete memoryless multiple access channel," vol. Doctor in de Wetenschappen Proefschrift dissertation. Leuven, Belgium: Katholieke Universiteit Leuven, 1982.

[72] A. Wyner and J. Ziv, "The rate-distortion function for source coding with side information at the decoder," *IEEE Transactions on Information Theory*, vol. 22, pp. 1-10, 1976.

[73] Z. Min, P. J. Smith, and M. Shafi, "A new space-time MIMO channel model," presented at The 6th Australian Communications Theory Workshop, 2005.

[74] G. J. Byers and F. Takawira, "Spatially and temporally correlated MIMO channels: modeling and capacity analysis," *IEEE Transactions on Vehicular Technology*, vol. 53, pp. 634-643, 2004.

[75] S. Wang, A. Abdi, J. Salo, H. El-Sallabi, and P. Vainikainen, "A time-varying MIMO channel model: theory and measurements," presented at The 6th IEEE Workshop on Signal Processing Advances in Wireless Communications, 2005.

[76] L. Ming, T. Lo, and J. Litva, "A physical spatio-temporal model of multipath propagation channels," presented at The 47th IEEE Vehicular Technology Conference, Spring1997.

[77] J. J. Blanz and P. Jung, "A flexibly configurable spatial model for mobile radio channels," *IEEE Transactions on Communications*, vol. 46, pp. 367-371, 1998.

[78] L. ByoungSun, K. Sewoong, M. Hyun Yook, L. Jewoo, S. Jeho, M. Cheol, and Y. Young Joong, "Modeling the indoor channel for the MIMO system using dual polarization antennas," presented at The 9th European Conference on Wireless Technology, 2006.

[79] G.-C. Zhang, X.-H. Peng, and X.-Y. Gu, "An improved urban macrocellular model for MIMO wireless systems," in *First International Conference on Communications and Networking in China*. China, 2006.

[80] A. Medles and D. T. M. Slock, "Optimal diversity vs multiplexing tradeoff for frequency selective MIMO channels," presented at IEEE International Symposium on Information Theory, 2005.

[81] M. Chiani, M. Z. Win, and A. Zanella, "On the capacity of spatially correlated MIMO Rayleigh-fading channels," *IEEE Transactions on Information Theory*, vol. 49, pp. 2363-2371, 2003.

[82] C. Chen-Nee, D. N. C. Tse, J. M. Kahn, and R. A. Valenzuela, "Capacity scaling in MIMO wireless systems under correlated fading," *IEEE Transactions on Information Theory*, vol. 48, pp. 637-650, 2002.

[83] S. L. Loyka, "Channel capacity of MIMO architecture using the exponential correlation matrix," *IEEE Communications Letters*, vol. 5, pp. 369-371, 2001.

[84] P. J. Smith, L. M. Garth, and S. Loyka, "Exact capacity distributions for MIMO systems with small numbers of antennas," *IEEE Communications Letters*, vol. 7, pp. 481-483, 2003.

[85] K. Ming and M. S. Alouini, "Impact of correlation on the capacity of MIMO channels," presented at The 38th IEEE International Conference on Communications, 2003.

[86] C. Oestges and A. J. Paulraj, "Beneficial impact of channel correlations on MIMO capacity," *Electronics Letters*, vol. 40, pp. 606-608, 2004.

[87] A. M. Tulino, A. Lozano, and S. Verdu, "Impact of antenna correlation on the capacity of multiantenna channels," *IEEE Transactions on Information Theory*, vol. 51, pp. 2491-2509, 2005.

[88] G.-C. Zhang, X.-H. Peng, and X.-Y. Gu, "Effect of fading correlation on the performance of cooperative systems with multi relay nodes," presented at IEEE International Symposium on Wireless Communication Systems, 2008.

[89] P. Murphy, A. Sabharwal, and B. Aazhang, "Building a cooperative communications system," 2007.

[90] G.-C. Zhang, X.-H. Peng, and X.-Y. Gu, "Performance analysis of an experimental wireless sensor network," *Wiley Journal of Concurrency and Computation: Practice and Experience*, 2010.

[91] G.-C. Zhang, X.-H. Peng, and X.-Y. Gu, "Practical investigation of performance trade-offs in cooperative-relaying wireless networks," presented at ACM International Symposium on Performance Evaluation of Wireless Ad Hoc, Sensor, and Ubiquitous Networks, Tenerife, Canary Islands, Spain, 2009.

[92] "MICA2_Datasheet," www.xbow.com/Products/Product_pdf_files/Wireless_pdf/MICA2_Datasheet.pdf.

[93] R. Narasimhan, A. Ekbal, and J. M. Cioffi, "Finite-SNR diversity-multiplexing tradeoff of space-time codes," presented at IEEE International Conference on Communications, 2005.

[94] T. S. Pollock, T. D. Abhayapala, and R. A. Kennedy, "Antenna saturation effects on MIMO capacity," presented at IEEE International Conference on Communications, 2003.

[95] V. Raghavan and A. M. Sayeed, "MIMO capacity scaling and saturation in correlated environments," presented at IEEE International Conference on Communications, 2003.

[96] I. F. Akyildiz, S. Weilian, Y. Sankarasubramaniam, and E. Cayirci, "A survey on sensor networks," *IEEE Communications Magazine*, vol. 40, pp. 102-114, 2002.

[97] S. Kumar, K. Kambhatla, F. Hu, M. Lifson, and Y. Xiao, "Ubiquitous computing for remote cardiac patient monitoring: a survey," *International Journal of Telemedicine and Applications*, vol. 2008, 2008.